Oscillons

Salmi, P.E.

Oscillons

Petja Salmi

In the front cover: a moving oscillon
In the back cover: radiation patterns with absorbing and periodic boundary conditions

Oscillons

PROEFSCHRIFT

ter verkrijging van
de graad van Doctor aan de Universiteit Leiden,
op gezag van Rector Magnificus
prof. mr. P.F. van der Heijden,
volgens besluit van het College voor Promoties
te verdedigen op dinsdag 23 september 2008
klokke 16.15 uur

door

Petja Salmi

geboren te Kuorevesi, Finland in 1975

Promotiecommissie:

Promotor:	Prof. dr. A. Achúcarro
Co-Promotor:	Dr. M. B. Hindmarsh (University of Sussex)
Referent:	Prof. dr. ir. W. van Saarloos
Overige leden:	Prof. dr. J. M. van Ruitenbeek
	Prof. dr. J. Smit (Universiteit van Amsterdam)
	Dr. P. M. Saffin (University of Nottingham)

An odd planet, and those on it are odd, too.
They're subject to time, but they won't admit it.
They have their own ways of expressing protest.

Wisława Szymborska

ISBN: 978-90-9023437-3

Contents

Chapter 1

Introduction

The traditional example (see e.g. [1]) of dissipative solutions is the surface of water. A disturbance, say throwing a stone into water, creates waves that travel to all directions away from the location where the stone hit the surface. Assuming further that the experiment takes place not at a small pond, but that the extent of water does not create any restriction, then the energy carried by the waves spreads to a larger and larger area. If an observer waits long enough, there is an arbitrarily low amount of energy left at any location from the initial energy input given by the stone. The disturbance has dissipated.

Imagine, however, that you could gently disturb the surface of the water and create a deviation from the flat surface (as a matter of fact, to a certain extent you even can, touching water with your fingertip and then slowly lifting it bends the surface slightly because of the surface tension). Imagine now further that this disturbace does not cause propagating ripples spreading out, but rather stays at its original location, say e.g. oscillating around the initial level of the surface. In case of the example of the unbounded surface of water this does not reflect reality, but it turns out that there are other physical systems, or at least classical field equations, that possess non-dissipative solutions. Such dissipationless solutions are often called *solitons* or, in some cases, solitary waves. These solutions can be time independent or there are solutions that are periodic in time. Typical examples of previous ones are topological defects that owe their stability to non-trivial vacuum structure. Most notable of such are monopoles, cosmic

strings and domain walls. The simplest example of topological defects are the kink solutions in one dimension. Though kinks are a standard case of time independent solitons their scattering behaviour provides a bridge to time dependent solitons, namely the breather, or doublet solution, in sine-Gordon model is one of the very few entirely analytically understood examples of non-dissipative solutions that are periodic in time. There are, however, time periodic, non-topological solitons in arbitrary space dimensions, so-called Q-ball solutions that will also be reviewed briefly.

This study is about time-dependent solutions that are neither strictly speaking entirely non-dissipative nor exactly periodic, but the time scale related to the dissipation of energy is far greater than the approximative period related to the solution. Like solitons in general, they go under several names and in this respect there is no entirely established precise terminology, but throughout this study these solutions are called *oscillons*. Unlike topological defects protected by a conserved topological charge or Q-balls that are stable as configurations minimising the energy, there is no obvious conservation law to explain why oscillons appear almost dissipationless. Due to this and because the problem is essentially time dependent and nonlinear the approaches are mainly numerical. The previous picture of the surface of water is illustrative because this study deals mainly field equations in two dimensions though results in higher dimensions will be presented as well.

The example of water continues to be a relevant one as the history of the discovery of solitons is connected to it in a familiar environment, namely in a channel that restricts the directions any waves created by disturbances can propagate. Solitons were namely discovered by Scottish engineer J. Scott Russell in 1834 when he followed a surface wave in a narrow shallow channel created by a boat coming to an abrupt halt. According to the publication the wave travelled at least for a mile before disappearing [2]. The satisfactory quantitative description was given by Diederik Korteweg and Gustav de Vries in 1895 [3]. This hydrodynamical soliton is briefly reviewed in the end of the chapter.

1.1 Kinks

Throughout this study with the dimension of the theory we refer to the number of spatial dimensions. In other words, one-dimensional means (1+1) space-time dimensions. There the action for a single, real scalar field is given by

$$S = \int \mathrm{d}^2\mathbf{x} \left[\frac{1}{2}\partial_\mu\phi\partial^\mu\phi - V(\phi) \right] , \tag{1.1}$$

where now $\mu = 0, 1$. We use here consistently natural units, unless explicitly otherwise stated, so that $\hbar = c = k_\mathrm{B} = 1$, where the constants are Planck's constant, speed of light and Boltzmann's constant, respectively. The Lagrangian from (1.1) is

$$\mathscr{L} = \frac{1}{2}\partial_\mu\phi\partial^\mu\phi - V(\phi) \, , \tag{1.2}$$

and the equation of motion reads

$$\ddot{\phi} - \partial_x^2\phi + V'(\phi) = 0 \, , \tag{1.3}$$

where the dot refers to derivation with respect to time. The energy-momentum tensor in the theory is given by

$$T_{\mu\nu} = \partial_\mu\phi\partial_\nu\phi - g_{\mu\nu} \left[\frac{1}{2}\partial_\rho\phi\partial^\rho\phi - V(\phi) \right] , \tag{1.4}$$

where $g_{\mu\nu}$ is the metric tensor and in flat space $g_{\mu\nu} = \mathrm{diag}(1, -1)$.

1.1.1 Quartic Theory

The most elementary example of a topological defect is the kink solution of a single real scalar field in one dimension. It is a non-dissipative solution owing its name to its shape when plotted as a function of position. The so-called Z_2 kink appears in a model known as ϕ^4 theory [4, 5], where one considers a symmetric double-well potential

$$V(\phi) = \frac{1}{4}\lambda(\phi^2 - \eta^2)^2 \, . \tag{1.5}$$

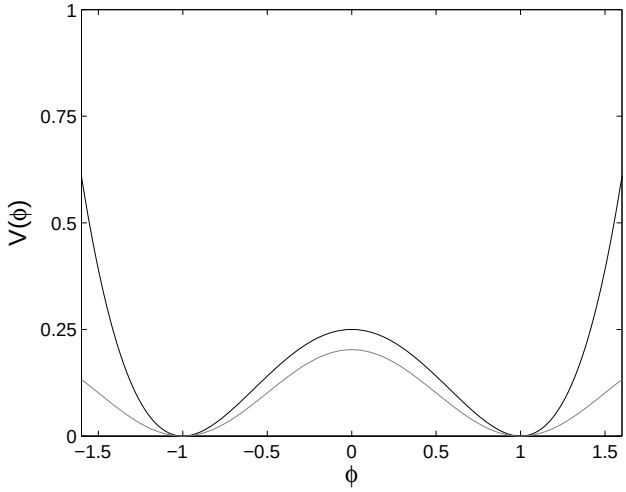

Figure 1.1. The quartic potential (1.5) for $\lambda = 1$ and $\eta = 1$ (black line) together with the potential (1.12) of sine-Gordon model for $\alpha = 1$ and $\beta = \pi$ (grey line), shifted by one unit along ϕ-axis in order for the two minima to coincide.

The potential has two minima, $\phi = \pm\eta$, assumed here to be distinct ($\eta \neq 0$), see also Figure 1.1. There is reflectional symmetry since $V(\phi) = V(-\phi)$ and the vacuum manifold has two-fold degeneracy. In addition to the trivial solutions, $\phi = -\eta$ and $\phi = +\eta$, there is the kink solution interpolating between these two. This can be found by solving (1.3) with above given potential. For time independent field ϕ the ordinary differential equation yields the kink solution centered at the origin

$$\phi_{\,\mathrm{kink}}(x) = \eta \, \tanh\left(\sqrt{\frac{\lambda}{2}}\eta \, x\right) . \tag{1.6}$$

A kink centered at any other position x_0 can be obtained by translation $x \to x - x_0$. Similarly a kink moving at arbitrary velocity less than the speed of light can be constructed by a Lorentz boost. An antikink solution that connects the two vacua in a reversed order can be obtained simply by flipping the sign in (1.6). The mass scale in the model is given by $m^2 = 2\lambda\eta^2$.

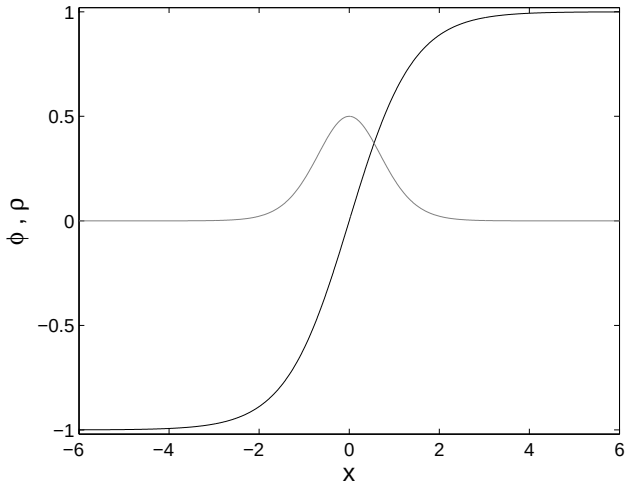

Figure 1.2. The profile of the kink $\phi_{\rm kink}$ in ϕ^4 theory, given by (1.6) (black line) and the energy density $\rho_{\rm kink}$, given by (1.7) (grey line) for $\lambda = 1$ and $\eta = 1$.

The energy density of a stationary kink is

$$\rho_{\rm kink}(x) = \left[\frac{1}{2}(\nabla\phi_{\rm kink})^2 + V(\phi_{\rm kink})\right] = \frac{\lambda\eta^4}{2}\,\mathrm{sech}^4\left(\sqrt{\frac{\lambda}{2}}\eta x\right) . \qquad (1.7)$$

This yields the total energy of the kink

$$E_{\rm kink} = \int_{-\infty}^{\infty} \mathrm{d}x\, \rho_{\rm kink}(x) = \frac{2\sqrt{2\lambda}}{3}\eta^3 , \qquad (1.8)$$

which can be interpreted as its rest mass. The attractive force between a kink and an antikink separated by the distance ℓ can be evaluated from the energy-momentum tensor (1.4) and is given by

$$F = 16\lambda\eta^4 e^{-\sqrt{2\lambda}\eta\ell} . \qquad (1.9)$$

From the point of view of topological considerations, there is a con-

served topological charge

$$Q = \int_{-\infty}^{\infty} \mathrm{d}x\, J(x) = \frac{1}{2\eta}\left[\phi(x=\infty) - \phi(x=-\infty)\right] , \tag{1.10}$$

where $J(x)$ is a topological charge density defined as

$$J(x) = \frac{1}{2\eta}\partial_x \phi\,. \tag{1.11}$$

This is the simplest example of topological conservation law, a kink configuration is characterised by $Q = +1$, while anti-kink has charge $Q = -1$. Any solutions with $Q = 0$ indicate that the field interpolates around the same vacuum value and thus can be continuously deformed to a vacuum solution. From the point of view of multi-soliton solutions, the ϕ^4 theory is very restricted. Because there are only two vacua, a kink can be followed only by an antikink. A model with greater number of vacua permits the existence of several solitons, in particular without antisolitons in between.

1.1.2 Sine-Gordon Model

The sine-Gordon model was initially proposed by Skyrme [6] as a toy model for nucleons. The vacua are labelled by an arbitrary integer. The model is defined by the potential

$$V(\phi) = \frac{\alpha}{\beta^2}(1 - \cos(\beta\phi))\,. \tag{1.12}$$

There are an infinite number of vacua, namely $\phi = 2\pi n/\beta$. The sine-Gordon kink has the form

$$\phi_{\,\mathrm{kink}}(x) = \frac{4}{\beta}\tan^{-1}\left(\exp(\sqrt{\alpha}x)\right) . \tag{1.13}$$

The antikink solution can be obtained by replacing x by $-x$ in (1.13). The energy density is given by

$$\rho_{\,\mathrm{kink}}(x) = \frac{4\alpha}{\beta^2}\,\mathrm{sech}^2\left(\sqrt{\alpha}x\right) . \tag{1.14}$$

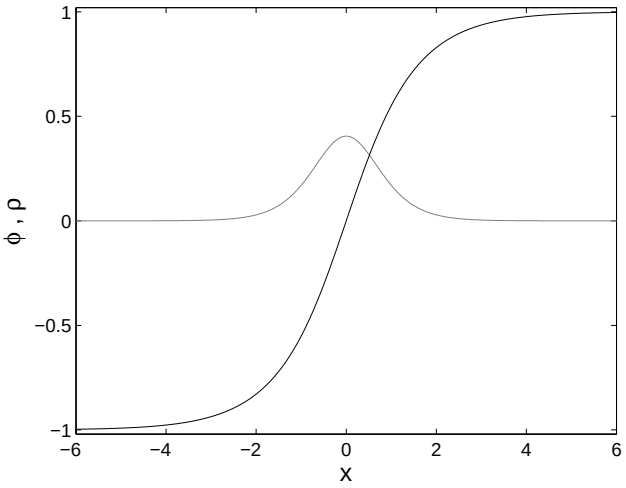

Figure 1.3. The profile of the kink ϕ_{kink} in sine-Gordon model, given by (1.13), scaled to interval $-1 < \phi < 1$ (black line) and the energy density ρ_{kink}, given by (1.14) (grey line) for $\alpha = 1$ and $\beta = \pi$.

The total energy of sine-Gordon kink is $E_{\text{kink}} = 8\sqrt{\alpha}/\beta^2$. The topological charge

$$Q = \frac{\beta}{4\pi} \int_{-\infty}^{\infty} \mathrm{d}x \frac{\partial \phi}{\partial x} \tag{1.15}$$

counts the net number of kinks (being negative for antikinks).

In the sine-Gordon model the attractive force between a kink and antikink separated by the distance ℓ is

$$F = \frac{20\alpha}{\beta^2} e^{-\sqrt{\alpha}\ell}\,. \tag{1.16}$$

1.1.3 Multi-soliton Solutions

Though the sine-Gordon model permits states with several solitons, the configuration of a kink and an antikink is of particular interest and can be

written as [7]

$$\phi_{\text{kink}-\text{antikink}}(x,t) = \frac{4}{\beta}\tan^{-1}\left[\frac{\sinh(v\sqrt{\alpha}t/\sqrt{1-v^2})}{v\cosh(\sqrt{\alpha}x/\sqrt{1-v^2})}\right]. \tag{1.17}$$

It is a solution of the equation of motion (1.3) with the potential taken to be (1.12). That the solution (1.17) describes the kink-antikink scattering comes apparent by studying the right hand side either in the distant past or far in the future. Focusing to the latter case and the limit $t \to \infty$, the solution (1.17) can be rewritten

$$\begin{aligned}\phi_{\text{kink}-\text{antikink}}(x,t) \quad &\to \quad \phi_{\text{kink}}\left(\frac{\sqrt{\alpha}(x+v(t-\Delta/2)}{\sqrt{1-v^2}}\right) \\ &+ \quad \phi_{\text{antikink}}\left(\frac{\sqrt{\alpha}(x-v(t-\Delta/2)}{\sqrt{1-v^2}}\right), \end{aligned} \tag{1.18}$$

where

$$\sqrt{\alpha}\,\Delta = ((1-v^2)/v)\ln(v)\,. \tag{1.19}$$

The solution splits into a kink-antikink pair moving apart with the relative velocity $2v$, the kink moving to left and the antikink to right. The collision has caused only a time delay given by Δ, or strictly speaking the time delay here is rather time advance because it is a negative quantity, $0 > \Delta$ as velocity $v < 1$. The kink and antikink attract each other according to (1.16) and undergo acceleration during the scattering process when approaching each other.

Similarly to (1.17), there exists an exact solution presenting two kinks and which can be written as

$$\phi_{\text{kink}-\text{kink}}(x,t) = \frac{4}{\beta}\tan^{-1}\left[\frac{v\sinh(\sqrt{\alpha}x/\sqrt{1-v^2})}{\cosh(\sqrt{\alpha}vt/\sqrt{1-v^2})}\right]. \tag{1.20}$$

Because the two-kink solution describes two identical solitons, it is not well-defined if in the scattering process the kinks pass through each other or rather bounce back off each other. The latter interpretation is slightly preferable [8], due to the repulsive force between kinks they cannot cross

the energy barrier at low speeds. Asymptotically there is no difference between backward and forward scattering. From (1.20) a solution describing two antikinks can be obtained again directly by flipping the sign, $\phi_{\text{antikink}-\text{antikink}}(x,t) = -\,\phi_{\text{kink}-\text{kink}}(x,t)$.

In addition to (1.17) where a kink and antikink pass through each other, there is another type of configuration consisting of a kink-antikink pair. This is a so-called breather, or doublet, solution and can be obtained from (1.17) by a simple replacement $\bar{v} = iv$ which still yields a real valued function

$$\phi_{\text{breather}}(x,t) = \frac{4}{\beta}\tan^{-1}\left[\frac{\sin(\bar{v}\sqrt{\alpha}t/\sqrt{1+\bar{v}^2})}{\bar{v}\cosh(\sqrt{\alpha}x/\sqrt{1+\bar{v}^2})}\right]. \tag{1.21}$$

While v represents the asymptotic velocity of the kink moving to left in (1.17), the breather is an oscillating bound state made of a kink and an antikink given in its overall rest frame as the solution is always centered at the origin. A travelling breather can be obtained further by Lorentz transforming (1.21). The oscillatory behaviour can be seen easily by rewriting the right hand side of (1.21). By defining $\omega = \sqrt{\alpha}\bar{v}/\sqrt{1+\bar{v}^2}$ and $\vartheta = 1/\bar{v}$ (see e.g. [9]) the breather solution becomes

$$\phi_{\text{breather}}(x,t) = \frac{4}{\beta}\tan^{-1}\left[\frac{\vartheta\sin(\omega t)}{\cosh(\vartheta\omega x)}\right]. \tag{1.22}$$

There is one parameter family of these solutions (1.22) labelled by ω ($\vartheta = \sqrt{\alpha-\omega^2}/\omega$). From (1.22) it is straightforward to see that the breather oscillates with a frequency ω. During the oscillation period it splits into a kink and an antikink, but at times $t = n\pi/\omega$ the kink and antikink disappear, the field is at the vacuum $\phi = 0$ and the breather's energy is purely in the kinetic form, see Figure 1.4. The total energy of the breather can be obtained just by inserting the solution (1.22) into the energy functional. This yields result

$$E_{\text{breather}} = \frac{16}{\beta^2}\sqrt{\alpha-\omega^2} = 2E_{\text{kink}}\sqrt{1-\frac{\omega^2}{\alpha}}. \tag{1.23}$$

The last form of the energy shows particularly clearly how the breather is

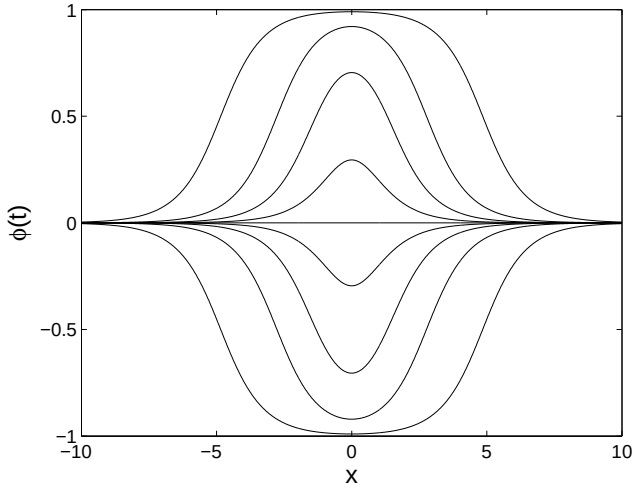

Figure 1.4. Snapshots depicting the evolution of a breather (1.22) over one period for $\omega = \pi/100$ and $\alpha = 1$ scaled to the interval $-1 < \phi < 1$. The time intervals between the snapshots are far from equal, most of the period the profile very close to either of the maximum excursions, i.e. a separated kink-antikink pair. The pictured breather has energy very close to that of two free kinks (difference only 0.5 per mille). When this is not the case and the breather has higher frequency ω, the profile of a breather never resembles to that of a kink-antikink pair. For instance, if $\omega > 1/2$, the maximum excursion is only two thirds of the distance between neighbouring vacua.

a bound state of a kink and an antikink. The breather has always lower total energy than that of two kinks at rest, and approaches that only at the limit $\omega \to 0$ corresponding to an infinitely long oscillation period. Together with the oscillation frequency ω the parameter $\bar{v}$ defines the size of the breather setting the maximum distance the approximate kink and antikink are apart before bouncing back. The field of the breather solution in the rest frame remains confined within the envelope [7]

$$\pm\frac{4}{\beta}\tan^{-1}\left[\frac{1}{\bar{v}}\,\mathrm{sech}\left(\frac{\sqrt{\alpha}x}{\sqrt{1+\bar{v}^2}}\right)\right]. \tag{1.24}$$

While the breather solution is a non-trivial configuration, the field interpolates between the same vacuum in a finite interval and thus topo-

logically the breather belongs to the trivial sector as the net topological charge given by (1.15) vanishes. The force between two kinks or antikinks is repulsive and therefore there exists no bound states with non-zero topological charge. This can also be seen by inserting $\bar{v} = iv$ into (1.20) which does not yield anymore a real function for the field ϕ.

All presented solutions consisting of several kinks and antikinks both describing scattering and the bound state are in the sine-Gordon model which in one dimension is a completely integrable system. There are no known corresponding exact solutions in ϕ^4 theory (a potential approximation can be found e.g. in [10]). Obviously there is no counterpart for two-kink solution (1.20) due to the vacuum structure of the quartic theory. Similarly, it forbids a kink and an antikink passing through each other in a scattering process, while they of course still can reflect. The reflection turns out to be inelastic, kinks release some amount of their energy into radiation, small amplitude oscillations around the vacuum. These oscillations are dispersive propagating waves, that will be assumed to be well described by a linear Klein-Gordon equation.

The scattering of the kink-antikink pair in ϕ^4 theory exhibits a very rich structure which has undergone a considerable amount of research. Not very surprisingly, when a kink and an antikink meet at high initial relative velocity, they reflect back and recede to infinity though some of the initial kinetic energy of kinks is always leaked into radiative modes. Once the collision velocity is low the kinks have time to lose enough energy in the collision so that they become trapped due to the mutual attractive force (1.9). However, there is no unambiguous threshold velocity separating reflection and trapping, noted for the first time in [11]. Instead, there exists an interval of initial velocities v, $0.19 < v < v_c = 0.26$, where the final state is either a widely separated kink-antikink pair or a decaying bound state depending very sensitively on v. In this region the kink and antikink can reflect once, escape to a finite separation and then return to reflect once more, but after this second reflection separate to infinity. This so-called two-bounce window, observed in [12], was explained quantitatively in [13] (see also [14]). While kinks lose translational kinetic energy during the first reflection and become bound by their mutual potential, this energy is not entirely lost into dispersive, propagating modes, but

at least partially stored in the internal mode, so called shape mode representing localised deformations of the kink solution, and roughly conserved. When the weakly bound pair comes together for the second time, it is possible that energy is retransfered to translational form allowing the kinks to escape. For this retransfer to be realised the time between the first and second collision has to satisfy a resonance condition. Thus the above mentioned velocity interval is split into these two-bounce windows. It is worth noticing that in the two-bounce window the scattering can be so closely elastic that similar elasticity is achieved again only at far higher velocities above critical speed v_c. Quite naturally, the mechanism of storing energy into internal modes is not in any way restricted to permit an escape only after two reflections. There exist three-bounce windows as well, found for the first time in a study of a modified sine-Gordon model [15] and then in ϕ^4 theory in [16]. The latter study then argued that these appear together with higher n-bounce windows on the edges of the two-bounce windows all which then makes the the interval to have a fractal structure.

Turning then the attention from reflection in the kink-antikink scattering to the other possible outcome, formation of the bound state. The bound state, dubbed as bion in [16], can form because energy is lost to radiation and the kink and antikink become trapped. This does not occur in the sine-Gordon model where scattering is elastic and kinks always pass through each other unscathed. As there is no loss of translational energy the kink and antikink stay free and never enter the sector of a bound state, i.e. the breather (recall that $E_{\text{breather}} < 2\,E_{\text{kink}}$ in (1.23)). It is noticeable that this and the complete integrability is strictly restricted to potential (1.12) and even a slight deviation of this shape yields a non-integrable model. This is illustrated by a modified sine-Gordon model defined by

$$V(\phi) = \frac{(1-r)^2(1-\cos\phi)}{(1+r^2+2r\cos\phi)}\,, \tag{1.25}$$

where r is a parameter in the range $-1 < r < 1$. Any non-zero value of the parameter r diverts the shape of a kink from (1.13) which brings some inelasticity to scattering process. It turns out that the model (1.25) has a very similar resonance structure as the one described in ϕ^4 theory when $-0.2 \lesssim r < 0$ [15].

Even though the scattering process in ϕ^4 theory is inelastic, the collision of a kink-antikink pair at low relative velocity has never seen to result to an immediate annihilation. This may be intuitive physically, the kinks in ϕ^4 theory retain some of the robustness of their sine-Gordon cousins [13]. In particular, it is not surprising that an intermediate bion state is formed in the above mentioned interval of bounce-windows, as an extremely slight variation of the relative velocity can eventually lead to a free kink-antikink pair instead of annihilation due to energy stored into the shape mode. Thus it is more than natural that any the bound state in this part of parameter space does not release its energy into radiation at once even when it does not dissolve into a free kink-antikink pair. Though there is no known breather solution in ϕ^4 theory (see [17]), one can continue looking for parallels between the two models and view the bion as an approximative breather (see e.g. [9]). One can seek some qualitative validation for this hypothesis by comparing the quartic potential (1.5) with the one defining sine-Gordon model (1.12) with appropriate rescaling. The Figure 1.1 shows clearly how they have fairly similar shapes in the region where kinks and the breather solution interpolate between the vacua. It has been also shown recently that the scattering process is in a way not entirely irreversible since collisions of the approximative breathers of ϕ^4 theory have created free kink-antikink pairs [18].

The bion state created by kink-antikink collision is then likely to become in this particular way initialised example of a one-dimensional oscillon, which will be defined and considered more extensively later on. There are some points one has to take into account though. One particular peculiarity of bions in contrast to oscillons have been reported in [16] where the simulations indicated erratic oscillations around the center of mass. In other words, based on the analysis of a time series (excluding the aftermath of the initial collision) it was argued that the bion-state oscillations are chaotic. This may be due to a residual of translational energy as such behaviour has not observed or reported when long-lived approximate breathers have been initialised with some ansätze. Another point to make is that while the energy stored in shape mode can explain bounce windows and the intermediate bion state, it is disputable how far the arguments based on its existence can be stretched. First, a long-lived

pseudo-breather can be obtained by initial data which is far away from the kink profile. More importantly, a shape mode can hardly explain the extreme longevity of small amplitude oscillations, where the kink-antikink structure is later on totally indistinguishable when the configuration at any time is far reaching the other minimum of the potential.

1.1.4 Quantum Effects

This thesis is about classical solutions in field theories, but here we briefly comment on quantum effects. The results given so far have been strictly at the classical level and quite general because all kind of rescalings of the coupling constant are classically allowed due to the invariance of Lagrangian. In the full quantum theory this is not true anymore, the relevant object there is not the Lagrangian, but $\mathscr{L}/\hbar$ where $\hbar$ is the Planck's constant. Now the coupling constant cannot be rescaled away, but it now usually enters any expression. All the previous results are modified, the energy of the kink, as well as its width and shape are all subject to quantum corrections. The classical limit is recovered at very weak coupling and perturbative analysis can be done using the coupling constant as the expansion parameter until this scheme breaks down. In the leading order the correction to the energy of a kink is only due to the interaction term, that is $\lambda\phi^4/4$ for Z_2 kinks, and it has been calculated in ϕ^4 theory and in the sine-Gordon model, the results can be found in [4] and [10], respectively. In both cases the quantum correction reduce the energy of the kink almost an equal amount as a function of the mass. The tendency for this correction to appear with a negative sign in one dimension is general and as can be seen based on variational arguments (see [9]). The energy of the kink in the sine-Gordon model to order β^2 can be found in [19].

After all said so far about the sine-Gordon model, it might not become as a surprise anymore that once again far more is known exactly about it also with respect to a quantised theory. It has been shown by Coleman [20] that the quantised sine-Gordon model does not have a well-defined ground state when $\beta^2 > 8\pi$. For smaller value of the coupling the sine-Gordon model is equivalent to a massive Thirring model provided that $g/\pi = 1 - 4\pi/\beta^2$, where g is the coupling constant of the Thirring model. This is

a very nontrivial duality, because the massive Thirring model is a canonical field theory describing fermions. In particular, when $\beta^2 = 4\pi$, $g = 0$ and the sine-Gordon model becomes the theory of a free Dirac field. The speciality regarding to this duality is that when the sine-Gordon model is strongly coupled (β is large), the massive Thirring model provides a description in the weak coupling limit (small g). Now the kink in the sine-Gordon model can be identified with a fermion of the massive Thirring model, there is a duality between solitons and particles.

We mention this result because it is interesting also from the point of view of the breather (1.22). The bound state of two fermions is also then a bound state of two kinks which is the breather. The energy states of the breather have been calculated in [10] and are given by

$$E_n = \frac{16\sqrt{\alpha}}{\bar{\beta}^2} \sin\left(\frac{n\bar{\beta}^2}{16}\right) , \tag{1.26}$$

where $\bar{\beta}^2 = \beta^2/(1 - \beta^2/8\pi)$ and $n = 1, 2, ... < 8\pi/\bar{\beta}^2$. Not surprisingly, quantisation yields a finite number of breather states. When the coupling increases these disappear by decaying into a free kink-antikink pair. The formula giving the energy of breather states is even more remarkable because it might be actually exact. All the breather states disappear at $\beta = 4\pi$ which is precisely when the interaction in the massive Thirring model switches from attractive to repulsive. Secondly, formula (1.26) gives the same result for the energy of a kink to order β^2 as the perturbative calculation [19].

Less can be said exactly about the kinks and their bound states in ϕ^4 theory at the quantum level though the theory is still renormalisable. Numerical studies have been conducted using different approaches and approximations. We communicate here results obtained in a study which considered kinks in the Hartree approximation [21]. The Hartree results for the energy of a kink are between the classical and semiclassical, leading order [4] values Another study [22] reported a similar observation as well as that the kink mean-field profile becomes broader than the classical one given in (1.6). The kink-antikink pair is far less stable than classically. The study [21] continued further examining kink-antikink scattering discussed earlier at the classical level. Though evidence was found for a critical ve-

locity v_c above which kink-antikink pair always reflect, this turns out to be far higher than the classical value $v_c = 0.26$ quoted before. Rather values around 0.76 (at $\lambda/m^2 = 1/12$) or 0.79 (at $\lambda/m^2 = 1/6$) were discovered. Even though the critical velocity naturally becomes coupling dependent and is not a universal quantity as in the classical theory, this does not explain the huge discrepancy. Quantum kinks are more likely to annihilate and produce radiation than their classical counterparts. While the study recovered that the kinks obey very similar behaviour in their final velocity above the critical speed, clear bion, or approximative breather, states were found only when the collision takes place at velocity very close to the critical speed. It was speculated that this observation can partially be due to the difficulty in recognising if a bound state has emerged in a strong radiative environment. It provides some, but very limited, consolation that on a qualitative level similar phenomena were observed as in classical kink-antikink scattering. This concludes the discussion of quantum effects and in the remainder we only return to it sporadically.

Returning for a moment to the static kink solutions, classical or quantised, they can be considered also in higher dimensions where they become domain walls. These are extended planar structures which have the kink profile in one direction. Obviously such domain walls are not finite energy solutions. There is an important non-existence theorem regarding lump solutions in higher dimensions.

1.2 Derrick's Theorem

The theorem by Derrick [23] states that there are no time-independent solutions of finite energy in flat space in more than one spatial dimension when there are only scalar fields in the Lagrangian of the form (1.2). This is due to the fact that energy functional of the static fields with respect to spatial rescaling is never zero when the fields are not in vacuum. This then implies that these field configurations cannot be stable solutions because their energy can be lowered indefinitely by shrinking them.

The energy functional in d spatial dimensions is

$$E[\phi] = \int \mathrm{d}^{\,d}\mathbf{x} \left(\frac{1}{2}(\nabla\phi)^2 + V(\phi) \right) = E_{\mathrm{grad}}[\phi] + E_{\mathrm{pot}}[\phi]\,, \tag{1.27}$$

where both E_{grad} and E_{pot} are positive. In spatial rescaling, $\mathbf{x} \to a\mathbf{x}$, where a is a positive constant there is one-parameter family of field configurations: $\phi_a(\mathbf{x}) = \phi(a\mathbf{x})$. For these the energy functional (1.27) yields

$$E[\phi_a] = a^{2-d}\, E_{\mathrm{grad}}[\phi] + a^{-d}\, E_{\mathrm{pot}}[\phi]\,. \tag{1.28}$$

In three or higher dimensions it is clear from (1.28) that $E[\phi_a] < E[\phi_{a=1}]$ for $a > 1$ and thus $\phi_{a=1}$ cannot be a solution extremising the energy. Looking for the stationary points more precisely by requiring that $a = 1$ is an extremum of (1.28) means that

$$-\frac{\mathrm{d}E}{\mathrm{d}a}\Big|_{a=1} = (d-2)\cdot E_{\mathrm{grad}} + d\cdot E_{\mathrm{pot}} = 0\,. \tag{1.29}$$

As already deduced in three or higher dimensions this immediately implies that both E_{grad} and E_{pot} must vanish permitting only trivial vacuum solutions. In two dimensions only E_{pot} must be zero, so Derrick's argument only excludes the potential term. The proof above can be easily generalised to include models consisting of any number of coupled scalar fields.

In a one-dimensional system Derrick's argument yields

$$E[\phi_a] = aE_{\mathrm{grad}} + \frac{1}{a}E_{\mathrm{pot}}\,. \tag{1.30}$$

The stationary point solved from (1.29) is $a = \sqrt{E_{\mathrm{pot}}/E_{\mathrm{grad}}}$. In particular, if one now requires that $\phi_{a=1}$ is the solution minimising energy, the contribution to the total energy is equally distributed between the gradient E_{grad} and potential energy E_{pot} parts. This holds for kinks in ϕ^4 theory and in the sine-Gordon model discussed earlier.

Derrick's argument seems very restrictive leaving only the trivial vacuum solutions in higher dimensions. There are, however, a number of ways to evade the theorem. First of all, the subtlety related to the potential term in two dimensions regarding Derrick's argument permits soliton solutions

in e.g. $O(3)$ sigma model in the plane [24, 25]. In higher dimensions one can include terms in the Lagrangian that involve either higher powers of derivatives of ϕ or higher order derivatives. Turning to gauge field theories changes the situation drastically because the field strength obeys a different scaling relation. Consequently, there are finite-energy solutions, like 't Hooft-Polyakov monopole [5, 26]. It should be repeated that in pure scalar theories Derrick's theorem forbids stable, finite energy solutions in two and higher dimensions. Naturally, the energy of an infinitely extending domain wall is divergent, but also, for instance, a global vortex on a plane, in spite of having a localised core, turns out to have so slowly decaying tails that its total energy is logarithmically diverging. Finally, and most importantly from the point of this study, Derrick's theorem does not say anything about time-dependent solutions of finite energy.

1.3 Q-balls

A standard example of non-topological solitons are so-called Q-balls. The term was proposed by Coleman [27], but earlier a similar construction was studied by Rosen [28] (see also [29, 30]). There exist variants, but the standard are Q-balls whose stability is protected by a global charge. Consider the Lagrangian for a complex scalar field in d space dimensions when the theory has a global U(1) symmetry

$$\mathscr{L} = \partial_\mu \phi \partial^\mu \phi^* - V(|\phi|^2)\,. \tag{1.31}$$

The conserved current here is

$$J^\mu(x) = i(\phi\,\partial^\mu \phi^* - \phi^*\,\partial^\mu \phi)\,, \tag{1.32}$$

and the conserved charge

$$Q = \int \mathrm{d}^d\mathbf{x} J^0\,. \tag{1.33}$$

One can now fix the charge Q and seek the lowest energy state by minimising

$$E_\omega = E + \omega(Q - \int \mathrm{d}^d\mathbf{x} J^0)\,, \tag{1.34}$$

where ω is a Lagrange multiplier and the energy E is given by the functional

$$E = \int \mathrm{d}^d\mathbf{x} \left[|\dot{\phi}|^2 + |\nabla\phi|^2 + V(|\phi|^2)\right]\,. \tag{1.35}$$

As we are not looking for a stationary solutions, the first term in (1.35) is the kinetic energy of the field ϕ, the only difference compared to (1.27). Re-organising terms in (1.34) the expression for E_ω can be written as

$$E_\omega = \int \mathrm{d}^d\mathbf{x} \left[|\dot{\phi} - i\omega\phi|^2 + \left(|\nabla\phi|^2 + V_\omega(|\phi|^2)\right)\right] + \omega\, Q\,, \tag{1.36}$$

where

$$V_\omega(\,\varphi^2) \equiv V(\varphi^2) - \omega^2\varphi^2\,. \tag{1.37}$$

Only the first term in (1.36) depends explicitly on time and, moreover, is positive definite. It should vanish at the minimum, i.e. $\dot{\phi} - i\omega\phi = 0$, so the field ϕ can be written as

$$\phi(\mathbf{x}, t) = e^{i\omega t}\,\varphi(\mathbf{x})\,. \tag{1.38}$$

Here φ can be chosen to be a real and positive valued function. The charge and energy of the configuration (1.38) are

$$Q = 2\omega \int \mathrm{d}^d\mathbf{x}\,\varphi^2 \tag{1.39}$$

$$E = \int \mathrm{d}^d\mathbf{x} \left[\omega^2\varphi^2 + (\nabla\varphi)^2 + V(\varphi^2)\right]\,. \tag{1.40}$$

The initial variational problem (1.34) can be now rewritten as

$$E_\omega = \int \mathrm{d}^d\mathbf{x}\left[(\nabla\varphi)^2 + V_\omega(\varphi^2)\right] + \omega\, Q\,. \tag{1.41}$$

Without loss of generality we can concentrate on positive values of the Q-ball frequency ω, i.e. $\omega > 0$ and consequently the charge $Q > 0$. One is interested in finding a localised solution that vanishes at infinity. One can furthermore assume that φ is spherically symmetric and monotonically decreasing. Under these assumptions the equation of motion for the field φ is

$$\frac{\mathrm{d}^2\varphi}{\mathrm{d}r^2} + \frac{(d-1)}{r}\frac{\mathrm{d}\varphi}{\mathrm{d}r} - \varphi\frac{\mathrm{d}V_\omega}{\mathrm{d}\varphi^2} = 0\,. \tag{1.42}$$

For the solutions φ regularity at origin demands $\mathrm{d}\varphi(0)/\mathrm{d}r = 0$, while the value $\varphi(0) = \varphi_0$ is to be determined by solving the equation. A localised, smooth solution must obviously fulfil $\varphi = 0$ and $\mathrm{d}\varphi/\mathrm{d}r = 0$ at $r \to \infty$ (the requirement for a finite energy in (1.40) may imply even more stringent conditions). Regarding the potential, a conventional choice is to require that the origin is the global minimum ($V'(0) = 0$) and choose $V(0) = 0$. The mass of the scalar field ϕ is given by

$$m^2 = \frac{\mathrm{d}V}{\mathrm{d}|\phi|^2}\Big|_{|\phi|=0}\,. \tag{1.43}$$

Q-balls were first considered by Coleman [27] assuming that the charge Q is large. The condition for the existence of such Q-balls is that $V(|\phi|^2)/|\phi|^2$ has a minimum that is not located at the origin and that the potential V grows more slowly than $m^2|\phi|^2$ over some range of ϕ (see Figure 1.5), i.e.

$$\min\left(\frac{V(|\phi|^2)}{|\phi|^2}\right) \equiv \frac{V(|\phi_{\min}|^2)}{|\phi_{\min}|^2} < m^2\,,\ \phi_{\min} \neq 0\,. \tag{1.44}$$

This condition will become more apparent later when a Q-ball profile given by a step-function will be considered. However, there is a mechanical analogy related to Eq. (1.42) which gives a qualitative understanding of the Q-balls solutions and will be discussed first. One can namely interpret

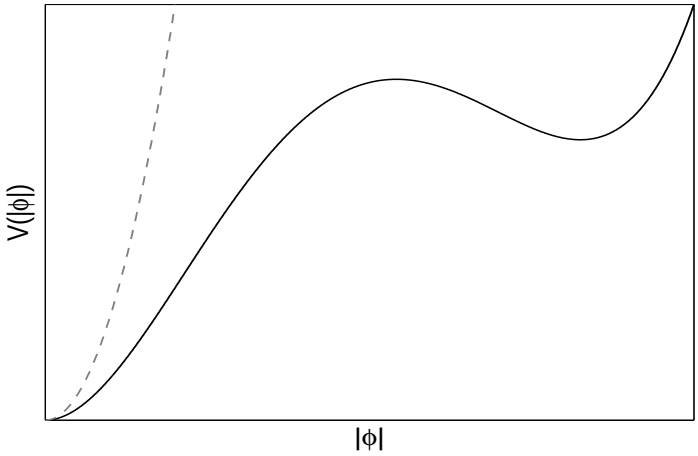

Figure 1.5. A generic potential V that allows Q-ball solutions. The dashed, grey curve shows the function $m^2\varphi^2$.

Eq. (1.42) as a Newtonian equation of motion for a particle moving under the influence of an inverted effective potential, $-\frac{1}{2}V_\omega$. In this picture, φ describes the position of the particle while the coordinate r plays the role of time (the same analogy can be recognised when considering the decay of the false vacuum, see e.g. the discussion in [31]). The above mentioned conditions for φ yield now that the point particle is released at rest and it just reaches the origin at infinite time and comes to a halt there. The second term in Eq. (1.42) is a velocity dependent friction which is also inversely proportional to time. That term is absent in one dimension ($d = 1$) and the energy of the particle is conserved. The main interest lies in the existence of Q-balls in higher dimensions ($d > 1$) and there the system is dissipative. When the particle is released at rest somewhere away from the origin, it must start higher up in the inverted potential in order to reach the origin (leaving aside the peculiarity in one dimension that the same level as the origin is sufficient there). On the other hand, if the particle starts far away and very high up the hill, the friction term decreases as time lapses and the particle will overshoot. Thus there is

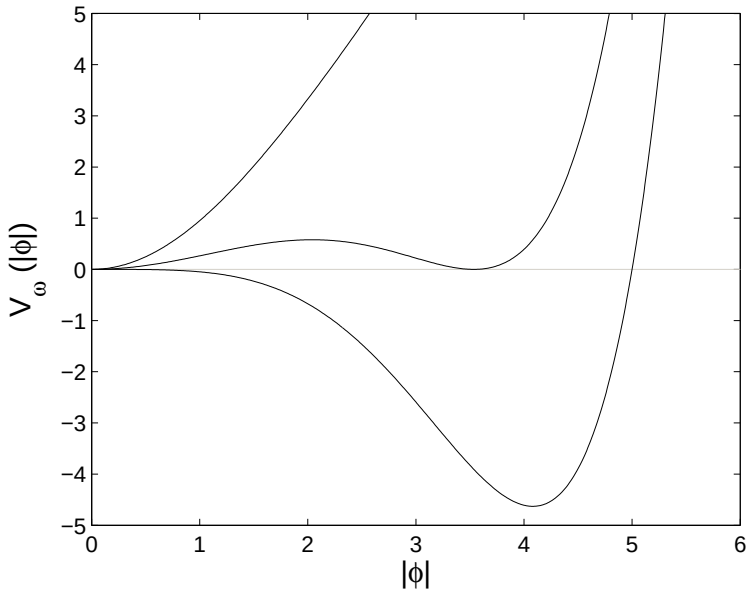

Figure 1.6. The effective potential $V_\omega(\varphi)$ for $\omega = 0$, $\omega = \omega_c$ and $\omega = m = 1$ (from top to bottom) for potential $V(\varphi) = \varphi^2 - A\varphi^4 + B\varphi^6$, where $A = 0.05$ and $B = 0.002$.

some value $\varphi_0 > 0$ that results in the particle arriving at the origin and stopping there.

This explains now the requirement (1.44) that the effective potential $V_\omega = V - \omega^2\varphi^2$ has a global minimum outside the origin, when $\omega < m$. This upper limit follows in the picture of the mechanical analogy from the requirement that the origin is a local maximum of the inverted effective potential so that the particle can stop there. Alternatively, it guarantees that φ vanishes at infinity. There is also a minimum value ω_c for which the effective potential just reaches zero somewhere outside the origin, see Figure 1.6. Hence, there exist Q-ball solutions in the range

$$\omega_c < \omega < m\,. \tag{1.45}$$

Consider then a Q-ball configuration with a fixed charge Q. The con-

figuration is stable with respect to decay to free scalar quanta if the energy of the Q-ball E_Q is less than the energy mQ of free scalars with an equal total charge

$$E_Q < mQ\,. \tag{1.46}$$

Then the Q-ball is the ground state of the theory. Solving the profile of a Q-ball from Eq. (1.42) is generally a numerical problem though few analytical approaches have been made (see [32, 33]). Thin and thick wall approximations give more insight into Q-ball solutions.

1.3.1 Thin and Thick Wall Approximations

In the thin wall approximation one assumes that the surface terms can be neglected and the field φ is given by the step-function, $\varphi = \varphi_0\,\theta(R_0 - r)$. This approximation is reasonable when the charge of the Q-ball is large. For this profile the charge and energy are easily computed

$$Q = 2\omega\varphi_0^2\,V_d \tag{1.47}$$

$$E = \left(\omega^2\varphi_0^2 + V(\varphi_0^2)\right)\,V_d\,, \tag{1.48}$$

where V_d is the volume of a sphere with radius R_0 in d dimensions and the gradient energy has been omitted. One can use the charge to express the energy

$$E = \frac{Q^2}{4\varphi_0^2 V_d} + V(\varphi_0^2)V_d\,. \tag{1.49}$$

For a fixed charge this has the minimum at $V_d = Q/(2\varphi_0(V(\varphi_0^2)^{1/2})$. When inserting this back to (1.49) one finds the virialisation in the thin wall approximation, both kinetic and potential terms have equal contribution to the total energy of the Q-ball. Naturally, this is an idealisation excluding the gradient energy. In this simplest thin wall approximation the energy of the Q-ball grows linearly with the charge as the energy-charge ratio is

given by

$$\frac{E}{Q} = \sqrt{\frac{V(\varphi_0^2)}{\varphi_0^2}}\,. \tag{1.50}$$

One can improve this result and calculate the contribution from the surface energy and see that the stability condition (1.46) is fulfilled. For this consider again the mechanical analogy. A field profile which stays constant for a large range of radii r means an unchanged value of the position φ for a long period of time. This can be arranged if the particle starts very close to the top of the hill of the inverted effective potential, i.e. almost at the minimum of the effective potential V_ω. On the other hand recall that the friction term in Eq. (1.42) will become negligible in the course of time. In order to prevent overshooting, the starting point must be then roughly at the same level as the origin. Thus the thin wall Q-ball can be approximated to be configuration with $\omega = \omega_c$ and the minimum of V_ω at φ_0. One can approximate further that the minimum of $V_\omega(\varphi^2)/\varphi^2$ is at φ_0 as well. By definition this is also the minimum of $V(\varphi^2)/\varphi^2$. Then

$$\frac{V(\varphi_0^2)}{\varphi_0^2} \approx \min\left(\frac{V(\varphi^2)}{\varphi^2}\right) < m^2\,, \tag{1.51}$$

where the inequality follows from the requirement (1.44). Inserting this to (1.50) yields $E < mQ$. This demonstrates that the condition (1.44) guarantees the stability of Q-balls as minimum energy configurations in the thin wall approximation. Coleman has shown further in this approximation that Q-balls which are stable with charge Q are stable for any charge $Q' > Q$ [27]. In the leading order the energy of a Q-ball is $E \simeq \omega_c\, Q$. One can improve this and take into account the contribution from the surface term that has been neglected so far. Because the friction term in the particle picture is irrelevant, one can integrate the simplified equation of motion (1.42) and insert that into (1.40) which results in a dimension-dependent correction.

One could now think that Q-balls exist only with a large value of the charge Q. This is not the case, even though the thin wall approximation breaks down as φ_0 increases for a fixed charge. There is namely another

limit one can consider and this approach is known as the thick wall approximation and applies to Q-balls with a small charge. It was first proposed in [34] for a generic quartic potential and later studied in a wider class of potentials in [35]. Instead of releasing the particle from the top of the inverted effective potential, look at the situation where ω is relatively large and φ_0 is far from being the minimum of $V_\omega(\varphi^2)$. Then φ_0 is close to the origin which suggests approximating the potential only with the lowest order terms. This was done in [34] by keeping only quadratic and cubic terms. One can study the variational problem with the reduced potential and show that there exist stable Q-balls with relatively small charge and with a boundary which is not localised in a narrow region. The consistency of the thick wall approximation sets constraints on the maximum charge for a Q-ball (note that in the case of a local gauge symmetry the charge of a stable Q-ball is in any case bounded from above [36]). This is natural, as the limit considers a Q-ball with a small charge and when the extra conditions are violated, the thin wall approximation may be applicable instead. However, it should be stressed that the condition (1.44) is no longer sufficient to guarantee the existence of Q-balls in the thick wall approximation and not all such potentials permit Q-ball solutions with thick walls, but the validity of (1.46) still guarantees the stability of a Q-ball.

While thin and thick wall approximations permit some analytical considerations of energy and charge, strictly speaking the precise determination of Q-ball stability and profile $\varphi(r)$ is rather a numerical challenge to be carried out for every potential specifically. Generally, the focus has not been on potentials permitting an analytic treatment, but rather on potentials inspired by particle physics phenomenology. Something about the form of the profile can be said though. It was shown in [37] that a Gaussian ansatz

$$\varphi(r) = \varphi(0)\, \exp(-r^2/r_0^2)\,, \tag{1.52}$$

is a physically reasonable approximation to the profile of thick wall Q-ball in the case considered. In another study [38] a better fit was provided by a kink-like hyperbolic tangent which can obviously approach the thin wall solutions more successfully. From the discussion regarding thin and

thick wall approximations one can notice that generally the charge of a Q-ball decreases with an increasing frequency ω. For the potentials considered in [35] it was shown that the charge of Q-ball in the thick wall approximation vanishes in the $\omega \to m$ limit (see also [39]).

Finally, quantum effects on Q-balls have been studied in [40] where it was shown that one-loop corrections can destabilise small Q-balls while large enough charge Q will guarantee a negative binding energy. For typical parameter values of the generic quartic potential considered, charge $Q \approx 7$ is sufficient to overcome the corrections and yield a negative binding energy.

1.3.2 Q-ball Interactions

Examining the dynamics of Q-balls is naturally restricted to numerical approaches as already the profiles cannot usually be determined analytically. Collisions of Q-balls have been studied e.g. in [38, 41–43]. Obviously, the interaction and the final state after the scattering depends on the chosen potential V, which in [41] was a general cubic potential of φ^2 (as shown in Figure 1.6), while in [38] and [42] the focus was strongly on specific supersymmetric scenarios and potentials involving logarithmic terms arising in gravity and gauge mediated supersymmetry breaking, respectively. Most studies have been carried out for two-dimensional Q-balls, but in [41] an investigation was done also in one and three dimensions. This study identified the key variables to be the relative phase, charge and incident velocity. The ansatz introduced in [41]

$$\phi = e^{i(\omega_1 t+\psi)}\,\varphi_{\omega_1}(|x-\ell|) + e^{i\omega_2 t}\,\varphi_{\omega_2}(|x+\ell|)\,, \tag{1.53}$$

describes two Q-balls separated by a distance 2ℓ in one dimension and can be generalised to higher dimensions. The subscript in the profile function stands for the corresponding frequency. While studying an isolated Q-ball with global symmetry the phase can be omitted, but the relative phase ψ, becomes an important parameter when considering two interacting Q-balls. In [38] the impact parameter, the alignment between the centers of the Q-balls with respect the direction of their velocity, was also varied. It was noted that it does not play such a defining role as the relative phase

until, of course, it becomes large enough to prevent the interaction.

Discussing now the phenomenology occurring in collisions at the qualitative level the interaction can result in coalescence, charge transfer or elastic scattering. Concentrating first on the effect of the relative phase, two Q-balls with equal charges ($\omega_1 = \omega_2$) attract if $\psi = 0$ and coalesce to form a larger Q-ball though some charge is lost in the process into small lumps or radiation. If the Q-balls are exactly out of phase $\psi = \pi$ the force between them is repulsive and, starting at rest, they drift apart unchanged. When the relative phase differs from these extreme values there is charge transfer between the Q-balls in such a way that the total charge in the Q-balls is conserved. After the charge exchange the Q-balls usually tend to repel. In [41] it was reported that in two dimensions the Q-balls often emerge at right angles to the initial direction of approach after the transfer process. Interpreting coalescence, often called also fusion, as an ultimate example of charge exchange it is quite natural that the amount of charge transfer decreases with increasing phase difference ψ and after some point the Q-balls start to scatter almost elastically. A peculiarity related to charge exchange is that the Q-ball which has lost charge may be accelerated during the process to far higher velocity than the initial one, up to a factor of ten reported in [42] though only relatively low initial velocities were considered in that study. At high initial velocities Q-balls pass through each other though charge is lost via radiation and velocities are reduced [41]. Finally, there is generally charge transfer in the scattering process of two Q-balls with unequal charges, $\omega_1 \neq \omega_2$. There is not much analytic understanding about Q-ball collisions. For instance, in a collision between a Q-ball and an anti-Q-ball, $\omega_1 = -\omega_2$, one would expect an annihilation as a likely outcome. Instead, they bounce back or pass through each other [41]. This indicates that the Q-balls can transfer their charge only very slowly.

A collision and the charge transfer can create an excited intermediate state where the Q-ball has excess energy compared to one with an equal charge. This may also occur if the Q-ball undergoes some other disturbance. Relaxation of excited Q-balls was considered in [44] with (2+1)-dimensional simulations. The numerical study monitored how the excess energy was radiated from the Q-ball in two-dimensional simulations. The

study concluded an exponential decrease in time, but the process is not rapid, relaxation proceeds slowly compared to the natural timescale of the fields, m^{-1}, the suppression factor being of the order 10^{-2}. Furthermore, Q-balls were deduced to be very robust objects retaining most of their charge during the relaxation process even when the initial excess energy clearly exceeds the energy of an unexcited Q-ball. In another study [45] the relaxation process was not seen to complete. The evolution of a three-dimensional lump was studied numerically assuming spherical symmetry. The lump emits charge until it reaches a quasi-equilibrium state, called Q-axiton according to the axion-breather studied earlier in [46]. A Q-axiton has far more energy than the corresponding Q-ball solution, in other words, $E \gg mQ$. It is a pulsating configuration with only a slight modulation in the amplitude (a Q-ball performing a breather-like motion after a disturbance was also reported in [41] and after a collision in [43] in one dimensional simulations). The authors assumed that Q-axitons evolve eventually to lower energy Q-balls of the same charge, but did not exclude the possibility that the state might be very long-lived. The meta-stability of an excited, pulsating, charge-poor Q-ball can hardly be attributed to any other mechanism than the one that makes oscillons so long-lived.

1.4 Oscillons

Let us return to the Lagrangian of a single real scalar field given in (1.2) but in an arbitrary space dimension. Before, in the case of kinks, the boundary conditions at infinity for the soliton state (kink or antikink) are different from that of a vacuum state, implying degenerate vacuum structure in the theory. When the field ϕ is asymptotically in the same vacuum there is no topological reason that would protect the field configuration from deforming into a trivial vacuum state as already mentioned in the case of the breather in sine-Gordon model. Nor is there any other obvious conserved quantity, like the global charge discussed in case of Q-balls. Thus there is nothing preventing a lump, a localised concentration of energy, from spreading and dissipating its energy. Still there exist extremely long-lived, oscillating energy concentrations that remain localised. These are oscillons. The term appeared for the first time in [47] where a sim-

ilar phenomenon was described in plasma physics (some non-relativistic applications will be discussed later on).

Oscillons are localised, non-singular, time-dependent finite energy solutions of nonlinear field theories. The oscillon performs anharmonic oscillations of the field amplitude about the global vacuum. It is characterised by a nearly constant radius and energy and the timescale of changes in these quantities are many orders of magnitude larger than the oscillation rate.

In some ways oscillons are like Q-balls without a charge [48]. They both are non-topological objects with oscillatory time dependence. However, unlike standard Q-balls with a global charge that have only a minimum size and can be arbitrarily large, all the observations suggest that oscillons have a preferred size, which is roughly a few in units of the inverse mass of the theory. The tails of the oscillon profile are often reported to decay exponentially as a function of the radial distance, $\exp(-\text{const.}\, m\, r)$, where m is the mass of the scalar field excitations. There are no known examples of long-lived, localised oscillations in massless scalar theories.

There is a well-defined energy related to any frequency. This is clear if one considers oscillons as approximative breather solutions. There is a one-to-one correspondence between the frequency of the breather (1.22) and its energy (1.23) as the bound state of kink and antikink. However, one should notice that for oscillons above space dimension $d = 1$, there is no obvious topological counterpart, like the kink for a breather (and we have seen that the one-dimensional sine-Gordon model is a very special system in every respect). Oscillons are not restricted to theories which have other soliton solutions. An example are oscillons in the one-dimensional model considered in [49] (see the second chapter where the formation of oscillons has been discussed). The potential (2.8 has a single minimum and thus the theory contains no nontrivial static solutions.

While the stability of Q-balls is guaranteed by a conserved charge, an oscillon owes its longevity to an unknown mechanism where the dynamical interplay between gradient pressure is balanced by attractive self-interaction of a real scalar field. The oscillation frequency is without any observed exception close to the mass of the scalar, i.e. very near the threshold for propagating modes. Assume that the oscillations have a

small amplitude ϵ: the gradient terms are then of the order ϵ^2 and balanced by quadratic non-linear terms in the equation of motion. Then the small-amplitude analysis (see e.g. [10, 49]) implies a linear dispersion relation $\omega = m\sqrt{1-\epsilon^2}$. However, oscillons appear also with relatively large amplitudes. Finishing the parallel between Q-balls and oscillons, it is intriguing that the frequency of Q-balls in the thick wall approximation, which clearly corresponds better to Gaussian shaped oscillons than the thin wall limit, approaches the mass of the field when the charge goes to zero.

We now turn to consider oscillons in three dimensions.

1.4.1 Oscillons in Three Dimensions

The discovery of longevity of certain oscillating energy concentrations goes back to the work by Bogolyubsky and Makhankov in 1976 presented in [50] and subsequently in [51], where the word pulson was introduced to describe the phenomenon. They studied ϕ^4 theory and the double-well potential (1.5) in three dimensions assuming a spherically symmetric geometry. In the study [50] a spherical bubble of different radii r_0 was initialised using the static domain wall form (1.6)

$$\phi(r) = \eta \tanh\left(\sqrt{\frac{\lambda}{2}}\eta\,(r - r_0)\right), \tag{1.54}$$

where the initial radius r_0 was set to be larger than the natural length scale in the model, $r_0 \gg (\sqrt{2\lambda}\eta)^{-1} = m^{-1}$. When the field equation was evolved numerically, it was discovered that the bubble evolution depends to a large extent on the radius r_0 and in a favourable case the bubble can live a number of oscillation periods. This observation has to be seen in contrast to a free, massive scalar field described by the Klein-Gordon equation. In that case an excitation decays quickly having a life-time of the order $5m^{-1}$. A similar kind of numerical examination was also carried out in the sine-Gordon model. In the second publication [51] different initial data was used taken this time to be the breather (1.22). The findings included a modulation of the oscillation amplitude as well as a minimum size of the amplitude, below which no oscillations take place.

The re-discovery as well as the introduction of the term oscillon in this context, was done by M. Gleiser in [52]. Rather than referring to pulsating their energy away, the term oscillon emphasises the remarkable persistence of these field configurations. The background of the study was the activity at the time in understanding the dynamics of phase transitions. The study in ϕ^4 theory included, not only the symmetric double well potential (1.5), but also an asymmetric one given by

$$V_{\rm A}(\phi) = \frac{m^2}{2}\phi^2 - \frac{\kappa}{3}\phi^3 + \frac{\lambda}{4}\phi^4\,. \tag{1.55}$$

By choosing the value of parameter κ appropriately the potential has two non-degenerate minima and then $V_{\rm A}$ becomes relevant in modelling a first order phase transition. Here also a study was carried out assuming spherical symmetry. In addition to an initial bubble profile taken to be that of a hyperbolic tangent (1.54), Gaussian initial conditions were used as well. While any bubbles in the symmetric double well potential cannot gain energy in going from one vacuum to another, there are so called critical bubbles in the potential (1.55) whose energy corresponds to the barrier for vacuum decay. The interest was how smaller, sub-critical bubbles behave. The study revealed that both asymmetric and symmetric double well potentials support oscillons and the life-time was now determined to be in the range $10^3 - 10^4$ in units of the inverse mass for both (1.5) and (1.55). There is a minimum energy of the initial bubble to evolve into a long-lived oscillon corresponding to a minimum size r_0. Smaller bubbles lose energy exponentially fast and disappear.

In addition a stability analysis with respect to radial perturbations was conducted. The standard technique is to expand a perturbation $\delta\phi(r,t)$ in normal modes, $\delta\phi(r,t) = {\rm Re}\sum \phi_n(r)\exp(i\omega_n t)$. The oscillon solution, $\bar{\phi}_0(r,t)$, satisfies the equation of motion, which for a scalar field ϕ in three dimensions assuming spherical symmetry reads,

$$\frac{\partial^2\phi}{\partial t^2} - \frac{\partial^2\phi}{\partial r^2} - \frac{2}{r}\frac{\partial\phi}{\partial r} + \frac{\partial V}{\partial\phi} = 0\,. \tag{1.56}$$

The amplitudes ϕ_n satisfy the radial Schrödinger equation

$$-\frac{\mathrm{d}^2\phi_n}{\mathrm{d}r^2} - \frac{2}{r}\frac{\mathrm{d}\phi_n}{\mathrm{d}r} + \bar{V}(r,t)\phi_n = \lambda_n\phi_n\,, \tag{1.57}$$

where the potential $\bar{V}(r,t) = 3(\bar{\phi}_0(r,t))^2 - 3$ and $\lambda_n = \omega_n^2 - 2$. The perturbations $\delta\phi$ do not grow, as long as the lowest frequency ω_0^2 is positive, i.e. $\lambda_0 > -2$. Because the potential $\bar{V}$ is time-dependent, only a numerical approach to solving the Eq. (1.57) is feasible. Such a study suggests that oscillon states at any time during the period are stable against radial perturbations [52].

A far more detailed examination was then carried out in [53]. On the numerical side the study continued with spherically symmetric bubbles that were initialised using a Gaussian profile or the domain wall profile given by (1.54). A dynamically increasing simulation lattice was utilised for an extensive study of the effects of initial size r_0 and amplitude of the bubble. It should be noted that oscillons turn out to live longer in the asymmetric potential (1.55) than in the symmetric double well potential (1.5). That is easy to understand in a non-degenerate case where oscillons become closer to critical bubbles which explains their increased longevity. Even when the potential (1.55) has two degenerate minima, it is shallower and narrower than (1.5) which softens the gradient energy of initial bubbles enhancing the lifetime. The numerical part of the study confirmed the results of [52]. More importantly several analytic approaches were made to explain observed properties of oscillons and will be discussed now.

The bubbles that have an initial radius smaller than some critical one do not evolve to long lasting oscillons. It was argued that this critical radius can be understood in a particle picture where the only degree of freedom is the amplitude of the deviation from the vacuum when ones fixes the value of the radius r_0. The study of a perturbation in linear order yields an evolution equation and the eigenvalue is a function of the amplitude and size r_0. One seeks now unstable fluctuations that bring the perturbation away from the vacuum interpreting these to permit oscillon configurations. Demanding that the eigenvalue is negative leads to a minimum size for the oscillon. This approach in zero-dimensional field

theory obviously neglects completely the contribution of the gradient energy which is a severe limitation. Though gradient energy turns out to be always subdominant for an oscillon, this rather indicates that long-lived configurations are, in some sense, smooth ones. In three dimensions, gradients in the absence of any stabilising conserved current and charge will inevitably bring a tendency for spreading of any energy concentration. An attractive potential for the self-interaction of the scalar field is necessary to act against this tendency. It is natural that oscillon configurations thus have very subdominant contribution from gradient energy. The smaller the oscillon configuration becomes, the larger gradients grow while the volume of attractive potential energy is decreasing. Heuristically it is easy to deduce that therefore there must be some lower critical radius below which the oscillon becomes unstable.

A similar kind of eigenvalue analysis can be employed for understanding the values of the amplitude for deviation from the vacuum that result a long lasting oscillations. For a range of amplitudes the eigenvalue is negative suggesting the possibility of oscillon solutions. The minimum value of the amplitude is simple to understand. In a linear theory oscillations are damped and energy leaks quickly from the envelope. Thus the amplitude must be large enough in order to the field to probe the non-linear regime of the potential. Huge deviations from the vacuum in turn result in too violent dynamics and spreading of energy. The final collapse of an oscillon can also be interpreted from the point of view of the minimum size for an amplitude. During the evolution the oscillon radiates energy and consequently its amplitude decreases. Once the amplitude falls below a critical value, the field evolution enters the linear regime. The oscillon loses its energy quickly and collapses. This is illustrated in the phase-space picture, Figure 1.7 showing the final spiralling that starts once the amplitude (at $\dot{\phi} = 0$) falls below a certain threshold value. Before decay, during the oscillon stage, the motion is restricted to a fairly narrow band in the phase-space.

Though no direct analytical result for the life-time of oscillons was obtained, the study pointed out an interesting connection between virialisation and the long-lived oscillon states. The virial theorem can be evaluated by starting from the equation of motion (1.56). Multiplying by $4\pi r^2\phi$ and

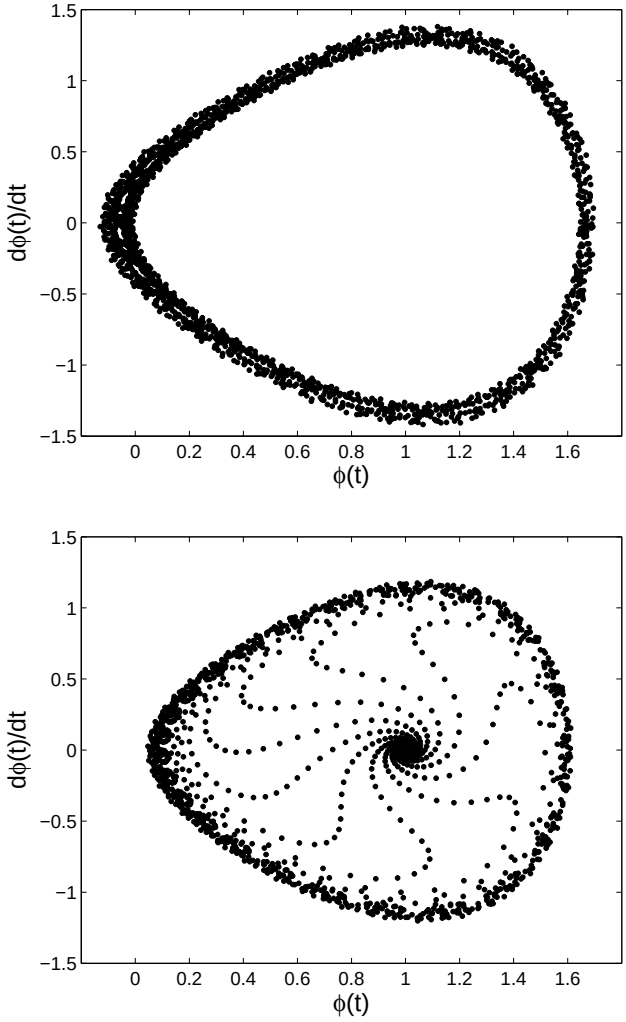

Figure 1.7. Phase-space portrait depicting oscillon evolution at the centre $r = 0$ in two time intervals of length 2000, in both the sampling occurred every $\Delta t = 1.0$. The upper panel shows evolution of during the oscillon stage in an interval starting at time $t = 2000$. The motion follows an egg-shaped orbit, the asymmetry is a natural consequence of the potential (1.5), which is steeper in the direction of increasing field ϕ (see Figure 1.1). The lower panel shows the evolution starting at time $t = 6000$. The spiralling indicates the collapse of the oscillon, which occurred around the middle of the interval. The oscillon was initialised by setting $r_0 = 3.0$ and amplitude $A = 1$. Partial reproduction of a figure presented in [53].

integrating over the radial variable r, using integration by parts, yields

$$4\pi \int_0^\infty \mathrm{d}r\, r^2\, \phi\, \ddot{\phi} + 4\pi \int_0^\infty \mathrm{d}r\, r^2\, (\phi')^2 + 4\pi \int_0^\infty \mathrm{d}r\, r^2\, \phi\, \frac{\partial V}{\partial \phi} = 0. \quad (1.58)$$

The second term in (1.58) is twice the total gradient energy. Assuming that the oscillon can be considered a periodic configuration and integrating over this period $\bar{T}$ and applying again integration by parts to the first term in (1.58) one arrives at

$$-\frac{1}{\bar{T}} \int_{\bar{T}} \mathrm{d}t\, 4\pi \int_0^\infty \mathrm{d}r\, r^2\, \dot{\phi}^2 + 2\,\langle E_{\mathrm{grad}} \rangle + 4\pi \left\langle \int_0^\infty \mathrm{d}r\, r^2\, \phi\, \frac{\partial V}{\partial \phi} \right\rangle , \quad (1.59)$$

where brackets indicate average over one period. The first term in (1.59) can be now identified as twice the (averaged) kinetic energy. The virial theorem reads

$$\langle E_{\mathrm{kin}} \rangle = \langle E_{\mathrm{grad}} \rangle + 2\pi \left\langle \int_0^\infty \mathrm{d}r\, r^2\, \phi\, \frac{\partial V}{\partial \phi} \right\rangle , \quad (1.60)$$

It was noticed in [53] that the longer the oscillons live, the better they fulfil the condition (1.60). This provided evidence for the existence of attractor field configurations which minimise the departure from virialisation.

Furthermore, it is illustrative to compare the virial theorem (1.60) to the maximum values of the energy. Over half of the period, the energy of an oscillon varies over between kinetic energy and potential and gradient energy and back. To a great precision the maximum kinetic energy equals the sum of the maximum potential and gradient energy, thus

$$\max\{E_{\mathrm{kin}}\} \simeq \max\{E_{\mathrm{grad}}\} + \max\{E_{\mathrm{pot}}\}\,. \quad (1.61)$$

This is natural as, at the moment of maximum excursion, the oscillon configuration does not have have any kinetic energy, very much like a pendulum at the highest point during the swing. When the oscillon configuration goes through the vacuum value, it is to a good extent flat especially for potentials that are symmetric around the minimum. Thus at that moment all the energy is in kinetic form. See the profiles in Figure 3.1.

In [54] a very detailed investigation was carried out to study the life-

time of oscillons as a function of the initial radius. The study continued to work with the symmetric double well potential in three-dimensional theory assuming spherical geometry using Gaussian initial profiles that had been shown to result in longer lifetimes in [53] compared to the domain wall profiles (1.54). The authors used a novel numerical technique which was not based on straightforward dynamically increasing lattice, but a method that blueshifts the outgoing radiation. In the monotonically increasing boosted coordinates most of the radiation is frozen in a transition layer and only a very little amount of energy is reflected back into the interior. This computationally efficient method permitted a very thorough scan of the parameter space and resulted in the discovery of the resonance structure of oscillon lifetime shown in Figure 1.8. There exist over a hundred resonances which rise above the overall lifetime profile. The resonances are well-fitted by assuming that the lifetime behaves as $\gamma^\star \ln|r - r_0^\star|$, where $\gamma^\star$ is a resonance-dependent exponent and $r_0^\star$ the precise resonant value. The authors draw a parallel to a similar type of behaviour describing gravitational collapse. Though the scaling suggests that by fine-tuning the initial radius r to resonance, the lifetime could become arbitrary long, no oscillons were observed to survive over 10^4 time units. The fine-tuning was later repeated with an increased precision in [55] resulting in the increase by a factor of two in the maximum lifetime.

Furthermode, also a bounce window to long living oscillons was discovered. Originally it was found in [53] that only initial bubbles with radii in the range $2.4 < r_0 < 4.5$ can evolve to an oscillon. The study [54] noticed that initial radii larger than $r_0 > 5$ can also result in the formation of long-lived oscillons. These oscillons do not continue to evolve with this initial large radius, but radiate strongly. However, the collapse does not always result in an immediate decay, but in the formation of a long-living state of a smaller size in the window $2.4 < r_0 < 4.5$. Though outside the axis in Figure 1.8, a very similar kind of resonances were found up to a radius $r_0 = 9$. The authors compared this with the fractal nature in kink-antikink scattering in ϕ^4 theory [16] discussed earlier, thus the name bounce window.

The virtue of the Gaussian shape to match the oscillon profile has been also used as a starting point for analytic considerations in three di-

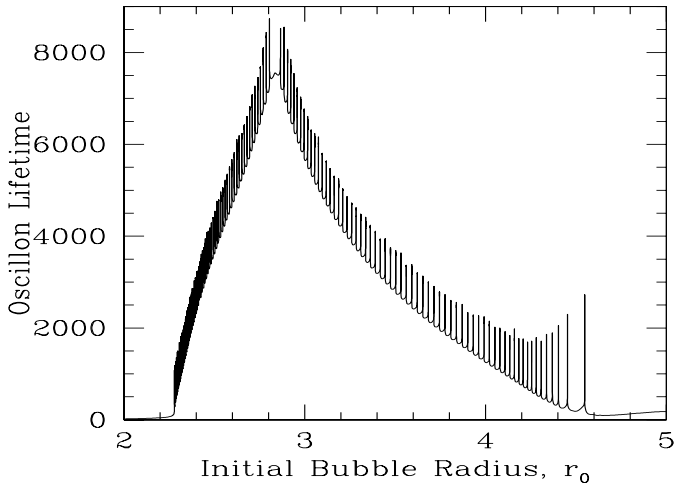

Figure 1.8. The resonance structure of the oscillon lifetime as a function of the initial radius r_0 from [54]. The minimum radius around $r_0 \simeq 2.3$ agrees well with the one reported in [53].

mensions [56]. The approach was already presented in [57]. The idea is to substitute a spherically symmetric Gaussian ansatz with a fixed radius and a time-dependent amplitude into the Lagrangian. After carrying out the integration over the spatial variable one is left with an effective Lagrangian as a function of the amplitude and its time derivative as well as the radius. From this one can derive an equation for the amplitude. In [57] the focus was on oscillons in higher dimensions, namely depending on the form of the potential the procedure yields inequalities which constrain the radius of the oscillon to be above a dimension-dependent minimum value. Depending on the form of the potential the approach may yield also an upper critical dimension above which long-lived oscillons cease to exist. In the case of the quartic potential (1.5) this was found to be six. While this method does not include the energy losses due to radiation due to the integration over space, this issue was addressed in [56] by estimating the amount of energy flow from the oscillon core assuming a constant oscillation frequency. This predicts the lifetime of an oscillon in three dimensions and the obtained

value agrees fairly well with the mean lifetime in Figure 1.8. However, it is not clear how well this approximation generally captures the evolution of the emitted radiation because it can be very sensitive to the oscillation frequency.

1.4.2 Quasi-breathers in ϕ^4 Theory

In what has been discussed so far oscillons have been seen to emerge from relatively generic initial profiles. Though oscillons are long-lived objects they are certainly not stable in the strictest sense because they emit radiation and thus there is always some energy loss. This also implies then a decrease in the oscillation amplitude and a change in the frequency. Therefore oscillons are not strictly periodic solutions to the equation of motion.

The alternative is to look directly for periodic solutions for the equation of motion, like that given by (1.56) in three dimensions. This approach was first taken in [58] and it has been since repeated in [54] and [59] culminating in work presented in [55] and [60]. Adopting the term suggested in [55], these solutions will be called quasi-breathers.

Originally Watkins [58] looked for frequency as a converging series around the mass m in the theory, motivated by similar kind of treatment of an anharmonic oscillator. This lead to an introduction of the following radial, periodic trial solution for the field

$$\phi(r,t) = \sum_{n=0}^{\infty} f_n(r)\cos(n\omega t)\,, \tag{1.62}$$

where the spatial dependence of each mode is encoded in the function f_n. Because in practice the frequency is close to the mass, $\omega \approx m$, the higher terms $n > 1$ correspond to radiation modes. One can truncate the series at some n and insert (1.62) in the equation of motion. Equalling the terms $\cos(n\omega t)$ leads to a set of $(n+1)$ coupled nonlinear ordinary differential equations. Alternatively, one can plug the trial series into the action and integrate over the period $\bar{T} = 2\pi/\omega$ as has been done in [59]. The differential equations can be solved numerically for a given frequency ω by standard techniques. A relaxation method was used in [58] while in [54]

and [59] the shooting method has been used where the values $f_n(0)$ are the shooting parameters and regularity demands that $\mathrm{d}f_n(0)/\mathrm{d}r = 0$. It turns out that the series (1.62) converges quickly and only a few terms $f_n(r)$ in the beginning are large near the origin and then decrease when r increases. The procedure gives thus numerically a field configuration oscillating with frequency ω.

Furthermore, by inserting the solutions at various frequencies in the energy functional one can obtain the energy density as a function of frequency which furthermore can be turned to the energy inside some sphere corresponding to the energy located in the core. Already in [58] it was noticed that there is a minimum value at the frequency $\omega_c < m$. This lead Watkins to suggest an interpretation of the final decay of an oscillon. Once the frequency of an oscillon reaches this critical frequency, there is no oscillon state with lower energy and thus any extra loss of energy must result in a dispersive state instead and cause the decay of the oscillon. The lifetime of oscillons was not determined in the study because the radiation rates were arbitrary small. While the study [58] considered only three-dimensional ϕ^4 theory, investigation has been carried out for a range of dimensions, $2 < d < 6$ in [59].

Though the ansatz (1.62) provides a methodical way to obtain oscillating solutions with a given frequency, there is a peculiarity related to them which was already noticed in [58], but, for instance, overlooked in [54] and explains the term quasi-breather. This can be already seen by considering the equation of motion in three dimensions (1.56) at large radius r. Asymptotically the field ϕ is close to vacuum (in many of the studies the potential has been chosen so that $\phi = 0$ is the minimum, but for the potential (1.5) consider a small perturbation around the vacuum η, $\phi \to \eta + \phi$). The field equation can be approximated in the linear theory by the Klein-Gordon equation (see e.g. [59])

$$\frac{\partial^2\phi}{\partial t^2} - \frac{\partial^2\phi}{\partial r^2} - \frac{2}{r}\frac{\partial\phi}{\partial r} + m^2\phi = 0\,. \tag{1.63}$$

This has the asymptotic solution

$$\phi(r,t) = A\,\frac{\cos(kr - \Omega t + \psi)}{r}\,, \tag{1.64}$$

where $k^2 = \Omega^2 - m^2$ and ψ is a phase. The decay of a solution (1.64) for the field ϕ is not sufficiently fast to yield a finite energy when integrated over the volume. Solutions of the form (1.64) are in this respect only weakly localised. They represent a standing wave which is a superposition of an outgoing spherical wave and an ingoing wave. The ingoing radiation has the stabilising effect that permits the existence of the strictly time-periodic solution.

A thorough and rigorous investigation of the complete system of differential equations that results from the introduction of ansatz (1.62) in three dimensions was carried out in [55]. Only for modes with $n^2\omega^2 < m^2$ there are exponentially fast decaying solutions for $f_n(r)$. However, there are always modes (in practice modes $n \geq 2$) for which $n^2\omega^2 > m^2$ and these behave asymptotically as (1.64) with a long tail. It is not possible to suppress all these slowly decaying oscillatory modes [55]. Consequently, the energy of the solution (1.62) inside a sphere of large enough radius R is proportional to R, while these solutions of infinite energy exist for all frequencies $\omega < m$.

At best one can look for solutions which minimise the oscillatory tail, but numerical search reported in [55] did not show any evidence for the tendency of this tail to vanish at any frequency. The solution of the form (1.62) with a minimal oscillatory tail is the quasi-breather. In the field-configuration space it is a solution close to the breather with finite energy, the only known example being the breather presented in the context of the one-dimensional sine-Gordon model.

Though these weakly-localised quasi-breathers are of no direct physical relevance, the study [55] continued to argue that they provide a model for oscillons even at the quantitative level. A comparison between direct Fourier decomposition (1.62) and real time evolution of generic initial conditions supports the description that the oscillon at the frequency ω has the core of a quasi-breather of the same frequency and whose tail is cut off at some radius r. Because an oscillon lacks the complete tail of a quasi-breather, outgoing waves carry energy away from the core region without a balancing factor: oscillon loses energy and is not strictly periodic anymore. The time evolution of the oscillon can be then characterised by a frequency $\omega(t)$ which follows approximately an adiabatic evolution through

a series of quasi-breather states. While the study [55] considered quasi-breathers only in three-dimensional ϕ^4 theory, these numerical solutions were constructed in [59] also in four and five dimensions. The existence of quasi-breathers provides attractors in field space which oscillons can approach to. Attention shifts then from oscillons to quasi-breathers.

These findings in higher dimensions are well in concordance with the classical result obtained by Segur and Kruskal [17] who showed that there is no such a stable breather in ϕ^4 theory as in sine-Gordon model in one dimension. The calculation, assuming a small amplitude, shows that the one-dimensional quasi-breather radiates and its energy decays asymptotically as $\log(t)^{-1}$. This result has support from a numerical study [61] which was not restricted to the assumption of a small amplitude of the breather.

The small amplitude analysis has been extended to higher dimensions in [60] where authors derive a master equation that determines the spatial dependence of the terms in the expansion. The major result is that there exist the minimum energy at some frequency ω for all dimensions $d > 2$, thus generalising the observation of Watkins. Interestingly, particularly considering this study, the energy is monotonically decreasing function of the amplitude in lower dimensions $d < 2$ two-dimensional models being a special case, the energy tending to a constant value when the amplitude goes to zero. However, there are no small amplitude quasi-breathers above three dimensions. This does not exclude long-lived oscillons in higher dimensional models (see e.g. [57]), but they do not have quasi-breather counterpart at small amplitude limit, the upper critical dimension being four.

The existence of quasi-breathers provide thus attractors in field space which oscillons can approach to. Attention shifts then from oscillons to quasi-breathers. However, the insight the quasi-breather description brings to oscillons is limited to the understanding of quasi-breathers themselves. While oscillons appear in wide variety of models, presumably there are then time-periodic solutions for a range of potentials. Do they exist then for all models that supports oscillons or even in larger set of theories, where they are not attractors?

1.4.3 Oscillons in the Standard Model of Particle Physics

So far the discussion has considered only theories involving scalar fields and this remains the primary framework of this study. However, oscillon solutions are not restricted exclusively to scalar theories, but have also been found in models including gauge fields. These, rather recent, discoveries will be reviewed briefly below. As gauge theories are natural in describing high energy phenomena, the existence of oscillon solutions in such models is very interesting and has the potential to greatly enhance their importance.

A series of papers [62–64] has shown that there may be room for an oscillon in the Standard Model of Particle Physics. The first study [62] considered spontaneously broken SU(2) gauge theory where gauge fields couple to a doublet Higgs. The model permits the introduction of a spherical ansatz [65–67]. There remain four physical, independent degrees of freedom consisting of three radially polarised W-bosons and the Higgs boson. At the classical level the theory is completely specified by the ratio of the Higgs boson mass m_{H} to W-boson mass m_{W} as the Lagrangian of the theory can be rescaled in an arbitrary manner and the choice where $m_{\mathrm{W}} = 1/\sqrt{2}$ and $m_{\mathrm{H}} = \sqrt{2\lambda}$ was used, λ being the scalar coupling. Time evolution starting from localised initial value data, given by a Gaussian deviation from the vacuum, was carried out numerically in this framework. The outcome of the time evolution is not extremely sensitive to the initial data, but configurations of small amplitude and a relatively large spatial extent were used. In some cases the fields dissipate completely, but under some conditions a localised, oscillating core remained. These oscillations displayed a gradual decay, but for the particular mass ratio $m_{\mathrm{H}} = 2m_{\mathrm{W}}$ ($\lambda = 1$) the field oscillated without any observable decay over $50,000$ in natural time corresponding to $14,000$ oscillations. The frequency of oscillations is just below the frequency related to the mass of the field, so that the measured value in the Higgs field was $\omega_{\mathrm{H}} = 1.4068$ and in the gauge field $\omega_{\mathrm{W}} = 0.7037$, both within less than a percent from the threshold for dispersive, radiative modes as for this mass ratio $m_{\mathrm{H}} = \sqrt{2}$. Though far from explaining the existence of oscillon, it is easy to understand why a special mass ratio $m_{\mathrm{H}}/m_{\mathrm{W}} = 2$ emerges. The oscillation frequency is just below the mass of the corresponding field. Necessarily in the presence of

several fields with different masses, a resonance can take place only with fixed integer mass ratios.

The bare SU(2) model with a spherical symmetry excludes photons and fermions and cannot uncover the effects of any non-spherical deformations either. The study was further extended to include two major ingredients in [63, 64], namely a fully three-dimensional spatial lattice eliminating any symmetry assumptions was used together with the introduction of the U(1) hypercharge field. This model then describes the full bosonic sector of the electroweak Standard Model, the additional gauge coupling is set to give the Z^0 boson the mass that matches its observed value. The major result of the study is that while the SU(2) oscillon solution is modified it remains stable in the full electroweak theory for the particular two-to-one mass ratio.

The initial conditions were the approximative solutions found in SU(2) theory for vector and Higgs bosons. The magnetic field was set to vanish. It turned out to be necessary to start with slightly larger amplitudes and spatial extend of fields, but an increase of 15% was sufficient to create an oscillon configuration in the SU(2)×U(1) model. After shedding some energy into electromagnetic radiation the oscillon settles to a configuration which does not radiate and is constructed primarily of excitations in $W^{\pm}$ and Higgs fields, while Z^0 is largely absent. In the electroweak model the radiated energy is almost entirely in the electromagnetic field while the oscillon arranges itself to be electrically neutral and decouples from the electromagnetic background. The Cartesian lattice breaks all the rotational symmetries but also explicitly slightly non-spherical initial conditions were examined and verified to converge to a similar oscillatory solution.

All this applies strictly to the specific mass ratio $m_{\mathrm{H}} = 2m_{\mathrm{W}}$ in the model. The study [64] includes an examination of the implications when the mass ratio is let to deviate from this. In the case of lighter Higgs the fields collapse inwards before dispersing, while a heavier Higgs mass results in a fast decay outwards. The demand of fine-tuning is vast, when the masses are off by 5% from the two-to-one ratio an almost immediate demise of the energy concentration takes place and even a variation by 0.5% results in decay after a few hundreds of oscillations.

For the favourable case $m_{\mathrm{H}} = 2m_{\mathrm{W}}$ the oscillon survives in three-dimensional simulations over similar timescales as in the SU(2) model. The frequencies of the electroweak oscillon were reported to be $\omega_{\mathrm{H}} = 1.404$ and $\omega_{\mathrm{W}} = 0.702$. Though the oscillon has small amplitude its large spatial extent compared to the natural scales of the model yields a very massive object. It has an energy of approximately 30 TeV localised in a region of radius roughly 0.05 fm. Consequently it is also well described by a classical analysis. In spite of the vast energy content, the small amplitude means that there is no winding in the Higgs field and the configuration is far from the sphaleron barrier during the oscillon stage though a decay or a collision of oscillons could change this situation. From the point of view of realistic phenomenology the electroweak model still excludes fermions. While couplings in particular to light fermions could create a decay channel, photons were not seen to generate such a destabilising effect. These issues will be discussed again in the context of the early Universe in the second chapter.

The electroweak model is not the only gauge theory that has oscillon solutions, but they have been found also in the Abelian-Higgs model. It is not very surprising that the two-dimensional Abelian-Higgs model supports oscillatory solutions as well because it is not very different from the SU(2) model with the spherical ansatz [65]. On the other hand, the mechanism by which oscillons are created and the region of the parameter space where they are formed are quite different. The study [68] found oscillons as remnants of vortex-antivortex scattering at low momentum. The Abelian-Higgs model [69, 70], introduced as a framework for spontaneous symmetry breaking has, like the SU(2) model with the spherical ansatz, only one free parameter at the classical level, conventionally defined as $\beta = (m_{\mathrm{S}}/m_{\mathrm{V}})^2$, where m_{S} and m_{V} are the scalar and vector masses, respectively. The model has vortex solutions [71] and, quite like a kink and an antikink, a vortex and antivortex attract each other and a vortex-antivortex pair on a lattice comes together. It was noted in [68] that the scattering at low enough values of the parameter β results in a long-lived oscillatory state, instead of a quick annihilation. The lifetimes of these oscillons were reported to be 10^4 to 10^5 in units of m_{V}^{-1}. The critical value of β below which the oscillon production takes place is $\beta_c \simeq 0.13$,

thus a relatively low mass of the scalar field is required, $m_S \lesssim 0.36\, m_{\mathrm{V}}$. The authors argue that the critical value can be understood by a screening mechanism caused by the gauge field. This gives a correction to the effective mass of the scalar field in the core of the vortex changing its sign at β_c, below which long-lived oscillations can evolve. It should be noted that quasistable breathers had been found earlier in the one-dimensional Abelian-Higgs model when sphaleron decay was studied in [72] and these were later seen also in two-dimensional simulations [73].

It is worth repeating that the extension of oscillon solutions from single scalar field models to cover gauge theories increase their appeal considerably as gauge theories are realised in Nature and the SU(2)×U(1) model in particular. Furthermore, a truly remarkable feature of the electroweak oscillon is related to the existence of an oscillon in the presence of several fields. At first sight, any extension of the field content and introduction of couplings can provide effectively a friction term and a decay mechanism. Especially this is true for a massless photon field, which can radiate at arbitrary low frequencies. From that point of view it is really surprising that there is an oscillon in the electroweak model. The discovery that the oscillon remains meta-stable due to some non-trivial decoupling mechanism, proves that oscillon solutions can be found in theories that have multiple fields and a lot of structure. Finally, oscillons in gauge theories can have a number of applications, e.g. in baryogenesis which will be discussed in the second chapter.

1.5 Solitons in Non-relativistic Theories

So far here the word soliton has been used almost as a synonym of any non-dissipative solution. This is not the traditional definition for solitons. A non-dissipative solution that can travel without a distortion to its shape should rather be called a solitary wave. The second requirement (see e.g. [7]) usually attached to solitons is related to the interactions of solitary waves. If they meet but re-emerge after the contact retaining their original velocity and shape, the wave is a soliton. Thus the kinks in sine-Gordon model are solitons in this strictest sense, while kinks in ϕ^4 theory are not.

Solitons or solitary waves are not restricted to the realm of relativistic field theories as the original discovery made by Scott Russell already proves. Also the second more stringent feature mentioned above was first discovered when studying a non-relativistic wave equation. The word soliton goes back to the work of Zabusky and Kruskal [74] carried out in the scattering of wave pulses of the Korteweg-de Vries equation. The KdV equation reads

$$\frac{\partial \phi}{\partial t} + \phi \frac{\partial \phi}{\partial x} + \delta^2 \frac{\partial^3 \phi}{\partial x^3} = 0 \,. \tag{1.65}$$

In the example of water, ϕ corresponds to the height of the surface of the fluid. The stationary solutions of (1.65) in a frame moving with velocity v are found by a standard technique. Substituting $\phi = \Phi(x - vt)$ yields a third order nonlinear ordinary differential equation. The solution can be written [74]

$$\phi = \phi_\infty + (\phi_0 - \phi_\infty) \operatorname{sech}^2 \left[\frac{x - x_0}{\Delta} \right] , \tag{1.66}$$

where ϕ_∞, ϕ_0 and x_0 are arbitrary constants related to the asymptotic level of the fluid, the height of the pulse and its location, respectively. Furthermore, the width of the pulse and its velocity are determined by these constants

$$\Delta = \delta \left[\frac{\phi_0 - \phi_\infty}{12} \right]^{-1/2} , \tag{1.67}$$

and

$$v = \phi_\infty + (\phi_0 - \phi_\infty)/3 \,. \tag{1.68}$$

Thus the pulse becomes narrower when the its amplitude increases or the parameter δ^2 decreases. The latter sets the magnitude when the third term in (1.65) becomes important and balances the steepening caused by the second term. Also the velocity and the amplitude of the pulse are related - bigger pulses travel faster.

The applicability of the KdV equation reaches beyond shallow water

waves and it can be used to describe one-dimensional, long-time asymptotic behaviour of a small amplitude waves in other media. For instance, it was re-derived in a study of magnetohydrodynamic waves in collisionless plasma in 1960 [75]. Another reason for revived interest in KdV equation was the numerical work conducted by Fermi, Pasta and Ulam [76] who studied a one-dimensional anharmonic lattice or alternatively, a vibrating string, which has nonlinear terms in the interaction between neighbouring mass points. The study, one of the early numerical ones, led to the unexpected discovery that nonlinear systems do not always tend to a quick equipartition. KdV equation is the governing equation of the Fermi-Pasta-Ulam problem in the continuum limit.

The major discovery of Zabusky and Kruskal [74] was that the wave pulses (1.66) scatter almost elastically, in other words after a collision they re-emerge with original velocities and shapes. This was understood later analytically by the work that essentially presented the inverse scattering method [77]. It turns out that the KdV equation defines a completely integrable system characterised by an infinite number of conserved quantities. The existence of solitary objects in KdV equation obviously slows down thermalisation and explains the earlier observation made by Fermi, Pasta and Ulam. The subsequent interest in solitons lead to a development of more techniques, like Bäcklund transformations, which can be utilised to construct multi-soliton solutions for completely integrable systems. This is the underlying reason for the existence of such exact solutions like (1.20) and (1.21), describing two kinks or the breather in a closed form in sine-Gordon model. However, one-dimensional sine-Gordon model is more or less the only known example of its kind among relativistic field theories.

Finally, the third completely integrable system usually mentioned is that given by the nonlinear Schrödinger equation

$$i\,\frac{\partial\phi}{\partial t} + \frac{\partial^2\phi}{\partial x^2} + \phi\,|\phi|^2 = 0\,. \tag{1.69}$$

Here the soliton solution is

$$\phi(t,x) = \sqrt{2}a\,e^{ia^2t}\,\mathrm{sech}(ax)\,. \tag{1.70}$$

It can be also interpreted as Q-balls in a non-relativistic theory. While the KdV equation (1.65) describes shallow water waves, the nonlinear Schrödinger equation (1.69) has been used to model deep water waves. As a remark it has been linked also to the formation of so called freak waves (also known as rogue or giant waves). These are defined as waves having height that exceeds by the factor 2.2 the significant wave amplitude which in turn is defined as the average of the largest third of waves. Not much is known about freak waves, they are presumably not particularly soliton-like objects. It has been argued [78] that the non-linear term plays an important role in the dynamics of freak wave generation though that process also depends crucially on the initial spectrum. Another example of non-linearities enhancing density contrast is given by the dynamics of the axion field presented in [46]. As will be seen, the amplitude of oscillons easily exceeds the typical height of linear, dispersive waves in the system by a factor considerably greater than two. Sticking to that uncomplicated definition, oscillons can be then considered as freak waves. However, much of this study shows that oscillons, at least in low dimensional theories, have soliton-like features. Interpreting oscillons as freak waves merely demonstrates how difficult it is to set definitions that would capture precisely the relevant phenomena. A good example is the breather itself. Though the solution (1.22) is entirely dissipationless, it cannot be called even a solitary wave if that is defined as a wave that can travel retaining its shape due to the non-trivial time dependence of the breather's profile.

A considerable part of this thesis deals with oscillons forming from collapsing domains, an observation which served to a great extent as a motivation for this study. Therefore it is appropriate here to bring up that localised, oscillating structures are found in granular media. These structures, also called oscillons, were observed to form in a vibrating layer of sand [79, 80]. In the experiment the layer in the bottom of an upright container was vertically driven by an external, harmonic force. The control parameters in the experiment are thus the drive frequency and the acceleration amplitude. The oscillons are small, two-dimensional circularly symmetric excitations which oscillate at a frequency half of that of the driving force, appearing during one cycle as a peak, on the next as a crater. The oscillons were reported to form at drive frequencies 20 to

30 Hz, but being quite sensitive to the strength of the amplitude. Another study [81] found them in a different band of the parameter space at higher acceleration. A phenomenological model has been suggested to explain the observations [82]. These oscillons in a granular media exist only due to the constant energy input by the external force that enables an interplay between dissipation and hysteresis. Therefore they are not closely related to oscillons in relativistic field theories that appear almost non-dissipative. Still it is very interesting to note certain similarities. The oscillons were reported to have persisted 5×10^5 container oscillations thus having a long lifetime. Secondly, the oscillons were observed to have short-range interactions, depending on the phase so that oscillons of like phase repel, while those of opposite phase attract and bind. It has been also suggested based on theoretical considerations that acoustic instability could create oscillons in stellar chromospheres [83]. It might be worthwhile to look for oscillons also in non-relativistic theories.

Chapter 2

Cosmological Framework

The previous chapter considered non-dissipative or meta-stable solutions in nonlinear field theories, the main subject of this study. This chapter departs from this topic. Though solitons are found in physical systems familiar to everyone like the example of Korteweg-de Vries equation shows, studying relativistic field equations brings a close connection with the realm of high energy physics, like the oscillon in the Standard Model of particle physics demonstrates. It is not excluded that some such solutions could be seen in accelerator experiments. However, in most cases such conditions, above all extremely high energy density and temperature, where extended objects could come into being are met only in the very early Universe. This follows from the Big Bang model which states that the Universe started much more dense and at higher temperature than it is at present, exceeding by far anything that can be reached in any terrestial laboratories.

While solitons are worth studying in their own right, lot of related research has been motivated by considerations related to the physics in the early Universe. In particular this applies to topological defects, which could form in cosmological phase transitions via the Kibble mechanism. The connection with the cosmology is not limited to the idea that the early Universe would merely provide the only experiment where high energy solitons could be created. In turn, defects could have a very strong, if not even defining, influence on the subsequent evolution of the Universe in many ways. Thus when looking for physical applications of solitons in rela-

tivistic field theories, cosmology is a very natural framework. For instance, it would be very difficult to review work carried out on gauged strings of Abelian-Higgs model (extension of Nielsen-Olesen vortex [71] to three dimensions) without referring to cosmology at all. Oscillons are no exception and many studies are intimately tied to e.g. physics of cosmological phase transitions or to considerations in an expanding background. For a survey of such research some preliminaries of cosmology are necessary. Finally, the last topic of this study, formation of oscillons from collapsing domains, is also about the dynamics of oscillons in a radiative environment which bears a similarity to the conditions in the early Universe.

For the above mentioned reasons the cosmological standard model is briefly described together with the present observations that have provided us with a very precise picture of the Universe. However, there are a number of open questions that will be listed. Then attention is turned to solitons in the early Universe and some of the questions they could solve or, equally well, raise. Phase transitions and formation of topological defects are considered, focusing on domain walls. Turning to nontopological defects, the Q-balls described in the previous chapter could form via fragmentation of Affleck-Dine condensate and contribute to dark matter as well as creation of baryons. In the end of the chapter oscillons are considered from the point of view of cosmology.

2.1 Cosmological Standard Model

The Big Bang model states that at some point in the distant past the Universe was in a state which was extremely hot and dense compared to the present. Since then the Universe has expanded and consequently temperature and density have decreased. The expansion is described by a time-dependent scale factor $a = a(t)$ that multiplies coordinate distances to yield proper, physical ones.

The first support for Big Bang cosmology goes back to the work by Edwin Hubble, but the strong evidence in its favour was the discovery of the Cosmic Microwave Background (CMB) radiation. This is the relic radiation from the time of recombination when neutral hydrogen was formed for the first time when the hot plasma had cooled down. At that moment

the mean free path of photons exceeded the size of the horizon, in other words the Universe became transparent. Therefore the CMB provides us with a snapshot of the Universe almost at its birth.

The CMB radiation is extremely homogeneous reflecting the state of the Universe at the time of the last scattering. There were, however, tiny fluctuations already present then, which came to seed the formation of structure we observe in the current Universe. These anisotropies in the CMB are arguably the most important source of cosmological information. Not exclusively, but to a great extent, it is thanks to the recent precise measurements of the CMB radiation that we have now a very good understanding of what are the constituents that make up the Universe. This is often referred as the cosmological Standard Model, or ΛCDM model. This stands for the fact that the energy density of the present Universe is dominated by dark energy and cold dark matter. Dark energy is an unknown essence that causes the current accelerated expansion of the Universe and cold dark matter is non-relativistic, weakly interacting non-baryonic matter. Conventionally, one gives the fractions of different components relative to the critical density ρ_c, $\Omega_i = \rho_i/\rho_c$. The dominant ones are $\Omega_\Lambda = 0.742 \pm 0.03$ and $\Omega_{\mathrm{CDM}} = 0.214 \pm 0.0027$, while the ordinary baryonic matter contributes a fraction $\Omega_\mathrm{b} = 0.044 \pm 0.003$ (the quoted figures are mean values based on the WMAP satellite data only [84]). The values are based on six parameter model that assumes a flat Universe, i.e. $\Omega_{\mathrm{total}} = 1$. The limits from the CMB data alone set the curvature to the limit $-0.063 < \Omega_\mathrm{k} < 0.017$ [84] when the flatness assumption is lifted. The CMB measurements alone do not set very stringent bounds on the equation of state for the dark energy either. However, combined with other observations there is a fairly tight limit, $-1.11 < w < -0.86$ [85], where w is the parameter for the equation of state, $w = P/\rho$, P being pressure. The spectral index n_s, determining the spectrum of the CMB fluctuations, is very close to unity, $n_\mathrm{s} = 0.963 \pm 0.015$ [84], which indicates almost scale-independent spectra.

While the present observations yield a spectacular precision, a theoretical understanding of these constituents is far less settled. There is no explanation for dark energy [84]. All the observations are consistent with a cosmological constant Λ, which has a constant equation of state

$w = -1$ and would be a natural candidate. However, to match its value with the observations requires extreme amount of fine-tuning from the particle physics perspective. Other possibilities include a scalar field, so-called quintessence, or an effect of inhomogeneities, i.e. a large void in the local Universe.

There are many candidates for dark matter. Theoretically the best motivated is undoubtedly the lightest supersymmetric particle (LSP) which is stable if R-parity is conserved. However, observations do not limit the options which range from axions with mass 10^{-5} eV to superheavy particles or objects of almost macroscopic size. Even for the tiny fraction of baryons the situations is not settled. The Standard Model of particle physics explains rigorously the interactions of baryonic matter, but it rather suggests that there were equal proportions of matter and antimatter. Thus the origin of this baryon asymmetry is not known. How this asymmetry has been generated, the process called baryogenesis, will be discussed later. To complete the list of open questions with a last one, while the amount of baryonic matter in the Universe is known very well, the observed ordinary matter in the present Universe does not add up to this value. There is an explanation for this according to which the majority of the baryons reside in the intergalactic medium at high temperature. This diffuse gas, warm-hot intergalactic medium, is invisible for current instruments and thus the present observations miss roughly half of the baryons observed at higher redshifts via Lyman-α forests.

Together with the constituents of the ΛCDM model, an integral part of the standard model is cosmological inflation. This is a period of rapid, accelerated, expansion that occurred in the very early Universe. The inflationary scenario explains why the observed Universe is flat, isotropic and homogeneous. Most importantly, it provides a mechanism for the creation of the small density fluctuations we observe in the CMB. One prediction of inflation is the almost scale-free spectrum which is well supported by the present observations. Inflation can be realised when the potential energy of a scalar field dominates the energy density. There is naturally no candidate for the inflaton, the field that drives inflation, within the experimentally accessible energy scales, but the inflaton must be sough in the extensions of the Standard Model of particle physics and is exclusively a

theoretical challenge. After inflation, hot Big Bang cosmology is restored in a phase of reheating where the energy of inflation is released into particle production.

2.1.1 Baryogenesis

The current measurement [84] of the baryon-to-photon ratio $\eta_{\rm b}$ yields

$$\eta_{\rm b} = \frac{n_{\rm b}}{n_\gamma} = (6.226 \pm 0.386) \cdot 10^{-10} \,. \tag{2.1}$$

In spite of being a very small number there is an apparent asymmetry, there is more matter than antimatter. While it is still possible that there are significant amounts of antimatter in the Universe, these cannot be closer than at cosmic length scales. Therefore by far the most likely explanation is that the number (2.1) reflects a true baryon asymmetry in the current Universe. One could take this baryon asymmetry as an initial condition, but that would not be a particularly explanatory approach. A. Sakharov was the first who suggested that the baryon asymmetry could arise via physical processes and identified the conditions which are necessary for baryogenesis [86]. Obviously the baryon number B must be violated in order any net baryon asymmetry to be generated. Secondly, CP, the product of charge conjugation and parity, must be violated. Otherwise every reaction that produces a particle is accompanied by a reaction creating an antiparticle. Finally, there is need for non-equilibrium conditions, an arrow of time. Even B and CP violating processes cannot create any asymmetry without a departure from equilibrium.

The Sakharov conditions are just the necessary requirements for a process to create baryons, while a model for baryogenesis can be considered successful only if it generates the right baryon fraction $\eta_{\rm b}$. Even the observed asymmetry (2.1) is relatively small, it turns out to be difficult to produce. One should also notice that for instance the B and CP violation has to cease at the point when the Universe reaches thermal equilibrium because otherwise any created asymmetry is washed out.

There are several scenarios for baryogenesis (for a review see e.g. [87]), many operating at widely different energy scales. Baryogenesis could have taken place already at Planck scale, 10^{19} GeV. The quantum gravity ef-

fects cause violation of quantum numbers. However, due to the unknown physics, Planck scale baryogenesis is in effect taking the baryon asymmetry as an initial condition [87]. Baryogenesis could have taken place at the scale of grand unified theories (GUT), 10^{16} GeV. GUT scenarios do not have problems to meet the requirements of Sakharov conditions and many models successfully produce the required baryon density (2.1). The major problem of GUT scale baryogenesis is related to the wider cosmological framework. Inflation inevitable dilutes any particle density that preceded to effectively zero. The reheating temperature to which the Universe was heated after inflation is expected to be well below GUT scale.

Models for baryogenesis that operate at or below inflationary scale include leptogenesis, electroweak baryogenesis and so-called Affleck-Dine baryogenesis. In the scenario of the leptogenesis the baryon asymmetry is achieved by weak interactions converting lepton number to baryon number. Electroweak baryogenesis could in principle create a baryon asymmetry within the Standard Model. In practice, it turns out that there is too little CP violation and the non-equilibrium conditions are not met. In the supersymmetric extensions of the Standard Model electroweak baryogenesis is still a viable, though tightly constrained, scenario. Another variant of electroweak baryogenesis is to combine it with low-scale inflation where the phase of reheating takes the Universe out of equilibrium and sets the stage for baryogenesis.

The Affleck-Dine mechanism [88] in turn is based on the existence of a number of scalar fields that appear in supersymmetric scenarios. These fields carry baryon and lepton numbers and have easily large vacuum expectation values due to flat directions in the potentials. Quartic couplings in the potential violate baryon number and CP conservation. The equation of motion for a homogeneous field, $\phi(t)$, in an expanding background reads

$$\ddot{\phi} + 3H\dot{\phi} + \frac{\partial V}{\partial \phi} = 0\,, \tag{2.2}$$

where H is the Hubble parameter, $H = \dot{a}/a$, $a = a(t)$ being the scale factor. At early times H is large and the system overdamped. Once H decreases, the field performs damped oscillations. The quartic terms

become negligible and the created baryon number is conserved without wash-out. An additional appealing feature of the Affleck-Dine mechanism is that the dark matter LSP is created in the same process and thus the scenario could explain why baryon and dark matter densities have the same order of magnitude, $\Omega_{\rm b} : \Omega_{\rm CDM} \approx 1 : 5$. We will return to Affleck-Dine baryogenesis when considering Q-ball cosmology.

2.2 Phase Transitions and Defect Formation

The picture of the hot Big Bang model is modified by the inflationary scenario where everything pre-existing is diluted away and which sets a weak upper bound for the highest relevant energy scale in the form of the reheating temperature. While it is not known, it is certainly well below Planck scale and could be for instance less than 10^9 GeV to avoid over-production of gravitinos. In any case, after reheating the Universe is left at a temperature than anything that could have been directly probed in controlled particle physics experiments. If one believes in Grand Unification, then there is every reason to expect that larger symmetries have been present in theories describing particle physics at such temperatures. With the decreasing temperature these symmetries have then broken down in phase transitions. The existence of phase transitions is not entirely speculative based on theoretical considerations, but we can be almost sure of the occurrence of two phase transitions, at the QCD scale (around 100 MeV) and at the electroweak scale (100 GeV). Below the phase transition is demonstrated with a very simple example in the context of ϕ^4 theory.

The quartic potential given in (1.5) is at the classical level, as is the potential (1.12) in sine-Gordon model. These are adequate descriptions when quantum effects are small and the system is at low temperature. The standard technique to incorporate thermal effects is to introduce so-called effective potential, $V_{\rm eff}(\phi, T)$, which is then also a function of temperature T, and can consequently then be used to qualitatively describe phenomena like phase transitions. The effective potential $V_{\rm eff}$ is nothing but the free energy density (see e.g. [31]) associated with the field ϕ

$$V_{\rm eff}(\phi, T) = \rho(\phi, T) - Ts(\phi, T)\,, \tag{2.3}$$

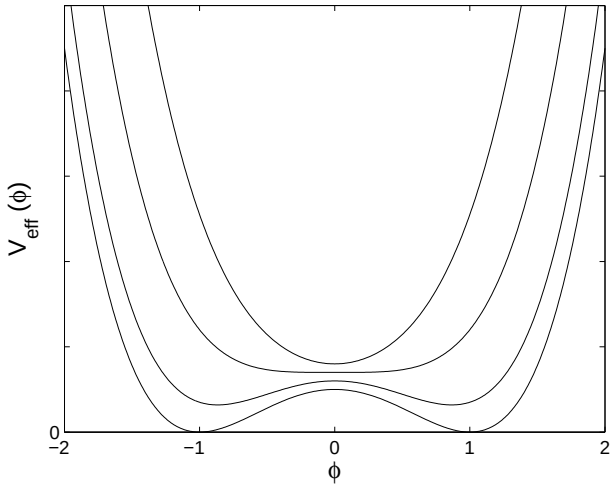

Figure 2.1. The effective potential (2.4) at temperature $T = 1.5\,T_c$, T_c, $0.5\,T_c$ and $T = 0$ (from top to bottom). $\lambda = 1$ and $\eta = 1$. The curves have been displaced vertically for clarity. Because there is no cubic term of ϕ in $V_{\rm eff}$, the result is a second order phase transition.

where s is the entropy density. One can calculate the effective potential when the free energy density of the system is known via the partition function Z e.g. for bosons in a scalar theory. The one-loop effective potential for (1.5) is (see [31])

$$\begin{aligned} V_{\rm eff}(\phi, T) &= V(\phi) + \frac{\lambda}{8}\,T^2\,\phi^2 - \frac{\pi^2}{90}T^4 + ... \\ &\simeq \frac{1}{2}\,m_{\rm eff}^2\,\phi^2 + \frac{\lambda}{4}\phi^4 + \frac{\lambda}{4}\eta^4 - \frac{\pi^2}{90}T^4\,, \end{aligned} \tag{2.4}$$

where the effective mass $m_{\rm eff}^2$ is

$$m_{\rm eff}^2\,(T) = \frac{\lambda}{4}\left(T^2 - 4\eta^2\right)\,. \tag{2.5}$$

At zero temperature $T = 0$ one recovers the original quartic potential (1.5). However, the two non-zero minima exist only at low temperature, while the effective mass $m_{\rm eff}^2$ changes sign at temperature $T_c = 2\eta$. Above that crit-

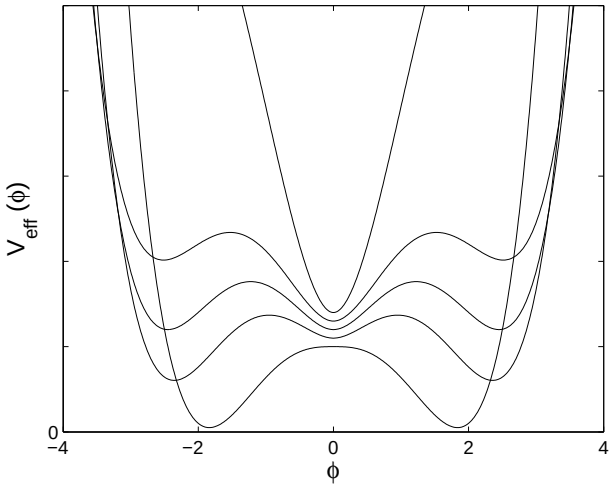

Figure 2.2. An example of an effective potential for a first order phase transition: $V_{\rm eff}(\phi, T) = \frac{1}{2}(T^2 - T_0^2)\phi^2 - \frac{1}{3}\kappa T|\phi|^3 + \frac{1}{4}\lambda\phi^4$, plotted at temperature $T = 1.5\,T_c$, $1.1\,T_c$, T_c, $0.9\,T_c$ and $0.5\,T_c$ (from top to bottom). The curves have been displaced vertically for clarity. $\kappa = 3\sqrt{6}/4$, $\lambda = 1$ and $T_0 = 1$. Notice the similarity with the effective potential $V_\omega(\varphi)$ for Q-balls shown in Figure 1.6; for Q-balls the field ϕ is, in some sense, on the verge of a first order phase transition [89].

ical temperature, $\phi = 0$ is the global minimum of the potential (2.4) and only with $T < T_c$ the field develops a non-zero vacuum expectation value. This is demonstrated in Figure 2.1, where the effective potential (2.4) is shown at various temperatures. The example at hand demonstrates a second order phase transition. This can be seen by solving the order parameter $|\phi|$ in the broken phase, $|\phi| = \frac{1}{2}\sqrt{T_c^2 - T^2}$. Thus $|\phi|$ is continuous at T_c.

In a first order phase transition there is some quantity or quantities whose expectation value behaves discontinuously. There the symmetric phase $\phi = 0$ remains metastable below the critical temperature T_c, see Figure 2.2. This metastable vacuum state is often called the false vacuum. There is a potential barrier separating the metastable and global minima. This barrier is overcome through thermal fluctuations that occasionally take the field over the barrier or by quantum tunneling. In each case

bubbles of new, broken phase appear and when they are larger than a critical size they expand. This process is called bubble nucleation. The bubbles grow until they coalesce and eventually the system enters the new, broken phase.

The order of the phase transition plays an important role in cosmology. A first order phase transition can potentially proceed relatively slowly so that it takes time before the transition is over, or in an expanding Universe it may not complete at all. In addition, a first order phase transition can provide a radical departure from equilibrium. Returning back to the topic of baryogenesis, the standard scenario of the electroweak baryogenesis is based on the idea that the electroweak phase transition is of first order, namely there are nonequilibrium processes near the bubble walls which can create baryon number B. This possibility is now excluded within the Standard Model of particle physics. The phase transition could be of first order only if the Higgs boson were light (see e.g. [90]), in practice having lower mass than the W-boson mass, $m_{\rm H} \lesssim m_{\rm W} = 80.4$ GeV, which is already ruled out by experimental searches. The electroweak phase transition may still be of first order in extensions of the Standard Model leaving the window open for production of baryons at the electroweak scale in conventional hot Big Bang cosmology (for a variant of electroweak baryogenesis combined with low scale inflation see e.g. [91]).

2.2.1 Kibble Mechanism and a Domain Wall Network

With the example of the effective potential (2.4) it is easy now to describe the formation of defects in ϕ^4 theory. With falling temperature the field then drops into either of the two vacua (or rather starts to oscillate about either of them), shown in Figure 2.1. Which one then apparently depends on some local fluctuations, thermal or quantum, at the time of crossing the critical temperature. In any case the correlation between vacua cannot take place on scales which have not yet been in causal contact. There is an equal probability for the field to fall into the vacuum $\phi = +\eta$ as $\phi = -\eta$ at length scales beyond the causal horizon $d_{\rm H}$ which in a static background is $d_{\rm H} = ct$ where c is the speed of light. Thus we expect that domains or islands of some characteristic size appear where the field ϕ has settled in

either of the two vacua $\phi = \pm\eta$. But in between those domains the field interpolates from one minimum of the potential to another and must go through zero. Thus in a one-dimensional system a kink forms to separate the two regions where different vacua were selected. In higher dimensions the formed defects are domain walls. See the upper panel in Figure 2.3 for an example of domains formed in two dimensions.

The above is a very simplified picture of the process known as Kibble mechanism named after T. Kibble who was the first to consider the formation of defects in cosmological phase transitions and the size of the created proto-domains [92]. There is naturally much more to add to the mechanism than the descriptive picture above. The causality constrain is obviously an upper bound. For cosmological applications one would like to know quantitatively the initial density of domains, because this converts to the initial number of domain walls, or other defects, the Universe will evolve with. For such purposes a precise value of the mean separation of defects at birth is important. The task is to find the right correlation length ξ, but the issue is not entirely without ambiguity. If the phase transition is not first but second order, the standard, equilibrium correlation length generically diverges at the critical temperature as $\bar{\xi} \sim (T - T_c)^{-\nu}$ where ν is the critical exponent (and is used as a base for universality classes). This still does not mean that after a second order phase transition the field everywhere ends up in the same vacuum. There is critical slowing down, it takes infinite time for the system to equilibrate while the phase transition is over in a finite time. Thus the equilibrium correlation length $\bar{\xi}$ does not set the distance scale over which different vacuum can be selected. Another distance scale is set by the Ginzburg length. This is the size of a domain in which thermal fluctuations are insufficient to lift the field from one vacua to another. It can be used to determine the mean distance between domains [92]. Alternatively, one can consider the length scale over which fluctuations have not had time to disappear due to critical slowing down and study how fast the cooling of the system takes place. This approach has been proposed by Zurek [93].

At this point we use the occasion to discuss briefly the subsequent evolution of domain walls to have a general example of a network of topological defects and in particular as it sets the starting point of the last

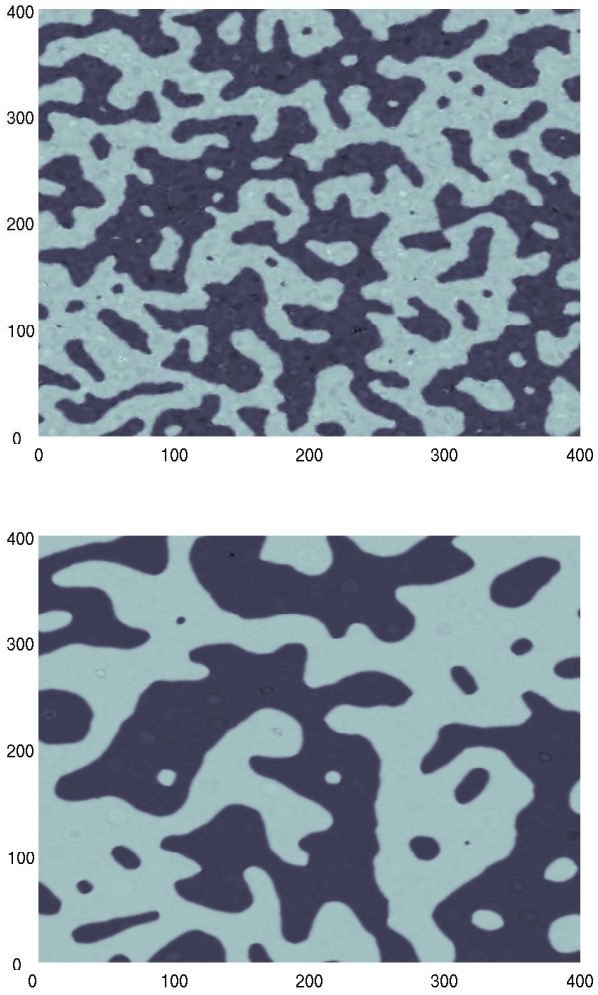

Figure 2.3. Two snapshots of the same region of size 400^2 at time $t = 20$ (above) and $t = 40$ (below) from a simulation where the field ϕ starts from the top of the local maximum of the potential (1.5) with a random momentum and is damped to condense (for details of the simulations, see last chapter). Typical lengthscale of any feature, like the size of the domains, has increased by a factor of two. In other words, the second snapshot is qualitatively like a magnification of one quarter of the first one.

chapter of this thesis. As discussed, the domains formed in the phase transition are separated by some characteristic length scale ξ. Once the system has cooled down, thermal fluctuations become weaker. Thus from the thermal point of view large enough domains are frozen-out. Instead of thermal fluctuations there is a completely different effect dictating the evolution of the network. A domain wall has surface tension σ_{wall} which is equal to its surface energy density (this is given by the energy of the one-dimensional kink, for instance (1.8) in the example of ϕ^4 theory). The domain wall evolves to minimise its surface area and thus straightens up. Consequently, the characteristic curvature radius of the walls grows with time. Of course, there is obviously another length scale in the network, which is the thickness of the walls. It is proportional to the inverse mass m^{-1}, which is $1/\sqrt{2\lambda}\eta$ in ϕ^4 theory, see (1.7). However, there is no reason why the large scale dynamics should depend on it. In practice, the network is well described by a single length scale ξ, which exhibits dynamic scaling with time, $\xi \sim t$. The scaling in domain walls has been studied numerically with field theory simulations in two and three dimensions and in static and expanding backgrounds. It has been argued that there could be a logarithmic correction to the linear scaling relation e.g. in [94, 95], but no indication of such was seen in [96]. This issue is still open, e.g. in [97] it was suggested that the deviations from linear scaling observed in numerical studies could be due to finite size effects.

The scaling is qualitatively probably best illustrated by comparing the two snapshots of a domain wall network in two dimensions presented in Figure 2.3. More qualitatively the scaling is demonstrated in Figure 2.4 where the time evolution of the total length of domain walls L_{walls} is shown for a two-dimensional network in a flat space. We determine the length of domain walls by counting the number of lattice sites where the field changes sign compared to its nearest neighbouring lattice points. The total length L_{walls} is inversely proportional to the mean curvature radius and consequently at least roughly to time as well, $L_{\text{walls}} \sim t^{-1}$. The same behaviour is also well captured by the Lagrangian density (1.2) integrated over the lattice, as the time-dependence of the two curves in Figure 2.4 agrees very well. Although the total energy is conserved in simulations, the dispersive waves have equal contributions on the one hand to kinetic

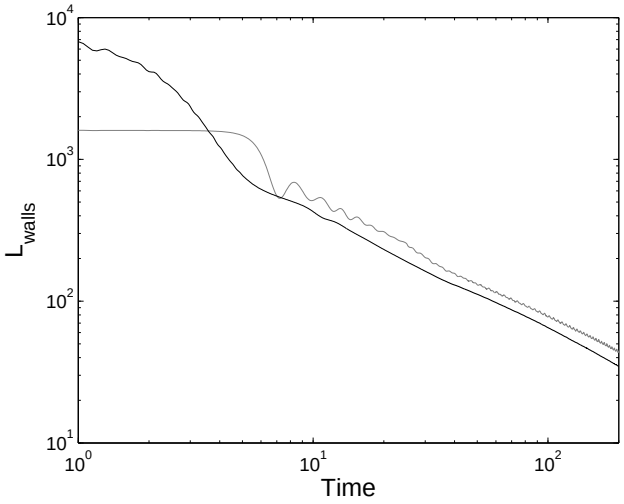

Figure 2.4. The total length of domain walls L_{walls} in a two-dimensional lattice whose physical size in linear dimension is $L = 400$. The curves show the number of zero crossings in nearest neighbouring lattice sites (black) and the Lagrangian $|\int \mathcal{L}|$ (grey) as a function of time averaged over 100 realisations. After the initial transients the curves track each other well. The slopes of the curves indicate a slightly slower decrease of L_{walls} with time than the predicted $1/t$. The data of the second half of the simulation ($100 \leq t \leq 200$) gives the best fit to a power law $L_{\text{walls}} \sim t^{-\delta}$ when the exponent $\delta = 0.9$. One possibility is that the domain walls scale as predicted, but the presence of oscillons can show up as a slightly slower decrease in these indicators.

and on the other hand to gradient and potential energy and therefore they have a negligible contribution to the Lagrangian density. Only soliton-like objects, as domain walls in this case, which have a static configuration with non-zero energy leave a signature in the Lagrangian density. Consequently, $|\int \mathcal{L}|$ grows linearly with the length of domain walls in the system L_{walls}, $|\int \mathcal{L}| = \sigma_{\text{wall}} \cdot L_{\text{walls}}$, where the proportionality constant σ_{wall} is the surface tension of the domain wall. This is thus a good indicator for defects.

The slopes of the curves in Figure 2.4 are not quite consistent with linear scaling, but indicate slightly slower decrease in time than t^{-1}. At least in these simulations this could be due to the presence of oscillons. The classical picture of scaling in a domain wall network has been now

also tested within the Hartree approximation [98] and it was concluded to be valid in the quantum theory in the semiclassical approach used.

2.2.2 Topological Defects in Cosmology

The formation and evolution of domain walls in ϕ^4 theory has many aspects that can be generalised. The Kibble-Zurek mechanism is not restricted to discrete symmetries and scalar theories, but other kind of topological defects, such as magnetic monopoles or cosmic strings, could form in an analogous way. Though it has been argued that in the case of local gauge invariance, the Kibble-Zurek mechanism would not be the quantitatively correct, this does not mean that there would not be defect formation in gauge theories, but just that the dominating process determining the density of defects could be quite different [99]. The evolution of a network of cosmic strings has a similar tendency to that of domain walls, strings straighten out due to the string tension. Scaling in the context of string networks is rather related to interaction processes between strings, which can be complicated. A major ingredient for evolution is the expansion of the Universe that stretches any defect networks.

Topological defects can solve and create many cosmological problems and they have had an impact on the development of many theoretical scenarios. Arguably the most notable was the so-called monopole problem. It turns out that the monopoles created at GUT scale would appear far too plentiful to be tolerable in any cosmological scenario [100] (for a review see e.g. [31]). The monopole problem was one of the issues that provided the initial motivation for the inflationary scenario (see the original work by Guth [101]). Decaying cosmic string loops in turn could for instance create baryon asymmetry via leptogenesis (see e.g. [102]). Presumably the first consideration of topological defects in cosmology dealt with domain walls [103]. It is very easy to see that a domain wall can quickly start to dominate the energy density in an expanding Universe. While the density of nonrelativistic matter behaves as $\rho \sim a^{-3}$, where a is the scale factor, the energy density of a domain wall decreases much more slowly, $\rho \sim a^{-1}$ because its area is growing due to the expansion and the surface energy density σ_{wall} remains constant. Obviously a realistic network of domain

walls exhibits a far more complicated dynamics, but the crude consideration above conveys the right picture. A domain wall network scales in the expanding Universe, but the network overpowers any matter component. Therefore domain walls at high energy scales are totally intolerable, they exceed the critical density ρ_c by orders of magnitude causing a quick collapse of the Universe. For this reason domain walls in standard scenarios are excluded. An interesting point to add is that the equation of state for a gas of non-relativistic walls is $P = -2\rho/3$ (see e.g. [31]). Thus the gas of domain walls causes a rapid expansion itself. Therefore it has been speculated that domain walls starting to dominate energy density of the Universe could be the reason for the current accelerated expansion. This does not seem likely in the light of the present observations. The equation state parameter for domain walls $w = -2/3$ is not compatible with the mentioned interval quoted e.g. in [85] that seem to converge to $w = -1$ and strongly favour cosmological constant at the moment. This finishes the very brief glance at topological defects, for a review see e.g. [89], but we now turn to nontopological defects.

2.3 Q-balls in the Early Universe

Nontopological defects do not owe their stability to a degenerate, nontrivial vacuum structure and therefore their formation do not require such a mechanism as described before where the field(s) ends up in a different vacua in separate parts of the space. This still does not mean that nontopological solitons could not be produced in a very similar manner to the Kibble mechanism. Formation of nontopological solitons in phase transitions was examined e.g. in [104]. The potential of the model considered has a global and a local minimum and permits nontopological soliton solutions where the field is confined in the vicinity of the local minimum. Below the critical temperature the field drops in either of the minima, but in contrast to the previous example, these are not degenerate, but the local minimum implies higher energy density and is the false vacuum. This is also called biased phase transition (see e.g. [9]). Analogously to the earlier discussion there are walls separating the two vacua, but because the true, global vacuum is energetically favourable, the regions of false vacuum shrink and eventually

disappear and the domain wall problem is avoided. While the walls have not disappeared, they protect the bags of false vacua and the nontopological solitons may form in these regions provided the walls survive long enough so that temperature is sufficiently low preventing dissolution of the solitons due to thermal effects. They are thus relics of the domains of false vacuum. The study [104] concluded that this kind of solitogenesis can be efficient to such an extent that the nontopological solitons could form all the dark matter in the Universe. Further studies considered also the evolution of the networks of nontopological solitons [105, 106]. The evolution was found to be very dependent on the parameters. New nontopological solitons can form from fusion of free scalars, solitosynthesis [105], but they may also almost entirely evaporate [106].

2.3.1 Q-ball Formation

Concentrating now on the formation of Q-ball, it has been argued in [107] that small Q-balls could be formed even via thermal fluctuations, but this mechanism is not likely to produce solitons in significant numbers. However, one expects a large number of Q-balls produced in the fragmentation of the Affleck-Dine condensate, i.e. the coherent field that has large vacuum expectation value.

Eq. (2.2) assumed a spatially homogeneous field $\phi = \phi(t)$. In practice this is only an idealisation which can be used to describe the baryogenesis in the model. However, already quantum fluctuations during the inflationary era create spatial inhomogeneities. These perturbations then grow and have been considered in a linear theory e.g. in [108]. However, when the modes grow large enough they become nonlinear and the complicated dynamics has to be studied numerically. Now the potentials considered, e.g. in the minimal supersymmetric extension of the Standard Model, are often very flat [109] and fulfil the condition (1.44) permitting Q-ball solutions [110]. During the nonlinear evolution Q-balls are formed and the system finds the most energetically favourable configuration, a number of Q-balls and radiation. The numerical simulations show that the condensate generically fragments into Q-balls [43, 111, 112]. The three-dimensional simulations showed the formation of large Q-balls [111] when

the potential was chosen to be that of the gauge mediated supersymmetry breaking one. Similarly, Q-balls were observed to form also in gravity mediated supersymmetry breaking scenario, which has a steeper potential, even when the initial fluctuations are very tiny [43]. The number of Q-balls in that case is larger and they are smaller, appearing with relativistic velocities. Almost all the initial charge of the condensate, in excess of 90%, ends up in the Q-balls. The gravity mediated scenario was considered further in [112], where two-dimensional simulations of the condensate were performed. Analytical considerations based on thermal distributions of Q-balls indicate that results achieved in two-dimensional simulations should apply to three dimensions as well. On the other hand two-dimensional simulations are computationally less demanding and larger number of them was feasible. Consequently, the authors explored a larger parameter space varying the initial energy-to-charge ratio of the condensate. They reported that the lumps initially formed are not Q-balls, but excited states and the relaxation process to a Q-ball lasts very long and can be quite complicated. Also the correlations between Q-balls deviates from random, i.e. the mean distance between Q-balls is less than one would expect for a random distribution, which could leave a distinctive imprint on the CMB.

2.3.2 Q-ball Cosmology

The Q-balls in supersymmetric extensions of the Standard Model carry baryon number and are often dubbed B-balls (for a review, see [113]). The stability of Q-balls in the pure scalar theory (1.31) was discussed earlier. In the extended models, the field ϕ couples to other fields, which creates a decay mechanism. This was first considered in [114] where the complex scalar field ϕ was coupled to fermions. As a consequence, the Q-ball evaporates via pair production on the surface. The original study calculated the evaporation rate $\mathrm{d}Q/\mathrm{d}t$ in the thin wall approximation. This was revisited in [35] where evaporation rate was calculated with numerical means for realistic Q-ball profiles which do not have infinitely thin walls. The evaporation rate increases with decreasing charge, thus the evaporation proceeds with an ever accelerating rate. In that respect evaporation of Q-balls resembles a little bit black hole evaporation.

The evaporation obviously changes the stability conditions, like (1.46), discussed before. Remarkably, Q-balls in very flat potentials can still be absolutely stable. For a constant potential, $V(\varphi) \approx V_0$, the relation between energy and charge is not linear, as in the standard thin wall approximation (1.50) where the potential energy plays a leading role, but sublinear. In three dimensions it is given by $E \sim m\, Q^{3/4}$ [115]. The larger the charge, the smaller the energy per unit charge and it is energetically favourable to store charge in large Q-balls. One can see this by looking at energy per unit charge $E/Q \sim m\, Q^{-1/4}$. From the point of view of cosmology this becomes highly interesting, because the potentials in the gauge mediated scenarios of supersymmetry breaking are very flat and the above relation is valid. When such a Q-ball is large enough so that energy per baryon number (charge) becomes less than the mass of the lightest baryon m_b the Q-ball can emit, the Q-ball (or B-ball) is entirely stable. This yields the minimum charge

$$Q \gtrsim \left(\frac{m}{m_\mathrm{b}}\right)^4 . \tag{2.6}$$

A factor of order hundred has been missed because of omitting a geometric factor in the energy-charge relation, but as we see very shortly it would have only a minor contribution. One can assume that the lightest baryon is a nucleon, $m_\mathrm{b} \approx 1$ GeV. We know the physics up to the electroweak scale, so the lightest scalar must have a mass at least $m \approx 100$ GeV. Already this yields a lower limit $Q \gtrsim 10^8$ which is now a crude underestimate. Expecting new physics at the TeV scale and setting $m = 10^3$ GeV suggests $Q \gtrsim 10^{12}$. The stable Q-balls are huge, estimations of the baryon number are rather of the order 10^{26} and the mass of the Q-ball 10^{24} GeV. This equals roughly 1 gram, making such Q-balls macroscopic objects. Even though Q-balls couple via strong interaction (QCD) to ordinary matter, their enormous mass screens it. Q-balls with mass 10^{24} GeV could pass through a star with only a minimal change to their velocity. Therefore, heavy Q-balls are in practice weakly interacting, a property which makes them a viable dark matter candidate provided that these really large Q-balls are formed as the simulations suggest [111]. On the other hand, there is no other mechanism in sight than the Affleck-Dine process that could

create such large Q-balls, for example thermal effects would not produce such heavy solitons [105]. Therefore the observation of stable dark matter Q-balls would be strong evidence of the Affleck-Dine mechanism.

In the gravity mediated scenario the potentials are not very flat, but asymptotically quadratic (see e.g. [116]). The straightforward thin wall approximation is a good one and the energy of the Q-ball increases linearly with charge as (1.50) suggests. Therefore such Q-balls are likely to decay due to evaporation effects as there is no such limit as (2.6). While such unstable Q-balls are not a good dark matter candidate themselves, they may provide an even more appealing cosmological scenario. Unstable Q-balls decay to baryons, and can then potentially create the baryon asymmetry. In addition to baryons, there are the decay products of the squarks that were trapped in the Q-balls. These are supersymmetric particles and decay to LSPs. Thus decaying Q-balls can potentially produce both baryons and dark matter and the common origin of these two constituents can now also explain why their fractions Ω_{b} and Ω_{CDM} are comparable [37] (the connection between Ω_{b} and Ω_{CDM} can be reached also in gauge mediated scenario with stable Q-balls if thermal effects transport baryon number to the surrounding plasma [117]). The unstable Q-balls are long-lived because their evaporation is suppressed by the surface-to-volume ratio. Therefore the baryon production takes place relatively late. This has some beneficial aspects from the point of view of successful baryogenesis. Q-balls protect baryons from sphaleron effects at high temperature and if the Q-balls decay at temperature below 100 GeV also wash out in the electroweak phase transition is avoided [37].

While the simulations in [43, 111, 112] showed the formation of Q-balls from Affleck-Dine condensate under Hubble damping, the study [118] investigated the effects of expansion on an isolated Q-ball in a potential which is of the form shown in Figure 1.6. In essence, Q-balls were found to be robust objects in an expanding background even when the Hubble parameter H is fairly large; they conserve their charge and maintain their constant physical radius. Only when the expansion rate is so strong that H and the Q-ball frequency ω start to be comparable, there are clear changes to the Q-ball profile function. There can be significant charge migration to the surface so that the Q-ball profile may deviate drastically from the solu-

tion in the static spacetime yielding an inhomogeneous rotation frequency. The stability of Q-balls against expansion naturally further validates them as a dark matter candidate. On the other hand the authors suggested that the enhancement of the surface charge may cause fragmentation of the Q-ball in the very early Universe. How the large charge density on the surface changes the evaporation rate has not been studied either.

As discussed, phase transitions can lead to the formation of Q-balls [104], but their presence can influence the phase transition in return. Q-balls can enhance the transition [107, 119], Q-balls are like bubbles that provide nucleation sites, but unlike the standard subcritical bubbles that disappear, Q-balls can be stable independent of their size. So they can grow gradually via charge accretion to reach the critical size and then expand to fill the space with the true vacuum. Q-balls can thus facilitate a first order phase transition that otherwise would not take place [119]. This is very similar to the effects oscillons can cause.

2.4 Oscillons in Action

In this section we discuss oscillons mainly in a cosmological framework. Most of the studies are numerical and while some include three-dimensional simulations in expanding backgrounds, in many cases lower dimensional toy models have been considered in testing various scenarios.

2.4.1 Electroweak Oscillon

Oscillons are nontopological defects and could principally cause similar effects in the early Universe, or even presently, as discussed in the previous section considering Q-balls. Many of these features and possibilities are illustrated very neatly by the electroweak oscillon [63, 64]. First of all, it is such a heavy object that the energies required for its formation are likely to be available only in the early Universe. If formed, very long-lived oscillons could ultimately contribute to the dark matter content of the Universe. If electroweak oscillons could have survived until today, they would be a good dark matter or ultra-high energy cosmic ray candidate [64]. The mass of an electroweak oscillon, 30 TeV, is in the middle of the window of other

dark matter candidates, far less than that of heavy Q-balls, but larger than that of axions or LSP's in standard scenarios. Oscillons as dark matter have been considered also in the context of the axion potential [46, 120] as will be reviewed shortly.

However, oscillons as dark matter would require them to be extremely long-lived and stable against expansion as well as e.g. interaction with the thermal bath of photons, and their survival until today seems quite a remote possibility. Rather more realistic is to expect oscillons to behave in many ways like unstable Q-balls in the early Universe. The analogy there reaches farther than the long relaxation time of oscillating, excited Q-balls. Like Q-balls, the electroweak oscillon could decay into fermions. Exactly as in the case of Q-ball evaporation, while coupling to fermions could destabilise the oscillon, it simultaneously offers an appealing scenario for baryogenesis discussed in [64]. A decay mode to light quarks would namely provide a mechanism for out-of-equilibrium production. If this mode is suppressed and oscillons decay only relatively late, the washout of the baryon asymmetry could be avoided. It was further suggested in [64] that during the decay of the electroweak oscillon the field configuration collapses inwards resulting in a very high energy density. At this stage it is possible that the sphaleron barrier could be crossed and the conservation of fermion number violated. In contrast to B-ball baryogenesis in the context of the Affleck-Dine condensate, the scenario described above is a variant of baryon production within the electroweak theory. The major obstacles to electroweak baryogenesis are the minor departure from equilibrium and the tiny amount of CP violation (see e.g. [87]). Oscillons clearly have principally the potential to create the necessary non-equilibrium, but it is far less obvious if there is a path to a successful baryogenesis in the electroweak model. As mentioned, the non-equilibrium conditions could be created by low scale inflation, but the very weak CP violation remains a severe, if not even fatal, problem for cold electroweak baryogenesis [121]. Whether the electroweak oscillon has any true implications for baryogenesis cannot be addressed without further studies.

2.4.2 Formation of Oscillons

To play a role in cosmology oscillons must come into being in the first place. There have to be localised fluctuations in the field which have large enough deviation from the vacuum to trigger the onset of an oscillon. The inflationary expansion leaves the Universe in a very homogeneous state, but in the light of several studies of the subsequent evolution the emergence of oscillons seems to be, if not entirely generic, at least fairly common.

The stage of reheating after inflation has in many models a very non-linear nature. The energy transfer from the inflaton to the matter fields can take place via parametric resonance, a very rapid amplification of long-wavelength modes of fields. This is often called preheating as the resulting state is not a thermal one. The effective temperature at this stage can be so high that symmetry restoration can take place locally [122]. The parametric resonance is followed by a phase characterised by the formation and interaction of bubble-like inhomogeneities, observed in simulations both after chaotic inflation [123] and $\lambda\phi^4$ inflation [124]. The dynamics of tachyonic preheating after hybrid inflation was studied in [122]. Tachyonic transitions occur in hybrid inflaton models when the inflaton rolls down the potential and is damped quickly. The simulations performed in [122] showed the appearance of local energy concentrations that the authors called "hot spots". These were formed both in two- and three-dimensional simulations. Simulations of a tachyonic transition in the SU(2) model have also led to oscillating energy concentrations [125].

While not every energy concentration is an oscillon, there are studies where this identification has been done. [126] reported two- and three-dimensional simulations of the growth of fluctuations in a supersymmetric hybrid inflation model. The study considered the classical evolution of the scalar sector of the theory and found roughly circular or spherical lumps forming. These were stable during the limited dynamical range of the simulations. The investigation of these inflaton condensate lumps showed that the field inside the energy concentration oscillates in time thus confirming that these lumps are long-lived oscillons and not concentrations of energy without any coherent structure that fade away rapidly. A significant result is that almost all the energy is concentrated in these lumps,

very much like the charge of the Affleck-Dine condensate becomes confined in Q-balls [43, 111]. This observation is supported by another study [127], which we review later, where the fraction of energy stored in oscillons was also found to be 50% of the total or more. Already qualitatively it is easy to reason that oscillons can be initially more abundant than topological defects as they result from the amplification of sub-horizon fluctuations without any bound related to causality. The authors did not observe any cosmic strings forming in the simulation volume in [126] and argue that the typical separation of cosmic strings in the model would be around the horizon size [128] (on the other hand, topological defects have much larger individual energies, which enhances their impact). A post-inflationary era during which the energy density is dominated by nontopological solitons could have significant cosmological consequences.

Some of these were discussed in [46] when growth of inhomogeneities in the axion field was studied (see also [120]). The axion solves the strong-CP problem of QCD and is a viable dark matter candidate (for current constraints see e.g. [129]). The axion results from the breaking of global U(1) symmetry, the Peccei-Quinn symmetry, but remains massless until the QCD phase transition where it acquires a light mass around 10^{-6} eV. The axion potential is essentially given by the sine-Gordon model (1.12) with a temperature-dependent coupling. Though the model has now a discrete symmetry, the domain wall problem there can be avoided. This is because the network consists of both domain walls and strings which cause a rapid decay of the walls (this kind of network has been studied e.g. in [95]). The three-dimensional simulations performed in [46] started with a white-noise distribution on large scales. The evolution results in large amplitude peaks in the energy density. Inside these energy concentrations, called axitons by the authors, the field performs rapid, large amplitude oscillations. This was seen clearly by studying the initially formed axiton configurations in one-dimensional simulations with longer dynamical range. The ultimate interest of the study was the enhancement of the inhomogeneities due to nonlinear axion dynamics. If the clumps are dense enough, they form gravitationally bound axion miniclusters. If a large fraction of axions condense into miniclusters, it has a great impact on the properties of axion dark matter as well as its experimental searches. Simulations suggest that

suitable seeds for the clustering form via oscillons as an intermediate state.

As a side remark, long-lived oscillons in three-dimensional sine-Gordon model would be very interesting for other reasons as well. In another context they have been called pion breather states [130] which could form in the QCD phase transition. In an uniformly isospin-polarised domain pions can be described by the sine-Gordon Lagrangian. It has been suggested that pionic breathers could form as remnants of the so-called disordered chiral condensate and they have been studied in [130, 131]. It was noted that if such objects would form in heavy ion colliders, like RHIC, they would yield a spectacular signal because their decay generates approximately 200 pions.

Studies of oscillon formation in less than three dimensions include [132] and [127]. In [132] a scalar theory was considered with a potential V inspired by the gravity meditated supersymmetry breaking scenario,

$$V(\phi) = \frac{1}{2}m^2\phi^2\left(1 + K\log\left(\frac{\phi^2}{M^2}\right)\right), \tag{2.7}$$

where $K < 0$ and M are constants. Tiny density contrasts were used analogously to the initial conditions applied in the study of Q-balls. The two-dimensional simulations showed that the energy density deforms into lumps which are close to a Gaussian shape.

The starting point of the study [127] was to use quasi-thermal initial conditions. The model, originally introduced in [49], is defined by the potential

$$V(\phi) = \frac{1}{2}m^2\left(\phi^2 - \frac{g}{2}\phi^4 + \frac{g^2}{3}\phi^6\right), \tag{2.8}$$

where g is a constant. Quasi-thermal initial conditions in this case stands for a thermal state of a free scalar field which naturally deviates from the thermal equilibrium in the completely nonlinear theory. However, starting the simulations initialised with the field ϕ at high initial temperature T this approach should be justified. The field was evolved numerically in a one-dimensional expanding background. Simulations showed the formation of oscillons in copious numbers when the temperature drops below $T \approx m/g$. The estimates based on a threshold in the energy density indicate that

half of the energy in the system is in oscillons, this fraction being quite insensitive to the initial conditions, like temperature.

In conclusion, oscillons form in several models with varying initial conditions and dimensionality. Because oscillons are more stable in low dimensions, their formation may be enhanced as well. It is worth noticing that both potentials (2.7) and (2.8) are convex functions and in contrast to quartic (1.5) and sine-Gordon (1.12) potentials they have no inflection points, but nonetheless they support oscillons.

2.4.3 Oscillons in Phase Transitions

The re-discovery of oscillons came about while studying the dynamics of phase transitions [52, 53], so the effects oscillons could have in phase transitions were considered from very early on. The issue has been studied specifically in a series of papers [133–135]. The starting point in all of them is an initial thermal state prepared using a technique based on Langevin equations. This is then followed by an instantaneous quench where the potential V is switched from single- to double-well form. In Figures 2.1 and 2.2 this corresponds to a change from the uppermost curve to the bottom one. Two-dimensional simulations showed a synchronous emergence of oscillons after the quench bearing likeness to a parametric resonance [133]. This is then yet another process where oscillons are formed and a very different one from the one reported in [127] where oscillons appear after a gradual cooling of the system.

Presence of the oscillons can affect the phase transitions in two ways. The emergence of oscillons can speed up the decay of the false vacuum considerably. Even though oscillons are typically small bubbles, they are persistent compared to conventional subcritical bubbles that fade away quickly. A coalescence of two oscillons can create a critical bubble that then expands. This phenomenon, called resonant nucleation, was found to be very efficient in [134] where two-dimensional simulations were performed, but it is also effective in three dimensions [135]. While the false vacuum decay is accelerated and the transition becomes weaker, later on the presence of oscillons has quite an opposite effect. They are bottlenecks for equipartition, delaying the diffusion of energy from low-wavelength

modes to higher ones [133].

Contact with the physics of the electroweak phase transition was made in [136]. It was concluded that thermal fluctuations at the electroweak scale cannot create oscillons since they are not strong enough to produce subcritical bubbles whose amplitude reaches beyond the inflection point of the potential to trigger an oscillon. This result could be altered with the existence of small-amplitude oscillons. The situation could be also different in phase transitions at higher energy scales. The resonant nucleation has been considered in the context of old inflation. The original inflation model by Guth [101] suffers from the fact that the false vacuum whose energy drives the inflation does not decay, as the expansion proceeds faster than the decay. Consequently, the inflationary phase does not terminate either. If the transition is greatly accelerated by the presence of oscillons this problem might be avoided [137].

It has been also speculated recently that resonant nucleation could help in understanding the dark energy. The smallness of the cosmological constant Λ is a puzzle. One suggestion how this tiny value could have emerged, is related to resonant tunneling in the vast landscape of vacua predicted by considerations in fundamental string theory. In other words, there has been a sequence of tunneling events from vacua with high energy to ones with lower energy [138]. Tunneling is however in general not a very efficient process unless it takes place via an intermediate state which fullfills resonance conditions. While this is a well-established phenomenon in quantum mechanics, it has been shown that there is no resonant tunneling from a homogeneous initial state in quantum field theory [139]. Relaxing the assumption of homogeneous false vacuum as an initial state, the resonant tunneling can occur, at least in a specific model [140], via an oscillon as an intermediate state.

Chapter 3

Oscillons in Two Dimensions

The majority of studies has considered oscillons in three spatial dimensions and assuming a spherically symmetric geometry. In this chapter we present numerical investigations of oscillons in two dimensions in theories with quartic and sine-Gordon potentials. The motivation to study two-dimensional models stems from the fact that they serve as a bridge between one-dimensional theories where there is the stable breather solution (1.22) and those in three dimensions which are physically most realistic. Oscillons in two-dimensional ϕ^4 theory has been studied before in [141], where a so-called adiabatic damping technique was introduced and exploited. Oscillons were not seen to decay in the performed simulations thus indicating a far longer lifetime than in three dimensions. Another difference with three-dimensional oscillons was the lack of the bounce window found in [54] and discussed earlier. Instead, initial conditions with all radii resulted in the onset of an oscillon solution in two dimensions. This was interpreted as evidence that the attractor basin in the field-configuration space is particularly large in two dimensions, which was again suggested in [142].

In contrast to the study [141], where radial symmetry in two dimensions was assumed, we perform fully (2+1)-dimensional simulations. These can also reveal a potential decay of the oscillon by coupling to nonradial deformations, which cannot be covered when restricting to radial, or spherical, symmetry. Furthermore we monitor quantities over the whole span of the simulations and concentrate largely on a study in frequency space

via Fourier analysis of oscillations. Our investigations here deal with the properties of oscillons when they are created with a Gaussian initial ansatz instead of as a consequence of the evolution after random initial conditions. However, we try to draw the connection by reporting on the boosted oscillons in the end of this chapter. First we present results from a stationary set-up using Fourier analysis to determine the time evolution of the oscillation frequency when an oscillon is created using a radially symmetric initial ansatz. Later we and study the collapse to radial symmetry for an elliptic ansatz.

3.1 The Models and Numerical Set-up

The Lagrangian for a single real scalar field ϕ in the presence of a potential V was given by (1.2). Now in two spatial dimensions, $\mu = 0, 1, 2$. The equation of motion thus reads

$$\ddot{\phi} - \nabla^2\phi + V'(\phi) = 0. \tag{3.1}$$

At the classical level the vacuum expectation value and couplings in the potential can be scaled out. In the degenerate double-well quartic potential (1.5) of ϕ^4 theory we set $\eta = 1$ and $\lambda = 1$ so that

$$V(\phi) = \frac{1}{4}(\phi^2 - 1)^2 \,. \tag{3.2}$$

In the potential of the sine-Gordon model (1.12) we choose the following scaling

$$V(\phi) = \frac{1}{\pi^2}\big(1 + \cos(\pi\phi)\big) \,. \tag{3.3}$$

Notice that both (3.2) and (3.3) have minima at $\phi = \pm 1$ and a local maximum at $\phi = 0$.

The field equation (3.1) is evolved on a two-dimensional lattice with periodic boundary conditions using a leapfrog update and a three-point spatial Laplacian accurate to $\mathrm{O}(dx^2)$. The lattice spacing for the data shown is set to be $dx = 0.25$ and the time step $dt = 0.05$. With that

choice the fluctuations in total energy on the lattice are less than 0.2% over 9×10^7 iteration steps. We tested our method by reducing both dx and dt from the above mentioned choice without observing significant difference in the quantities of main interest here. Unless otherwise stated the simulations for the data shown were carried out in 800^2 lattices.

In a lattice with periodic boundary conditions, the emitted radiation returns to a certain extent back to the region of the oscillon. Nevertheless, we choose here periodic boundary conditions rather than absorbing ones because we wish to explore the stability of the oscillons to the small perturbations from any radiation emitted, and because we wish to allow them to move without hitting any boundaries. In [141] the so-called adiabatic damping was used to remove radiation in (1+1)-dimensional simulations by introducing dissipative zones on the one-dimensional grid. In practice, this can be done by setting a location dependent friction coefficient in the equations of motion. However, it is not entirely clear how to implement the adiabatic damping technique in a two-dimensional rectangular lattice so that the isotropy of the system is simultaneously strictly conserved, though spatially dependent damping has been used in a study of excited Q-balls in (2+1)-dimensional simulations [44]. Periodic boundary conditions were used also in the study of the electroweak oscillon. The line of reasoning is that as long the region where the oscillon is localised is a small fraction of the total lattice, the radiation is sufficiently diffuse not to affect the oscillon drastically and the only potential influence would be destabilisation [63, 64]. In the electroweak model the implementation of the adiabatic damping method would be also much more challenging as it had to accommodate gauge invariance. The requirement of diffuse radiation is well realised with our choice of the size of the grid. Results from studies with absorbing boundaries are reported in the next chapter.

3.2 Properties

We start with a Gaussian ansatz

$$\phi(r) = \eta \left(1 - A \cdot \exp(-r^2/r_0^2)\right) \tag{3.4}$$

where r is the distance to the center of an oscillon $r = (x_1^2 + x_2^2)^{1/2}$ and the width of the distribution was set to be $r_0 \simeq 2.9$ (in units of $(\sqrt{\lambda}\,\eta)^{-1}$), suggested to be an optimal choice for a long living oscillon in three dimensions [53]. As mentioned in the introduction earlier studies have established the sensitivity both to the spatial size r_0 and the amplitude of the deviation from vacuum. For the data shown, the amplitude is $A = 1$ so that the center of the oscillon is located in the local maximum of the potential. This choice sets the initial deviation from vacuum to be drastic and ensures that we observe the non-linear features of the theory and not a small, linear perturbation around the vacuum. Too large amplitude leads to a violent dynamics and does not create an oscillon.

It should be immediately noted that the Gaussian ansatz does not provide the right description of radiation far from the oscillon core. This can be seen by studying a small, radially symmetric spatial perturbation φ around the vacuum. For a quartic potential (1.5) the substitution $\phi = \eta - \varphi(r)$ into (3.1) leads at lowest order to

$$\frac{\mathrm{d}^2\varphi(r)}{\mathrm{d}^2 r} + \frac{1}{r}\frac{\mathrm{d}\varphi(r)}{\mathrm{d}r} + m^2\varphi(r) = 0, \tag{3.5}$$

where $m^2 = 2\lambda\eta^2$. This Bessel equation has solution $\varphi = C_1 \cdot J_0(mr) + C_2 \cdot Y_0(mr)$, where J_ν and Y_ν are the Bessel functions of the first and second kind, respectively. Both are oscillatory with an amplitude decaying asymptotically as $r^{-1/2}$, thus much more slowly than (3.4). Repeating the calculation for sine-Gordon potential (1.12) yields the same result with $m^2 = \alpha$. The parameter m defines a mass in the theory as $m^2 = V''(\phi)$, where ϕ is at the minimum of the potential. The linearised wave equation (3.5) serves as the starting point when the absorbing boundary conditions are derived in the following chapter.

3.2.1 ϕ^4 Potential

The shape of the oscillon profile in ϕ^4 theory is shown in Figure 3.1. Deviation from the Gaussian form is clearly visible, but not drastic. The maximum excursion of the center even exceeds the initial displacement A when the preferred shape is taken. Figure 3.2 illustrates the broadening

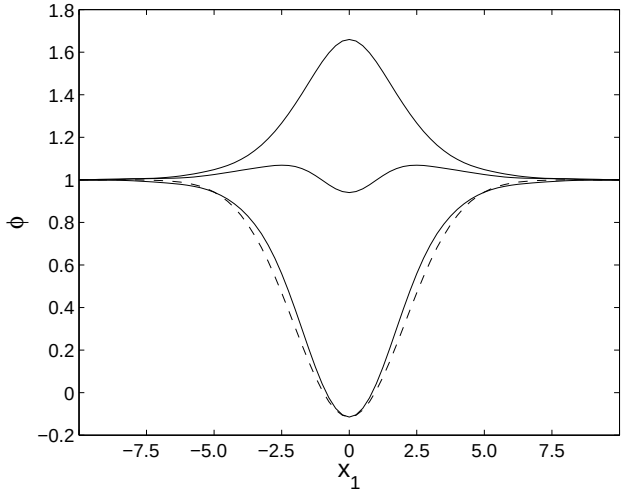

Figure 3.1. Oscillon profile at the extrema (above and below the vacuum expectation value) and at crossing the minimum of the potential in ϕ^4 theory. Dashed line shows a Gaussian form with the same amplitude and width r_0 of the initial profile.

of the energy density $\rho(\boldsymbol{x})$ in the extremum and contraction to a highly concentrated spike as the centre of the oscillon crosses the minimum of the potential when kinetic energy dominates the density. The value of the field at the centre of the oscillon as a function of time is plotted in the Figure 3.3. The oscillation over one period is not symmetric, as the field makes a larger excursion and changes more slowly where the potential is flatter whereas it changes rapidly in the region of steeper potential. Variation of the amplitude does not become apparent over this short period of time.

Figure 3.4 shows the total energy and the energy inside shells of radius $r = 0.5r_0$, $1.5r_0$ and $2.5r_0$ around the centre of the oscillon over the complete simulation time (4.5×10^6). Size $r = 0.5r_0$ shows large fluctuations depending on the phase of the oscillation, which can be well understood on the basis of the behaviour of $\rho(\boldsymbol{x})$ over a period shown in Figure 3.2. On the contrary the shell $r = 2.5r_0$ shows a relatively thin line and provides a

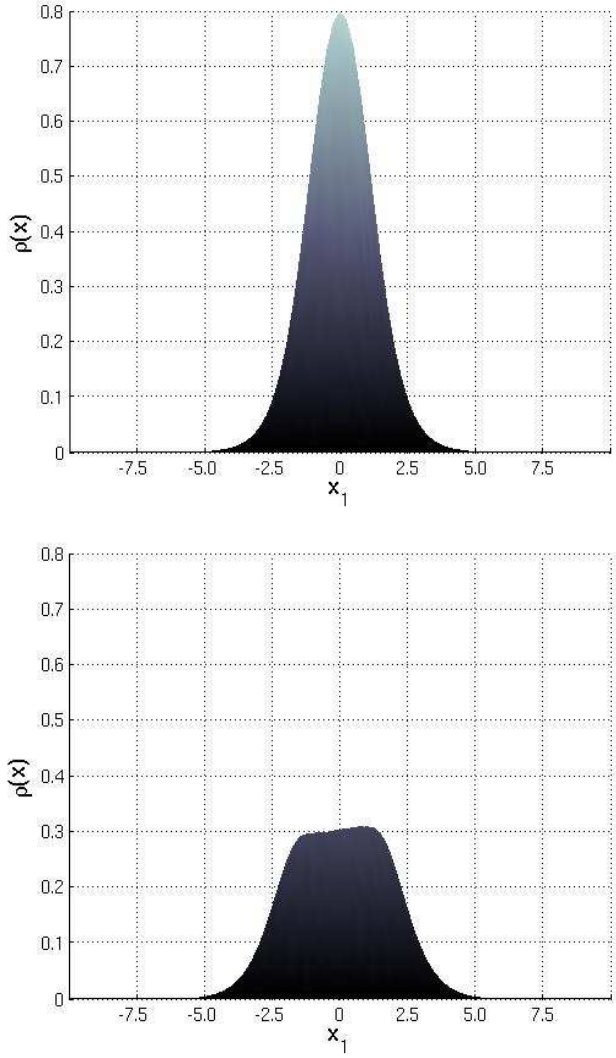

Figure 3.2. Energy density $\rho(\boldsymbol{x})$ of an oscillon in ϕ^4 theory at the moment of crossing the minimum of the potential (above) and at the moment of maximum excursion (below), corresponding to the field ϕ shown by the lowest solid line in Figure 3.1.

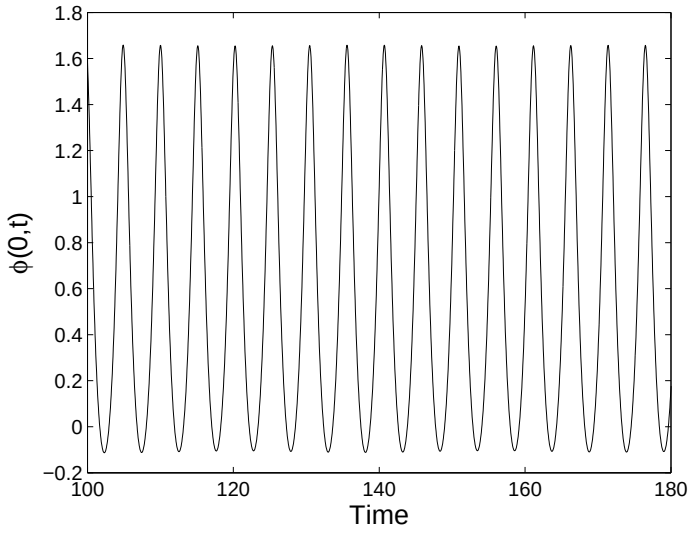

Figure 3.3. Field at the centre of the ϕ^4 oscillon $\phi(t, 0)$ as a function of time t.

good estimator for the energy of an oscillon. This is further confirmed by comparing the energy inside shells of radius $r = 2.5r_0$ and $5r_0$. They track each other well as can be seen in Figure 3.5, where they are plotted for a shorter time interval from the beginning of the simulation. Figure 3.5 also shows clearly a period in the beginning when the oscillon radiates energy rapidly. After that the rate of energy loss is much weaker and the data suggests some evidence for the existence of flat plateaus where the energy stays at a constant value and abrupt drops between them. These plateaus could be interpreted as a series of metastable states. The existence of excited, or metastable, states of oscillons has been speculated, see e.g. [58, 141]. However, here this feature turns out to be caused by the radiation on the lattice, see Figure 4.4 and the related discussion in the next chapter. In the end of the simulation more than 70% of the energy is still localised in an area covering less than 0.5% of the lattice.

The power spectrum of oscillations was studied by performing Fourier transforms of the field at the centre $\phi(t, 0)$ in consecutive time intervals. The length of the interval for the data shown is 5000 in natural units, which

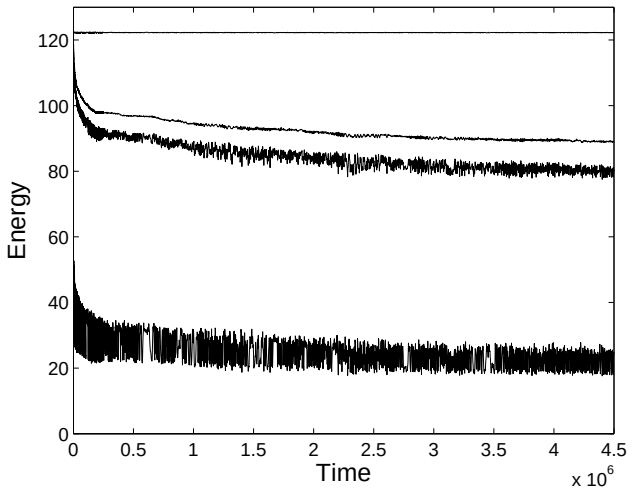

Figure 3.4. Total energy in the lattice and energy inside the consecutive shells with radius $r = 2.5\,r_0$, $1.5\,r_0$ and $0.5\,r_0$ around the center of the ϕ^4 oscillon (from top to bottom) as a function of time t.

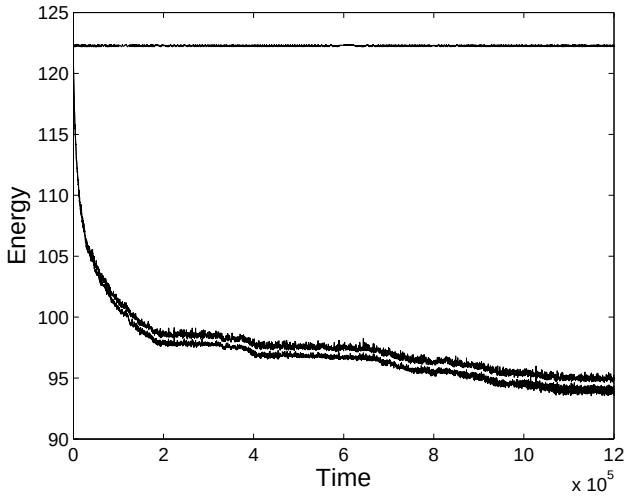

Figure 3.5. Detail from Figure 3.4, showing the total energy in the lattice and the energy inside shells with radius $r = 5\,r_0$ and $2.5\,r_0$ around the center of the ϕ^4 oscillon (from top to bottom).

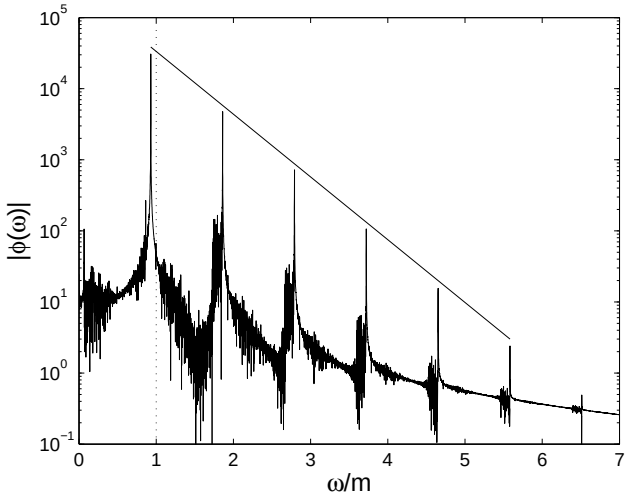

Figure 3.6. Power spectrum of field at centre of ϕ^4 oscillon $|\phi(\omega)|$ taken in time interval $2.5 \cdot 10^5 < t < 2.55 \cdot 10^5$. Solid line is a guide to the eye for an exponential fit to the amplitudes of the first six peaks, $\exp(-b\,\omega/m)$ with a slope $b = 2.03$. Vertical dotted line shows the radiation frequency $\omega = m$.

amounts to just over 0.1% of the total length covered by the simulation. An interval of that length includes approximately 10^3 oscillations. A typical example of the power spectrum is shown in Figure 3.6. There are very distinctive peaks that rise several orders of magnitude higher than the background between them. The first, highest peak just below frequency $\omega = m$ indicates the oscillation frequency, the other peaks are located at the integer multiplies of that one. Up to seven peaks can be identified in the power spectra.

There is a significant change in the shape of the peaks during the time evolution. In the beginning, when the oscillon radiates and the core loses energy reasonably fast, peaks are fairly broad, but later on when the oscillon 'stabilises' they become extremely narrow. During the early evolution it is possible to make a fit to the Breit-Wigner formula

$$F(\omega) = \frac{K}{(\omega - \omega_0)^2 + (\Gamma/2)^2}\,, \tag{3.6}$$

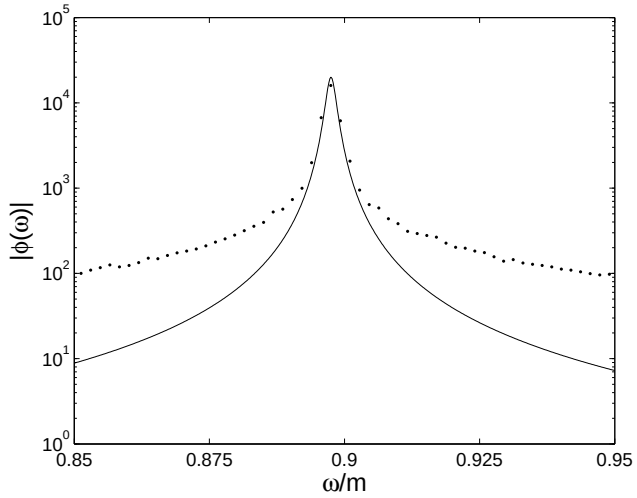

Figure 3.7. Fit (solid line) to Breit-Wigner form of first peak (dots) ϕ^4 oscillon taken in time interval $10^4 < t < 1.25{\cdot}10^4$: $\omega_0 = 0.8975, \Gamma = 0.0020$ and $K = 0.02$.

where ω_0 is now the peak frequency. A fit to the first peak is shown in Figure 3.7. It cannot be considered very accurate, but it gives an order of magnitude estimate of the decay width Γ during the era in which the oscillon radiates its energy strongly. Later on the peaks have no width in the restricted time interval where the Fourier transformation is made (our choice for the length of the interval is fairly optimal as longer intervals tend to reveal a shift of the peak frequency, not improve the width).

The amplitudes of the peaks in Figure 3.6 clearly obey an exponential decay law as a function of the frequency ω. The deviations at the level shown in the figure are most likely due to the limited accuracy of discrete Fourier transformation. The data also includes a low frequency peak (just next to the $|\phi(\omega, 0)|$ axis), with a frequency approximately 0.06. There is a slight variation of the amplitude, a beat, with the corresponding period around 100 in natural time units (though not present in Figure 3.3), which we believe is the cause of the structure.

Not only the shape of the peaks but also their frequency changes during the time evolution. There exists a strong correlation between the energy

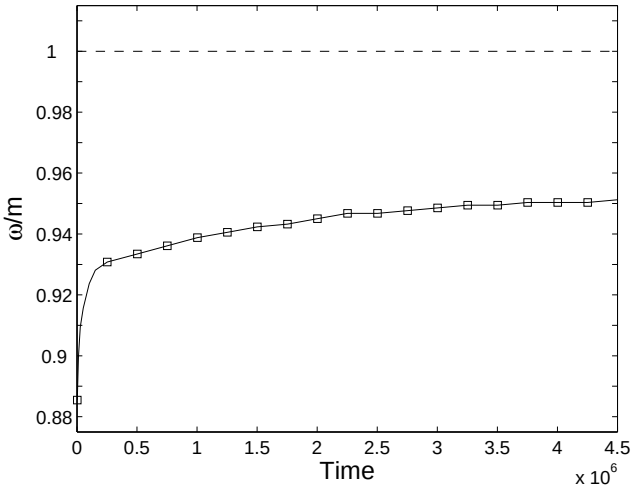

Figure 3.8. Oscillation frequency corresponding to the location of the highest peak as a function of time for a ϕ^4 oscillon. The precision of the measurement of the frequency is 0.002 at the scale of ω/m due to the limited time interval the Fourier transformation is made. Some data points close to the frequency axis are not marked with $\Box$ for clarity. Dashed line shows the radiation frequency $\omega = m$.

in the oscillon (shell radius $r = 2.5r_0$ in Figure 3.4) and the oscillation frequency, i.e. location of the highest peak, shown in Figure 3.8 as a function of time. During the early period when the oscillon radiates strongly, the frequency increases rapidly, but then the growth slows down drastically as the rate of energy loss becomes tiny. The time evolution of the oscillation frequency is the key which predicts the lifetime of an oscillon: as long as the frequency stays below radiation frequency, the oscillon cannot directly radiate all of its energy and disappear. As the rate of energy loss decreases, the increase in frequency slows down. Turning it the other way round this is in agreement with [58] and [59] who have reported the radiation rate decrease as ω/m increases. The minimum of the radiation rate is located at $\omega/m \simeq 0.97$ in the three-dimensional theory.

Though we have not evolved oscillons in our simulation longer than 4.5×10^6 time units, we can give bounds on the lifetime of an oscillon on the basis of the evolution of the oscillation frequency. Even a linear fit

to the second half of the points in Figure 3.8 suggests that the radiation frequency is not reached before a time of a few times 10^7, or about 10^7 oscillations. This is now based on the assumption that oscillons do not decay before reaching the radiation frequency $\omega = m$. While this remains an assumption in this context, it is however supported by the consideration of small-amplitude quasi-breathers [60] suggesting that the energy of a two-dimensional quasi-breather is monotonically decreasing and does not have a minimum for any frequency $\omega < m$. Lifetimes of the same order 10^7 were reported in [141] where oscillons were investigated in two dimensions, but with (1+1)-dimensional simulations assuming radial symmetry. However, the lifetime can be much longer since the slope of the line in Figure 3.8 is clearly flattening out and the radiation rate is a strongly decreasing function of frequency, as reported in [58, 59].

Setting the original amplitude A too high (e.g. $A = 10$ in the direction where the potential is steeper) will not lead to an oscillon, the initial concentration of energy does not stay localised but spreads rapidly. Starting with a configuration that has a larger amplitude and consequently more energy than the one shown in Figure 3.1 can still evolve to an oscillon but with a modulated amplitude. This effect becomes most apparent in the case of the sine-Gordon potential.

3.2.2 Sine-Gordon Potential

Persistent oscillations in the radially symmetric sine-Gordon equation were studied in [143] and extreme sensitivity both to the form and the amplitude of the initial deviation from the vacuum were observed. A complicated initial profile was used to obtain a minimally radiating pseudobreather. We have not been able to create a 'minimal' oscillon with a Gaussian initial ansatz - though the profile of an oscillon in the sine-Gordon potential is also fairly close to Gaussian (Figure 3.9), oscillations have modulated amplitude (Figure 3.10) whose period depends on the initial amplitude A. Figure 3.11 shows total energy in the lattice and energy inside shells of several radii around the centre of the oscillon in a simulation that spans the evolution up to time 10^6. There is no apparent evidence for energy plateaus in Figure 3.11.

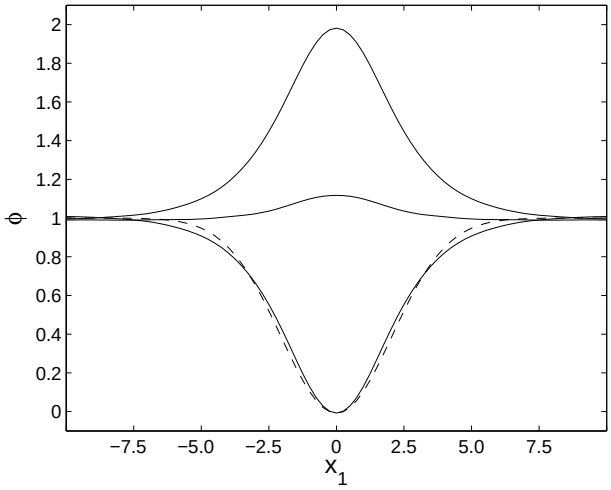

Figure 3.9. Oscillon profile at the extrema (above and below the vacuum expectation value) and at crossing the minimum of the potential in sine-Gordon model. Dashed line shows a Gaussian form with the same amplitude and the width r_0 of the initial profile.

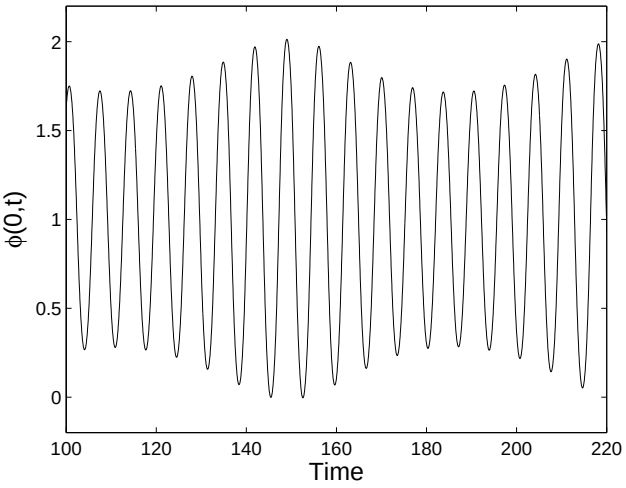

Figure 3.10. Field at the centre of the sine-Gordon oscillon ($\phi(t,0)$) as a function of time t.

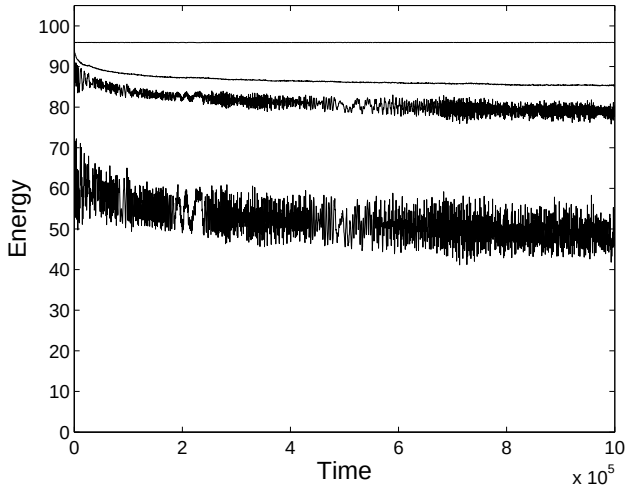

Figure 3.11. Total energy in the lattice and energy inside the consecutive shells with radius $r = 5.0\,r_0$, $2.0\,r_0$ and $1.0\,r_0$ around the center of the sine-Gordon oscillon (from top to bottom) as a function of time t.

The same choice of the interval for Fourier transformation was used as in ϕ^4 theory that now corresponds to 0.5% of the total time of the simulation. The study in frequency space shows similar basic features as in ϕ^4 theory with some significant differences. There are no even powers of oscillation frequency ω_0 present in the spectrum as can be seen in Figure 3.12 and at the very best only the first four peaks are visible in the power spectrum. The sine-Gordon potential (1.12) is symmetric around minima in contrast to the quartic potential (1.5) as illustrated in Figure 1.1. Necessarily, in the ansatz (1.62) there cannot be a time-independent component, i.e. $f_0 \equiv 0$. Furthermore, due to the symmetry of the potential around the minimum, all amplitudes f_n with even n vanish. As the amplitudes of the peaks decrease exponentially also here, but only half of them are present compared to Figure 3.6 of ϕ^4 theory, this suggests that the ansatz (1.62) would be a particularly good approximation for an oscillon in sine-Gordon potential, or potentially in any other symmetric potential that allows oscillons. There is no sign of low frequency structure in Figure 3.12 in contrast

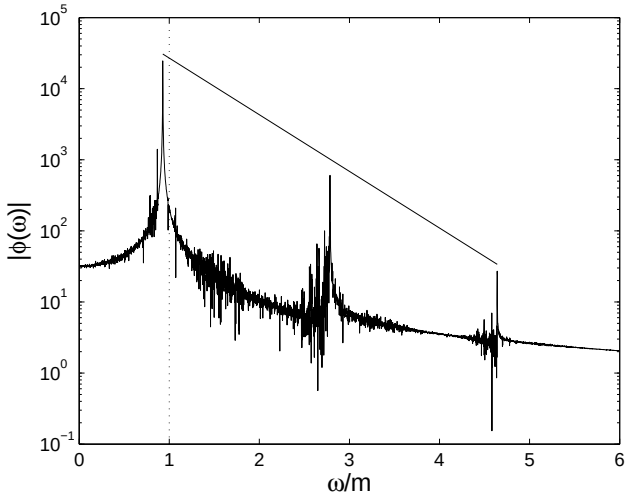

Figure 3.12. Power spectrum of field at centre of sine-Gordon oscillon $|\phi(\omega)|$ taken in time interval $1.5 \cdot 10^5 < t < 1.55 \cdot 10^5$. Solid line is a guide to eye for an exponential fit to peak amplitudes, $\exp(-b\,\omega/m)$ with a slope $b = 1.84$. Vertical dotted line shows the radiation frequency $\omega = m$.

to Figure 3.6.

The time evolution of the frequency of the first peak in the power spectrum of the sine-Gordon oscillon is shown in Figure 3.13 from a simulation that was evolved for 10^6 time units. The oscillation frequency starts initially closer to the lowest radiation frequency compared to the quartic potential, but there is no drastic increase either, which may be due to the weaker coupling to radiative modes as even multiples of the oscillation frequency are absent. Also here the increase in the oscillation frequency slows down in the course of time and even linear extrapolation yields a life-time estimate, i.e. intersection with the radiation frequency, around 10^7 time units, but it could be much larger, especially as the study of the power spectrum suggests weaker radiative modes.

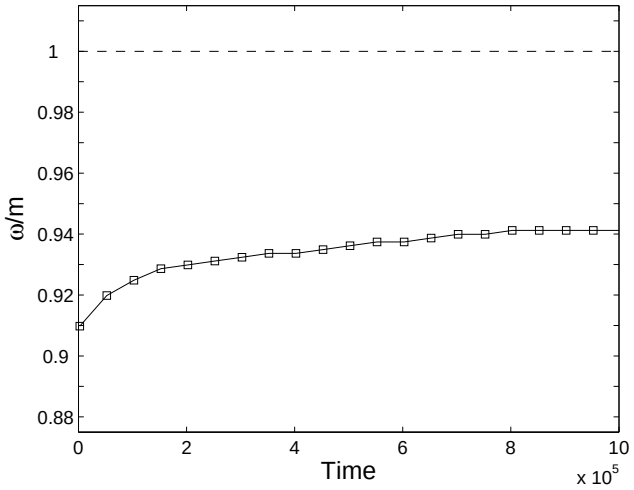

Figure 3.13. Oscillation frequency as a function of time for the sine-Gordon oscillon. The precision of the measurement of the frequency is 0.003 at the scale of ω/m. Dashed line shows the radiation frequency $\omega = m$.

3.3 Elliptical Oscillons

The relative ease to create an oscillon together with the energy shells pointing to the existence of successive plateaus and thus a series of metastable states gives rise to the question of whether the field configuration of an oscillon is unique. A very modest approach to the uniqueness is a study of an initial configuration which is not radially symmetric. As our numerical method was not restricted to spherical symmetry, we start with a Gaussian ansatz with different width in x_1 and x_2 direction. Oscillons emerging from the collapse of asymmetric bubbles were studied in [142] using a sort of effective radius as a measure. We investigate here the time evolution of the ellipticity via the quadrupole moment ϱ_{ij} of the energy density $\rho(t, \boldsymbol{x})$

$$\varrho_{ij} = \frac{\int d^2x\, x_i x_j \rho(t, \boldsymbol{x})}{\int d^2x\, \rho(t, \boldsymbol{x})}\,. \tag{3.7}$$

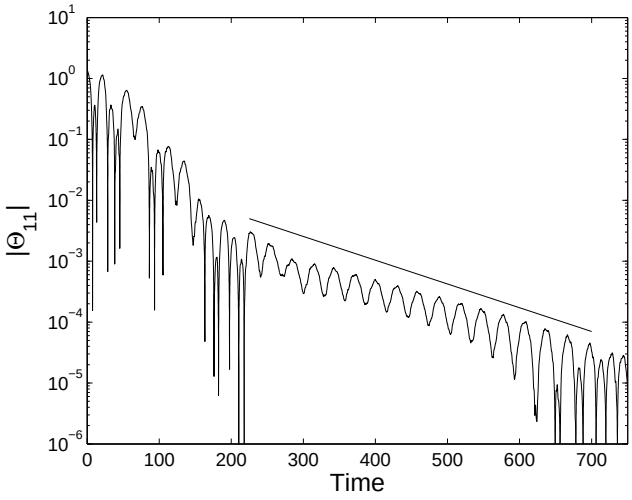

Figure 3.14. Ellipticity, $|\Theta_{11}|$, of an oscillon as a function of time in ϕ^4 theory. Here $r_0 = 3.9$ is the initial width of the major axis, whereas the minor axis has been set to have width 2.6. Straight, solid line is a guide to eye of an exponential fit, $\exp(-\varsigma t)$ with a slope $\varsigma = 0.009$.

Ellipticity is given by the eigenvalues of the traceless matrix

$$\Theta_{ij} = \varrho_{ij} - \frac{1}{2}\,\delta_{ij} \sum_{n=1}^{2} \varrho_{nn}\,. \tag{3.8}$$

Because the major and minor axis are along x_1 and x_2 the off-diagonal entries Θ_{12}, Θ_{21} vanish (a good check for the numerical accuracy of the method: $|\Theta_{12}|, |\Theta_{21}| < 10^{-15}$) and then the ellipticity is given directly by the diagonal elements of (3.8). We measured ϱ_{ij} in a square of length 20 in physical units located in the center of the lattice. Lattice size was set to be 4800^2 and thus no boundary effects will be important until far after time = 600. Figure 3.14 shows $|\Theta_{11}|$ as a function of time when initially the ratio of the major to the minor axes was set to be 3 : 2 (with the width in the x_1 direction being $r_0 = 3.9$). The oscillon rapidly approaches a spherical profile and ellipticity disappears in exponential phases.

The orientation of the major axis changes in a way that is not ob-

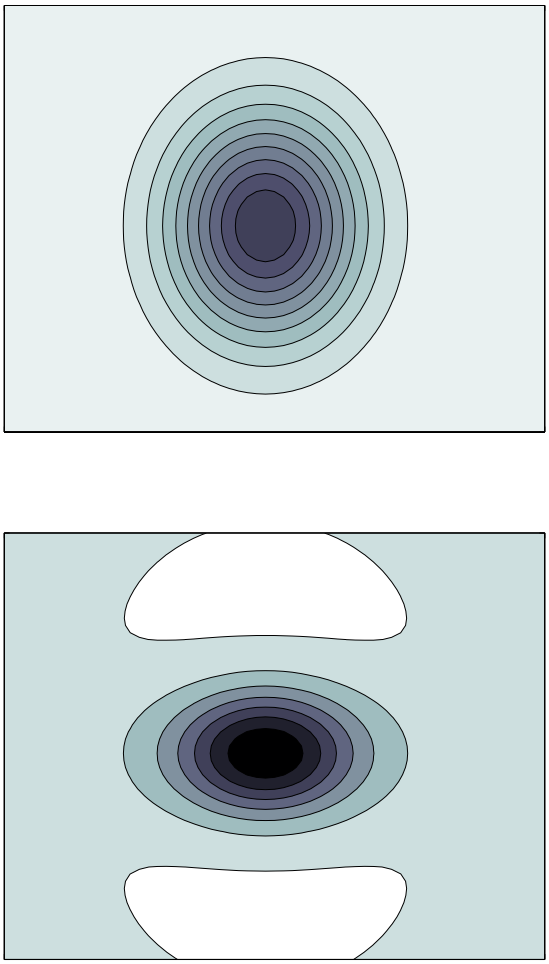

Figure 3.15. Contours of $\phi(\mathbf{x})$ for the initial elliptic Gaussian profile and after two oscillations (time = 10.6) in ϕ^4 theory. The field ϕ varies from -0.4 (darkest grey) to values slightly above 1.0 (shown in white).

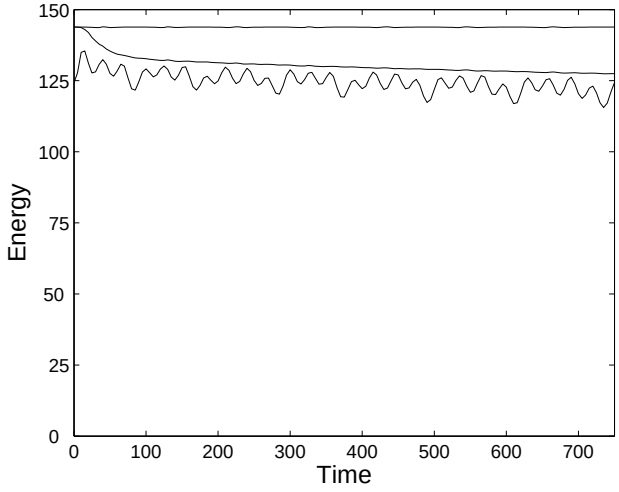

Figure 3.16. Total energy and energy inside shells of radius $r = 2.5\,r_0$ and $r = 1.0\,r_0$ around the center of the ϕ^4 oscillon as a function of time (from top to bottom). Here $r_0 = 3.9$ is the initial width of the major axis.

viously periodic (zero crossings of Θ_{11} appearing in the Figure 3.14 as almost vertical lines, which is demonstrated much more illustratively in Figure 3.15). This is in fact the only erratic behaviour of oscillations we have observed and is distantly reminiscent of the chaotic time evolution of the bion states reported in [16] and discussed in the context of the kink-antikink scattering. Figure 3.16 shows total energy and energy inside two shells around the oscillon core. Though spherically symmetric shells are not an entirely adequate method to measure energy of an elliptic configuration, they give a reasonable estimate and show that while ellipticity disappears exponentially, decreasing by four orders of magnitude, the energy inside the oscillon core has decreased by just over 10% indicating a quick collapse to a spherical shape.

Figure 3.17 shows the ellipticity and 3.18 the total energy and energy inside shells in a simulation with the same set-up but for the sine-Gordon potential. The main features are qualitatively similar, ellipticity decays rapidly and oscillon collapses into spherical profile. Here the orientation

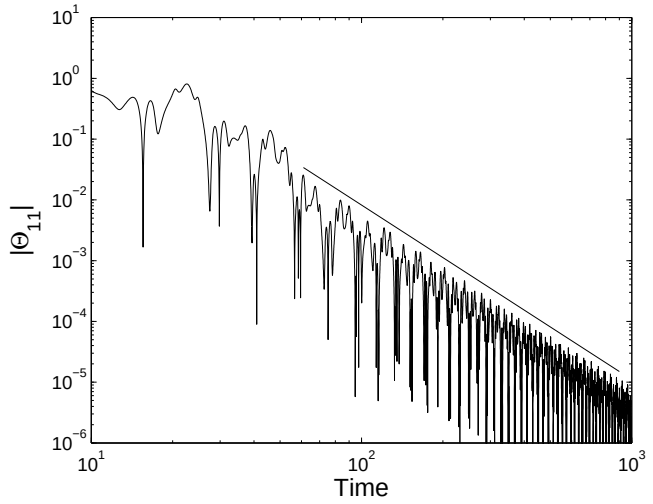

Figure 3.17. Ellipticity, $|\Theta_{11}|$, of an oscillon as a function of time in sine-Gordon model. Straight, solid line is guide to eye of a power law fit, $t^{-\varepsilon}$ with a slope $\varepsilon = 2.87$.

of major axis changes frequently in an almost periodic way. Moreover, the decay of ellipticity $|\Theta_{11}|$ (in Figure 3.17) matches better to a power law than an exponential fit. It is very tempting to interpret this result on the basis of the obtained differences of oscillons in frequency space between quartic and sine-Gordon potentials. As both even and odd multiples of the oscillation frequency are present in case of the quartic potential, the first radiative frequency, twice the basic frequency, has far greater amplitude than in the sine-Gordon potential where the first radiative mode has stronger suppression, its frequency being three times the basic oscillation frequency. Therefore it seems plausible that an oscillon in the quartic potential (3.2) can radiate its asymmetry exponentially, while initial deviation from spherical symmetry decays only with a power law in sine-Gordon potential.

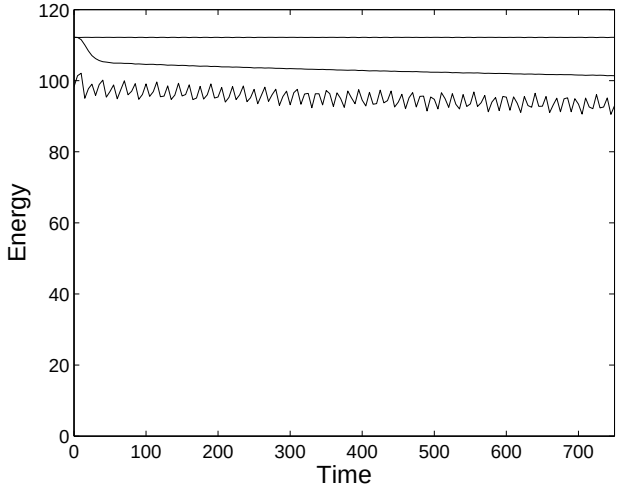

Figure 3.18. Total energy and energy inside shells of radius $r = 2.5\,r_0$ and $r = 1.0\,r_0$ around the center of the sine-Gordon oscillon as a function of time (from top to bottom). Here $r_0 = 3.9$ is the initial width of the major axis.

3.4 Colliding Oscillons

If created in Nature via some mechanism like collapse of domains, oscillons would have translational momentum initially. We prepare moving oscillons to draw the connection between oscillons given birth in simulations with random initial conditions and stationary oscillons created with e.g. a Gaussian ansatz. In practice the oscillon that starts with a Gaussian initial profile is first allowed to evolve for a few oscillations and then the configuration is Lorentz boosted. For all the data shown the velocity of moving oscillons is set to be $v \simeq 0.5$. We point out already here that oscillons originating from collapsing domains seem to generally have higher velocities, as will be seen later.

Fast moving oscillons become some sort of waves in the laboratory coordinates: they have typically at least two 'phases', part of the wave front lies above, part below the minimum of the potential. There is a precise correspondence between boosted oscillons and the objects travelling on wave

fronts originating from collapsing domains. We have also checked that a boosted oscillon is persistent like a stationary one and can wrap around the lattice (with periodic boundary conditions) travelling long distances without demise.

We finish by reporting the results of studies where oscillons were made to collide. There is a twofold reasoning for this study. We want to examine what kind of interactions oscillons have and thus try to understand their character this way. Secondly, if created in large numbers in phase transitions, encounters are inevitable and the behaviour of oscillons in those collisions has thus impact on the subsequent evolution of the system. The general rule is that a collision does not destroy an oscillon: we have never witnessed that the first collision between oscillons would have lead to the demise of either of them.

Figure 3.19 shows snapshots from a collision between immobile and moving (velocity $v = 0.5$) oscillons. After the collision there is one fast moving oscillon continuing in the direction of original translational momentum and a fairly stationary oscillon whose center, however, has moved slightly from the original location. This example seems thus almost interactionless. However, amount of interaction and momentum transfer depends on the relative phases of oscillons at the moment of collision and can result in two moving oscillons. This effect can be examined as the set-up for collision has been prepared by creating the immobile oscillon at an arbitrary time on the lattice. Therefore we can control the phase of stationary oscillon via the moment of its creation. The effect of the phase is demonstrated in Figure 3.20 where the set-up is otherwise the same as in Figure 3.19, but the initially stationary oscillon is time 1.3 behind the previous one corresponding to approximately 1/4 of the period. Here both the oscillons move left after the collision. In all collisions, some energy initially bound in oscillons is released to radiation, very much like in the collisions of kinks in ϕ^4 theory. The radiations can be seen in snapshots in small amplitude waves.

Figure 3.21 shows snapshots of a collision between two boosted oscillons with the same velocity ($v = 0.5$) travelling into opposite directions. As can be seen, oscillons pass through each other. We have also changed the alignment of oscillons so that the collision does not occur head on. Fig-

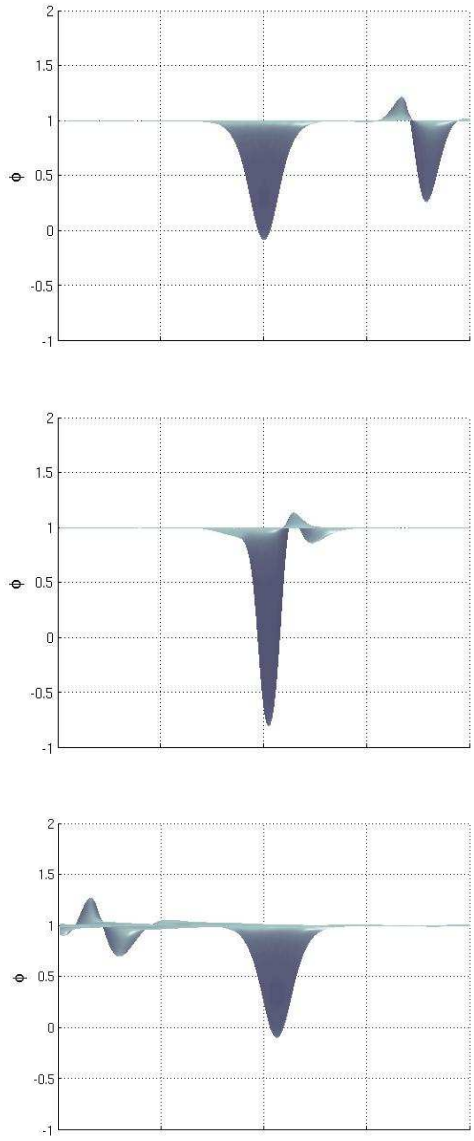

Figure 3.19. Sequence of snapshots at times $t = 0, 36.25, 80$ of an on-axis collision of two oscillons, one immobile (originally located in the middle) and one moving (from right to left), in ϕ^4 theory. After the impact there is one moving oscillon and a stationary one which is slightly displaced from the original position. The structure between the oscillons in the last snapshot is radiation (small-amplitude waves) created in the impact.

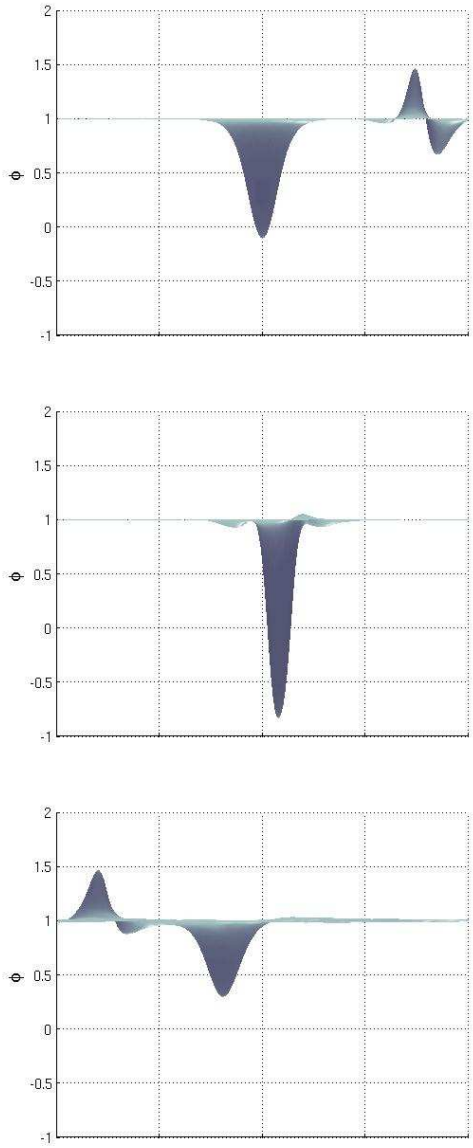

Figure 3.20. Sequence of snapshots at times $t = 0, 36.75, 100$ of an on-axis collision of two oscillons in ϕ^4 theory. The phase at collision set $1/4$ of the period different compared to Figure 3.19. Both oscillons move to left after the impact.

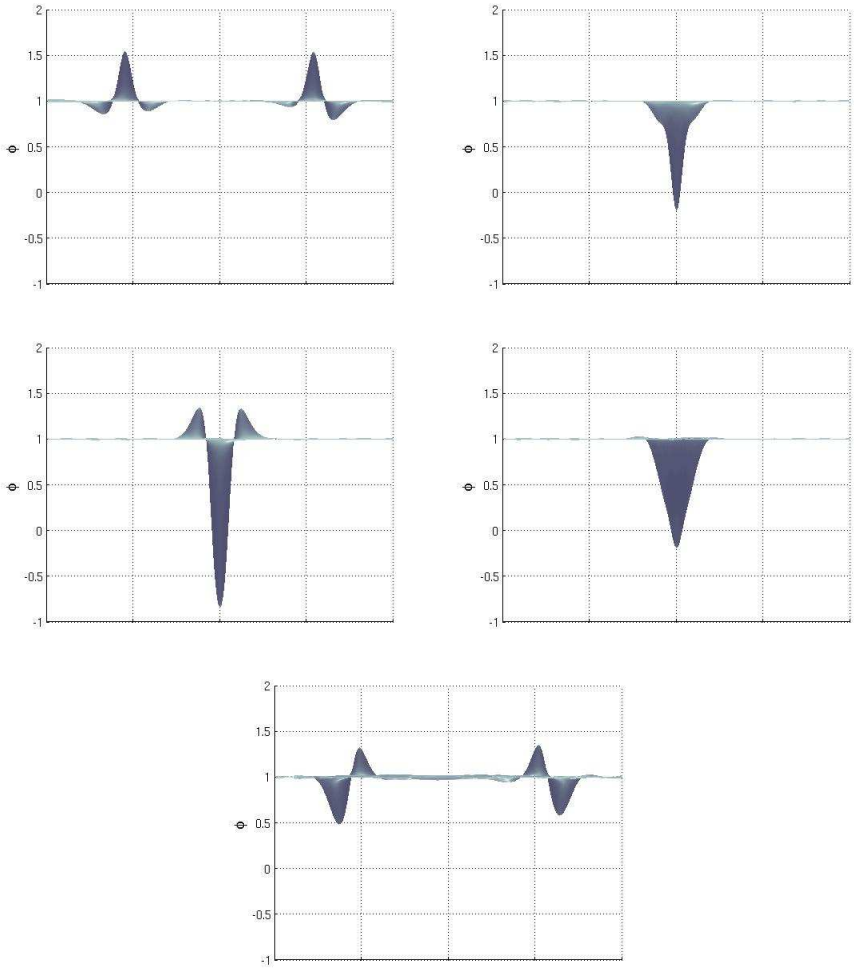

Figure 3.21. Sequence of snapshots at times $t = 0$, 29.5, 30.5, 31.5, 60.5 of an on-axis collision of two oscillons in ϕ^4 theory.

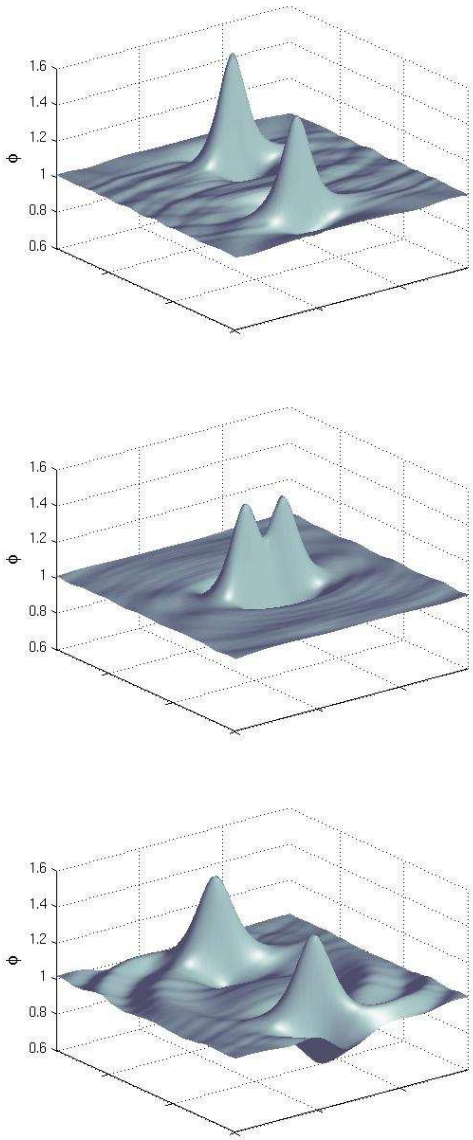

Figure 3.22. Sequence of snapshots at times $t = 0$, 22, 49 of an off-axis collision of two oscillons in ϕ^4 theory. Radiation appears particularly clearly as ring-like waves in the last snapshot.

ure 3.22 shows snapshots where the deviation in the alignment between the centers of oscillons is 5.0 in physical units. The set-up leads to an attractive scattering, oscillons do not behave as classical particle like objects, but their paths bend towards each other, the angle between initial and final velocity being approximately 20°. The radiation is particularly well visible in the last snapshot; there are ring-like waves centered at the point of impact. Collisions with a non-zero impact parameter are examined more systematically in the last chapter.

3.5 Conclusions

In this chapter oscillons were studied in two dimensions for ϕ^4 and sine-Gordon potentials numerically using periodic boundary conditions. We evolved stationary oscillons for 10^6 time units or longer. This is in good agreement with the results obtained in [141] where (1+1)-dimensional simulations were carried out assuming radial symmetry, but three orders of magnitude larger than the life time, $10^3\, m^{-1}$, reported in [132] where two-dimensional simulations were performed e.g. for potential (2.7). Furthermore, we examined the power spectrum of oscillations and observed that the basic oscillation frequency is just below the radiation frequency. Study in frequency space not only suggested much longer life time on the basis of the time evolution of the oscillation frequency than we could directly probe, but also points to the validity of the separable ansatz (1.62) in two dimensions. Though we have not evolved the oscillon in sine-Gordon potential as long, the analysis of the power spectrum suggests that it might be even more persistent than oscillons in ϕ^4 theory in spite of the modulated amplitude.

Furthermore, we considered here collapse to a radial shape after asymmetric initial conditions. The quick decay of elliptic perturbations is in good agreement with [142] indicating a large attractor basin for oscillons in two dimensions. Collapse to a spherical shape in three dimensions has been considered only in case of the electroweak oscillon, but with a very small asymmetry [64].

Studies of Lorentz boosted oscillons and collisions between them show also persistence of these objects and point to a behaviour that is very

similar to solitons. As our study was carried out on lattices with periodic boundary conditions, the radiation oscillons emit comes to some extent back to the centre of the lattice where oscillon is located. This can be viewed as a small perturbation and the long survival of oscillons in the set-up as their persistence to radiation. On the other hand, incoming radiation can also have an opposite effect pumping energy back into oscillon and thus extending the lifetime [58]. Even in the latter case our study has relevance in the situation where oscillons could absorb energy from the environment, like a weak heat bath or a laboratory experiment in a closed system. We turn now to the absorbing boundary conditions.

Chapter 4

Absorbing Boundary Conditions

In the previous chapter we studied oscillons in two dimensions omitting the effects of radiation on the lattice with periodic boundary conditions. In this chapter we re-visit the stability and time evolution of oscillons using now lattices with absorbing boundaries that will remove the radiation from the simulation box. This method also allows us to directly monitor the strength of radiation oscillons emit. Absorbing boundary conditions are an alternative to the, already mentioned, adiabatic damping technique, introduced in [141]. This approach has been successfully used also in [59] within the spherically symmetric approximation in a one-dimensional lattice varying the physical dimension in ϕ^4 theory.

While implementing the absorbing boundary conditions in any dimensional rectangular grid is principally straightforward, we also carry out (1+1)-dimensional simulations assuming radial symmetry after deriving the absorbing boundary condition in polar coordinates. First of all, the radial symmetry seems to be a valid approximation as the results of the previous chapter also demonstrate. More importantly, such simulations are computationally far less demanding and a much finer grid can be used. It turns out that such improved resolution together with longer dynamical range is also necessary in order to study the time evolution quantitatively.

Alongside with the absorbing boundary conditions we also introduce

a method inspired by the classical spectral function which we use for investigations in frequency space. The full power of this method becomes more apparent in the next chapter when moving oscillons are considered. This present chapter is organised as follows. The numerical set-up is reviewed in the following section. Then the spectral function in the classical approximation is introduced. We discuss the implications of absorbing boundary conditions first using quartic theory as an example. Then the main results are presented in ϕ^4 theory. We then go on to repeat the study in the sine-Gordon model. Finally, we report the results on a class of convex potentials. The equations of the absorbing boundary conditions are presented in the appendix.

4.1 Numerical Set-up

We continue to use the leapfrog update and a three-point spatial Laplacian accurate to $\mathrm{O}(dx^2)$. In the interior of the computational grid the field equation is still given by (3.1) and is evolved accordingly. At the boundaries a set of new equations is needed to absorb the massive radiation emitted by the oscillon. These equations are presented in the appendix in two and three dimensions, both in Cartesian coordinates and assuming spherical symmetry in polar and spherical coordinates, respectively.

The (2+1)-dimensional simulations are performed setting the lattice spacing to be $dx = 0.25$ and the time step $dt = 0.05$ as when periodic boundary conditions were utilised. Now total energy is naturally not conserved, so there is no such a direct measure for the numerical accuracy as with periodic boundary conditions. Later on we report on the precision we expect in (1+1)-dimensional simulations. In order to be able to straightforwardly compare with the previous results we also keep the size of the grid in 800^2. This means that for an oscillon located at the centre of the lattice its core is roughly at a distance of 100 units from the (nearest) boundary.

We continue by performing (1+1)-dimensional simulations assuming radial symmetry in two spatial dimensions. These permit the choice of a much finer lattice spacing which was varied keeping the ratio of time step and lattice spacing fixed and matching to the one used in (2+1)-

dimensional simulations, $dt : dx = 1 : 5$. Similarly the size of the one-dimensional grid was chosen so that the physical distance from the center of the oscillon to the absorbing boundary was always precisely 100 units. The majority of the simulations are performed on a grid of 10,001 lattice points and $dx = 0.01$, $dt = 0.002$.

We set the field ϕ and the field momentum $\Pi = \dot{\phi}$ at the origin $r = 0$ to have the same value as on the next lattice site with a non-zero value of the radius r. The good agreement with the data from (2+1)-dimensional simulations indicates that this boundary condition does not affect the results considerably. Another difference is that, while in (2+1)-dimensional simulations gradient energy is calculated from the difference in the value of the field on two nearest neighbouring lattice sites in each direction, we use three consecutive points in the grid to achieve precision accurate to $\mathrm{O}(dx^2)$ in (1+1)-dimensional simulations. In other words, the gradient is defined as

$$\frac{\partial\phi(t,r)}{\partial r} = \frac{\phi(t,r+dx) - \phi(t,r-dx)}{2\,dx}\,. \tag{4.1}$$

The shown data from (2+1)-dimensional simulations is averaged over a time interval (always short compared to the total span of the simulations) to suppress fluctuations and highlight the tendency in energy decrease.

4.2 Spectral Function in the Classical Approximation

The classical one-particle spectral function for a real scalar field ϕ can be defined through the Poisson bracket as

$$\Phi\,(t,\boldsymbol{x}) = -\,\langle\{\phi(t,\boldsymbol{x}),\phi(0,\mathbf{0})\}\rangle\ , \tag{4.2}$$

where the angle brackets denote an average over initial conditions. For a system in thermal equilibrium at temperature T, one can show [144, 145]

$$\Phi\,(t,\boldsymbol{x}) = -\frac{1}{T}\,\langle\,\Pi(t,\boldsymbol{x})\,\phi(0,\mathbf{0})\,\rangle\,, \tag{4.3}$$

where Π is the field momentum $\dot{\phi}$.

The numerical implementation of the correlator in (4.3) is straightforward in leapfrog discretization. In [145] the following symmetrized definition was suggested

$$\Phi\left(t,\boldsymbol{x}\right)=-\frac{1}{T}\left\langle \Pi(t+\frac{dt}{2},\boldsymbol{x})\,\frac{1}{2}\left(\phi(0,\mathbf{0})+\phi(dt,\mathbf{0})\right)\right\rangle . \tag{4.4}$$

The classical spectral function at zero spatial momentum $\Phi(t,\boldsymbol{p}=\mathbf{0})$ can be obtained from a volume average of (4.4). The spectral function in frequency space, $\Phi(\omega,\mathbf{0})\equiv\Phi(\omega)$, can in turn be derived by performing a Fourier transform.

We do not attempt to define temperature in what follows here, rather an isolated oscillon is at zero temperature though some temperature could be associated to the weak radiation background. We merely adopt the correlator of the field and field momentum as a useful quantity to monitor in order to determine frequencies present in the system under study. We simultaneously point out that our choice, inspired by the spectral function, is not unique, but other correlators, like e.g. the equal time correlator of ϕ and Π, could be used equally well. The choice of the reference point $\boldsymbol{x}=\mathbf{0}$ of the field ϕ in (4.3) obviously does not play a role in a homogeneous system where no lattice site is in special position. This is obviously not strictly true when we place a stationary oscillon in the middle of a lattice. Instead of choosing one lattice site, simulations averaging over all points in the lattice were performed. However, even though homogeneity cannot be directly assumed, an approximation of the spectral function at zero momentum where the correlator in (4.3) is replaced by the product of the average value of Π at given time and of ϕ at a reference time $t=0$, $\Phi(t)=\bar{\Pi}(t)\cdot\bar{\phi}(0)$, turns out to yield the same information in frequency space. Computationally this approximation is much more economical and will be used during the rest of this study. We show examples of the spectral function when discussing specific models.

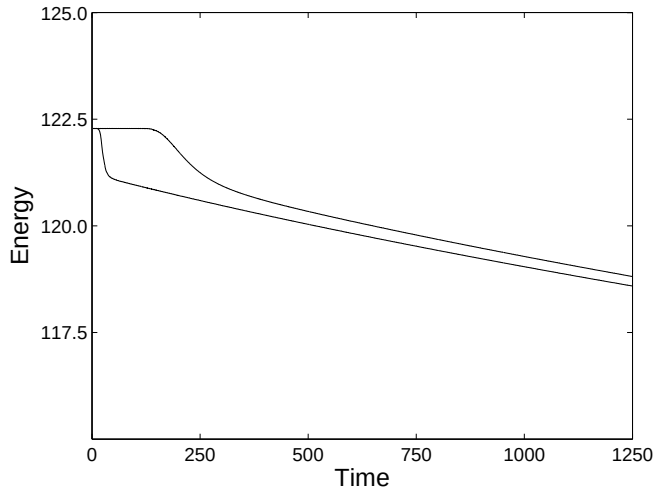

Figure 4.1. Total energy (top) in the two-dimensional lattice and energy inside a shell with radius $r = 5r_0$ (bottom) in ϕ^4 theory.

4.3 Quartic Potential

We continue to use both the same scaling given in (3.2) (the minima located at $\phi = \pm 1$ and the local maximum at $\phi = 0$) and the same initial data (3.4) with the same parameter values as in the previous chapter: $r_0 \simeq 2.9$ and $A = 1$, unless otherwise stated.

4.3.1 (2+1)-dimensional Simulations

Figure 4.1 shows the total energy in the lattice and energy inside a shell of radius $r = 5r_0$ around the centre of the lattice where the oscillon is located during the early stage of the simulation. The oscillon is well localised inside the shell of this size which, in turn, covers only a small fraction (less than 2%) of the entire lattice. From now on 'energy inside the shell' refers to a shell with this radius. The data shown are obtained by averaging the energy in a time interval whose length is 5 units, which corresponds roughly to the period of one oscillation. In the beginning more energy is shed by the oscillon when it settles from the Gaussian initial data into

its preferred shape (see Figure 3.1). This phase yields an abrupt drop in energy in the centre of the lattice which is followed then by a more steadily decrease. The total energy in the lattice remains constant for some time until the radiation reaches the boundaries of the grid. The decrease in the total energy is more gradual compared to the abrupt drop of the energy inside the shell; the spherical wave leaves the shell simultaneously in any direction whereas the waves arrive in the middle of the edge considerably earlier than in the corners of the rectangular lattice. However, apart from these apparent initial differences, clearly these two ways to measure energy track each other well later on. This is also a crucial check for the quality of the absorbing boundary conditions. The difference between these two quantities at any given time corresponds to the energy of the radiation emitted by the oscillon, which is moving away from the centre and to be annihilated at the boundaries. Therefore there is only a time delay, related to the size of the grid, until the total energy reaches the same value as the energy inside the centre of the lattice. The agreement improves further later on, when the oscillon radiates less. As an example the total energy in the lattice at time $t = 10^5$ is a mere 0.007% more than inside the shell of radius $r = 5r_0$. Consequently, we use the total energy in the lattice as the energy of an oscillon instead of the energy inside some arbitrary radius.

Naturally, the boundary conditions are not perfect, but some reflection inevitably takes place. This is unavoidable already due to the number of approximations made in the derivation of the equations at the boundaries, even before any effects related e.g. to the numerical accuracy. The absorption at the boundary is at its best when the direction of the incoming wave is perpendicular to the boundary. The greatest amount of reflection takes place at the corners which causes stronger waves in the direction of the diagonal of the lattice. This creates an anisotropy in the radiation background on the lattice which has quite a drastic consequence. In the course of time the oscillon slowly drifts away from the original location in the centre along the diagonal of the lattice. The displacement is considerable, but has never resulted in the oscillon being close to the boundaries of the lattice in the simulations. The maximum wave amplitude close to the boundaries is of the order 10^{-6} at the end of the simulations. We are unable to comment on how much this is caused by the incomplete absorp-

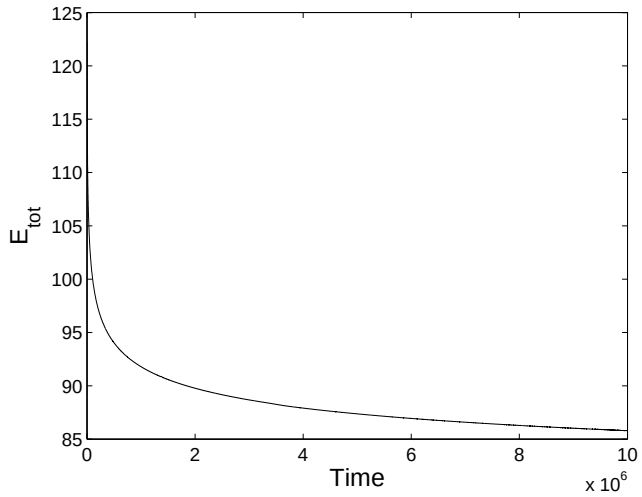

Figure 4.2. Total energy in the two-dimensional lattice in ϕ^4 theory over the whole span of the simulation, 10^7 time units.

tion leaving some remnant radiation in the simulation box or if it is still due to emission by the oscillon.

4.3.2 Properties in ϕ^4 Theory

Figure 4.2 shows the total energy in the lattice over the whole simulation that reached 10^7 time units. The data is now averaged over 100 measure points in a time interval of length $12,500$ units. Total energy is naturally a monotonically decreasing function of time, but the rate of decrease slows down raising the question of whether the total energy approaches asymptotically a constant value. This is demonstrated in Figure 4.3 where we plot the total energy E_{tot} subtracted by a number of constant values E_0 as a function of time on a logarithmic scale. For the smallest value shown, $E_0 = 55$, the curve of this difference is visibly bending upwards, while the inset shows clearly that $E_0 = 85$ yields an abrupt collapse. In conclusion, a power law is ruled out for these extreme values of the constant E_0. Intermediate values between these are closer to a straight line. Because the power law suppression of the radiation component is not strong, it is

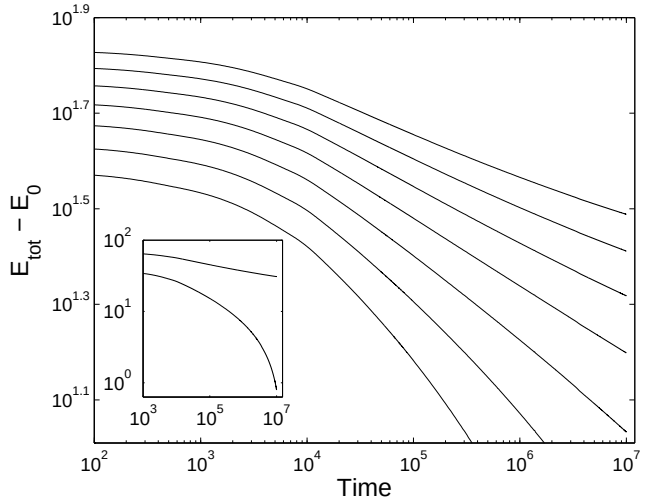

Figure 4.3. The difference of the total energy and a constant, $E_{\rm tot} - E_0$, on a logarithmic scale: $E_0 = 55, 60, 65, 70, 75, 80$ and 85 from top to bottom. The inset shows the utmost values $E_0 = 55$ and 85 over a larger scale on the energy axis.

difficult to single out the most likely value of E_0, but Figure 4.3 provides clear evidence for the existence of a unique constant E_0 and a power law. Thus the time evolution of total energy is governed by

$$\big(E_{\rm tot}(t) - E_0 \big) \sim t^{-\delta}\,, \tag{4.5}$$

where δ is a positive exponent governing the suppression of the radiative component with time. We discuss the physical interpretation of the asymptotic value of the energy E_0 at the end of this chapter.

Before turning to the analysis of the spectra we present a comparison between absorbing and periodic boundary conditions, used in the previous chapter. Figure 4.4 shows the total energy and energy inside a shell of radius $r = 5r_0$ in a simulation with periodic boundary conditions (shown already in Figure 3.5) together with the total energy in a lattice with absorbing boundary conditions with the same choice of parameters and no data set averaged. In the beginning the latter two track each other fairly

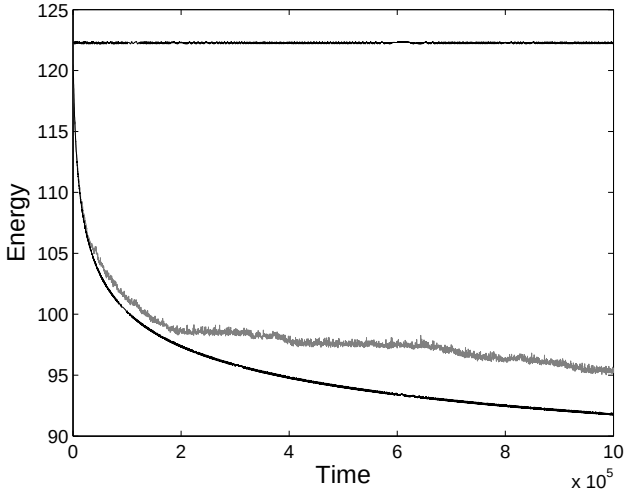

Figure 4.4. Total energy in a two-dimensional lattice with periodic boundary conditions (top) and with absorbing boundary conditions (bottom) and energy in a shell of radius $r = 5r_0$ (grey) on a lattice with periodic boundary conditions.

well, but later on there is clearly much more energy located in the centre of the lattice with periodic boundary conditions compared to simulations with absorbing boundaries. In the former case, the periods of almost constant energy inside a shell led us to speculate that the oscillon would go through a number of metastable states during its evolution. There is no sign of these plateaus when the study was repeated now with absorbing boundaries, but the data shows radiation with a slowly decreasing steady pace as also already demonstrated by Figure 4.2. Partially this excess energy shown by the simulation with periodic boundary conditions can be also attributed to radiation circulating around the lattice, but clearly the oscillon is excited compared to the evolution on a lattice with absorbing boundaries that remove radiation. Thus the interaction of an oscillon with radiation enhances its energy. Whatever the effects are on the quantitative level, we do not observe the demise of oscillons on the lattice with absorbing boundaries either, even though there is greater decrease in energy and the simulation has a longer time span.

4.3.3 Spectrum

We use the method based on the spectral function for the study in frequency space here for two reasons. First of all, the drifting of the oscillon does not allow observing oscillations simply via monitoring the field ϕ on a fixed lattice site. Secondly, as an average over the lattice the quantity Φ captures also the relative strength of the radiation in the simulation box.

Figure 4.5 shows the spectral function $\Phi(\omega)$ obtained by a Fourier transform in an interval of length 5000 in time units at an early stage (above) and towards the end of the simulation (below). The oscillation frequency ω_0 is naturally the most pronounced mode, its multiples appearing in the spectra exponentially suppressed. This suppression is slightly stronger later in the evolution, the slope is roughly 7% steeper in the right panel of the Figure 4.5. This is a marginal effect which is easily within the errors one can expect for the fit. Thus it is arguable if this could be an indication of an adjustment into a long living state where the modes that can carry radiation, $n > 1$ in (1.62) (setting $\omega = \omega_0$), have an extremely weak interaction.

The results using the spectral function Φ are qualitatively very similar to those obtained by the Fourier transform of the field $\phi(t, \boldsymbol{x})$ in the centre of the oscillon in the previous chapter where periodic boundary conditions were used. In fact, the agreement is even at the quantitative level in the suppression of the peaks with the increasing frequency ω. The value of the decay constant b is in good agreement with the one obtained using periodic boundary conditions in Figure 3.6. The discrepancy is well within the precision one expects for determining it from data and secondly the suppression evolves with time as well. Turning to the differences, here the signal in the spectral function at a later stage is very clean; there is hardly any noise present, the curve shown is a smooth line compared to Figure 3.6. We point out that fast Fourier transform of Jacobi functions in an interval yield a very similar signal, like the exponential suppression of the amplitudes of higher multiples of the basic frequency. An example is given in Figure 4.6 where the Jacobi function $\mathrm{sn}(\omega, 1/2)$ is shown. The resemblance is not co-incidental - Jacobi functions are solutions to a type

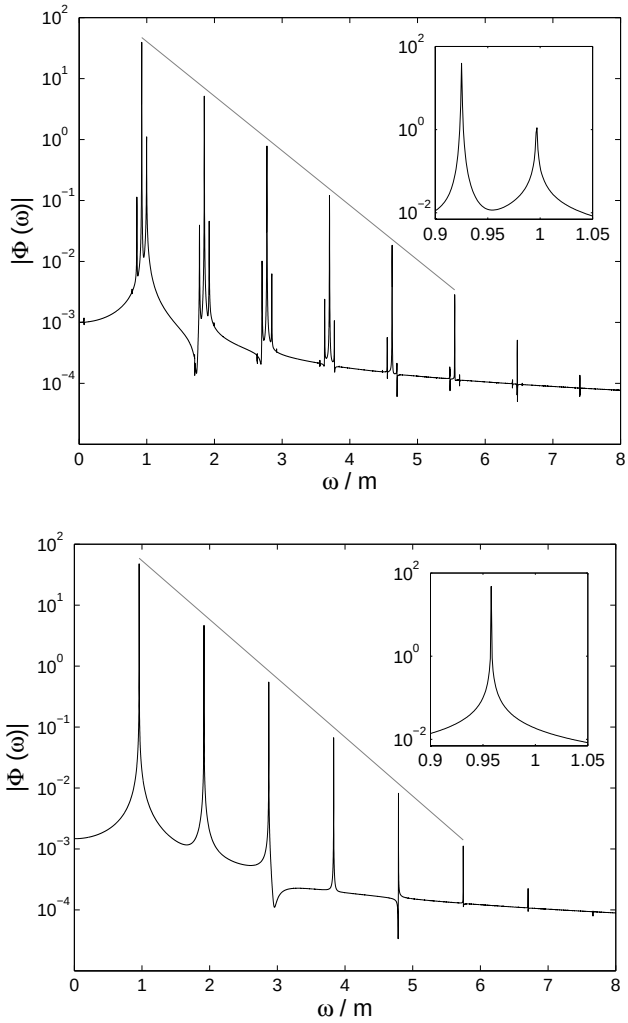

Figure 4.5. The spectral function $|\Phi(\omega)|$ over an interval of 5000 time units starting at time 10^5 (above) and at time $7.5 \cdot 10^6$ (below). The grey line is a guide to eye of the exponential $\exp(-b\,\omega/m)$ with slope $b = 2.06$ (above) and $b = 2.23$ (below). The insets show the spectrum around the radiation frequency $\omega \simeq m$.

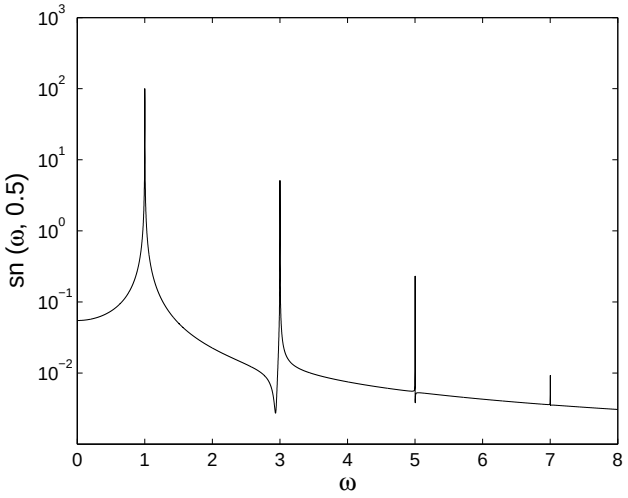

Figure 4.6. The Fourier transform of the Jacobi function $\mathrm{sn}(t, 1/2)$. The height of the first peak is normalised to 10^2 and its location to unity.

of elliptic non-linear differential equations of the form

$$\frac{\mathrm{d}^2 z}{\mathrm{d}t^2} = C_1\, z + C_2\, z^3\,. \tag{4.6}$$

One arrives at this kind of ordinary differential equation by omitting the spatial dependence in the equation of motion (3.1) in ϕ^4 theory. The volume averaging while obtaining the spectral function Φ naturally integrates out the spatial degrees of freedom (the spatial part of a small-amplitude quasi-breather in ϕ^4 theory is also determined by elliptic partial differential equations [60]).

The insets of Figure 4.5 show how the peak of the oscillation frequency ω_0 moves to the right indicating a higher frequency and simultaneously becoming narrower. The peak corresponding to radiation at $\omega = m$ is clearly present in the first inset, but disappears from the spectrum at late times. We interpret this as another piece of evidence of the efficiency of the absorbing boundary conditions and that they successfully remove radiation from the lattice.

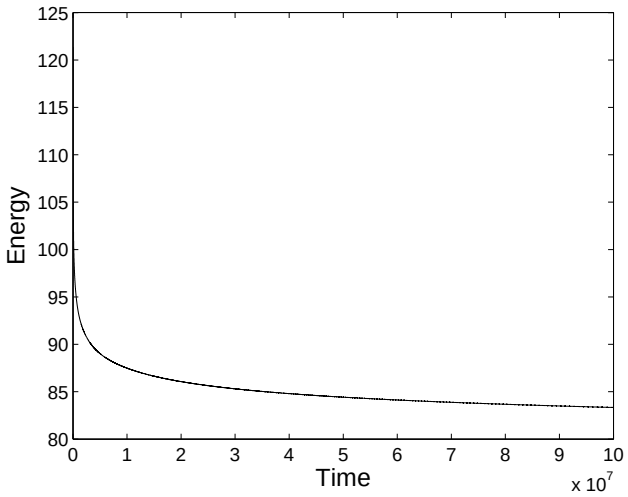

Figure 4.7. The energy inside a shell of radius $r = 5r_0$ from (1+1)-dimensional simulation in ϕ^4 theory.

4.3.4 (1+1)-dimensional Simulations

Performing (1+1)-dimensional simulations assuming radial symmetry on a one-dimensional grid is computationally less demanding and allows to reach roughly an order of magnitude larger time span. Equally important is the suppression of fluctuations in energy due to the finer lattice spacing that permits greater accuracy. No data set obtained in (1+1)-dimensional simulations is averaged over any time interval. Most of the discussion regarding (2+1)-dimensional simulations applies also here. However, the oscillon does not deviate from its original location due to the boundary condition at the origin. We therefore use the energy inside the shell of radius $r = 5r_0$ as a measure of the energy of an oscillon together with the total energy in the lattice.

There is no sign of the demise of the oscillon in 10^8 time units of evolution. Figure 4.7 shows the energy inside the shell over the whole simulation. The larger span in time permits now a more quantitative determination of the radiation losses so the values of the parameters E_0 and δ in (4.5) can be derived. Figure 4.8 shows the difference between the energy inside the

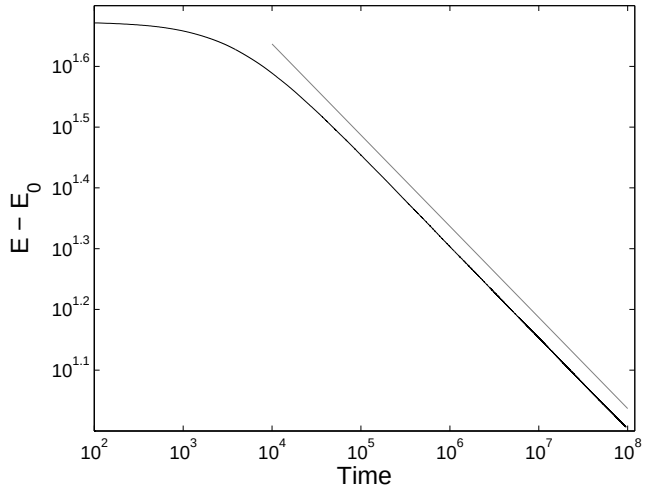

Figure 4.8. The difference of the energy inside a shell of radius $r = 5r_0$ and constant $E_0 = 73.25$. The grey straight line is a guide to eye showing a power law $(E - E_0) \sim t^{-\delta}$ with the negative slope $\delta = 0.15$.

shell and a constant $E_0 = 73.25$ on a logarithmic scale. The grey line is a guide to eye showing a negative slope -0.15. There is very good agreement to this over three orders of magnitude providing strong evidence for the power law decay of the radiative component governed by the exponent $-\delta = -0.15$.

4.4 Sine-Gordon Model

We continue to use the same scaling for the potential of the sine-Gordon model (3.3) so that locations of the minima are the same as in ϕ^4 theory, but here with mass $m^2 = 1$. We start with the same Gaussian ansatz as in ϕ^4 theory given by (3.4).

Figure 4.9 shows the total energy in the lattice. The maximum time in the (2+1)-dimensional simulation is 10^6 units. The data points shown are an average done in a time interval of length 2000 which contains 20 measure points. The search for a power law is shown in Figure 4.10. It is considerably more difficult to distinguish the straightest line from bending

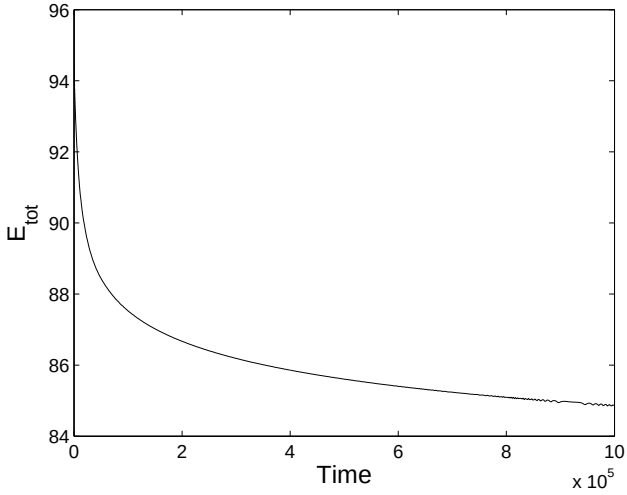

Figure 4.9. Total energy in the two-dimensional lattice in sine-Gordon model over the whole span of the simulation, 10^6 time units.

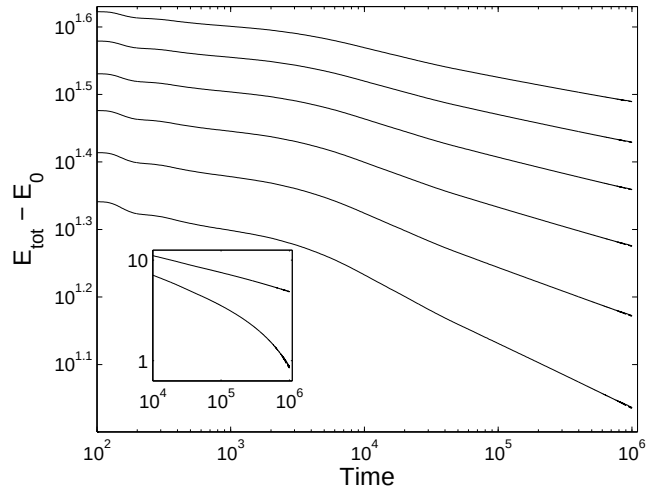

Figure 4.10. The difference of the total energy and a constant, $E_{\mathrm{tot}} - E_0$, on a logarithmic scale: $E_0 = 54, 58, 62, 66, 70$ and 74 from top to bottom. The inset shows the values $E_0 = 54$ and 84 over a larger scale on the energy axis.

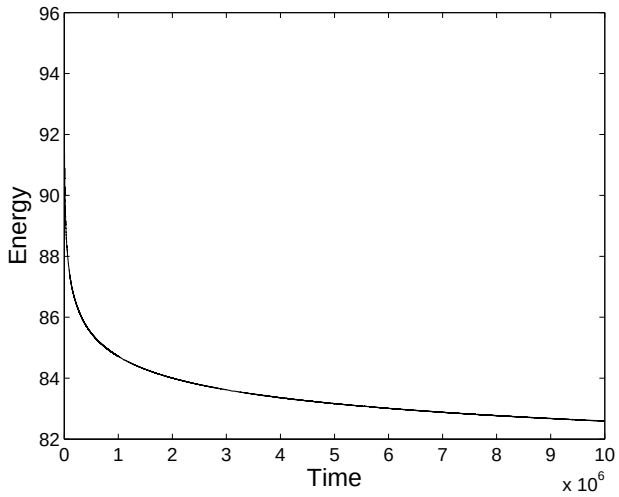

Figure 4.11. The energy inside a shell of radius $r = 5r_0$ from a (1+1)-dimensional simulation in sine-Gordon model in two dimensions assuming radial symmetry.

up- or downwards here than for the quartic potential in the previous section due to a shorter span of the simulation combined with an even flatter slope governing the decay of the radiation component. However, clearly the largest value for the constant $E_0 = 84$ can be ruled out as shown in the inset.

We turn immediately to the results from (1+1)-dimensional simulations with the assumption of radial symmetry in two dimensions. Figure 4.11 presents the energy inside the shell. Subtracting $E_0 = 72.25$ from this yields the curve shown in Figure 4.12. The grey line is a guide to eye of a slope $-\delta = -0.11$. We are lacking time span and data quality of ϕ^4 theory, but at the qualitative level the result definitely supports the power law suppression (4.5) in radiated power.

Returning to (2+1)-dimensional simulations, Figure 4.13 shows the spectral function $\Phi(\omega)$ obtained by Fourier transform in a time interval of length 5000 units at an early stage (above) and at the end of the simulation (below). Also here the signal is cleaner later on when emission of radiation

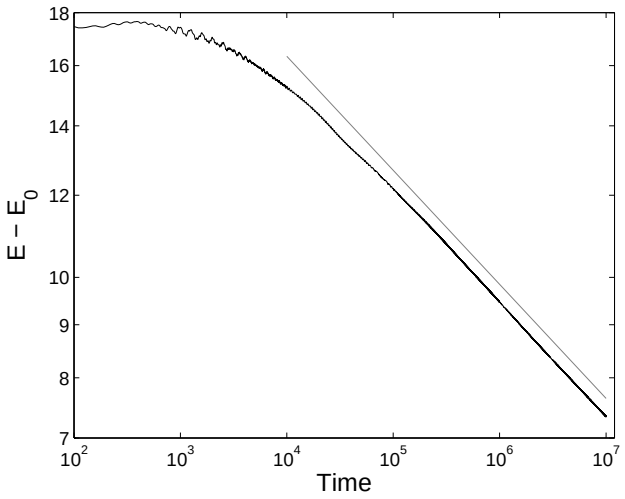

Figure 4.12. The difference of the energy inside a shell of radius $r = 5r_0$ and the constant $E_0 = 75.25$. The grey straight line is a guide to eye showing a power law $(E - E_0) \sim t^{-\delta}$ with slope $-\delta = -0.11$.

has declined. There is no sign of time evolution in the suppression of the higher amplitudes. The signal is far cleaner than when periodic boundary conditions were used, the example shown in Figure 3.12. However, the decay constant b governing the suppression of the peaks with increasing frequency ω is in excellent agreement with the one obtained using periodic boundary conditions.

4.5 Convex Potentials

The majority of studies on oscillons has been carried out in the context of ϕ^4 theory (see e.g. [52, 53, 55, 59]) or in the sine-Gordon model as we have done so far. Both potentials (1.5) and (1.12) have degenerate vacua and inflection points. Studies [132] and [49] considered potentials (2.7) and (2.8), respectively. These have just a single minimum and are convex functions. In [132] the study dealt with potentials that are nearly quadratic. In particular a quadratic potential with a negative logarithmic

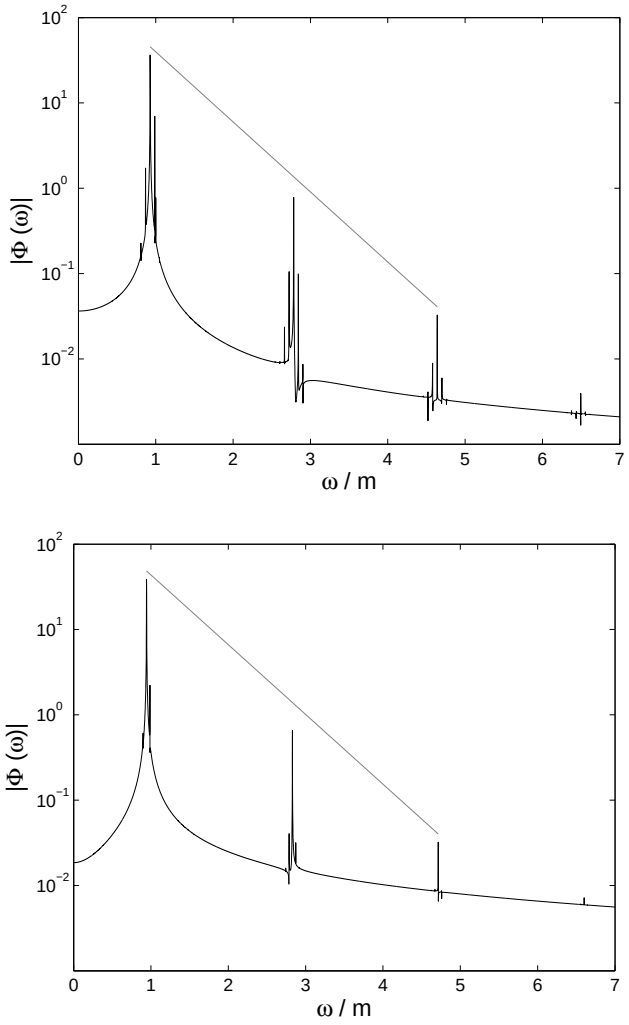

Figure 4.13. The spectral function $|\Phi(\omega)|$ over an interval of 5000 time units starting at time 10^5 (above) and at time 10^6 (below). They grey line is guide to eye of the exponential $\exp(-b\,\omega/m)$ with slope $b = 1.88$.

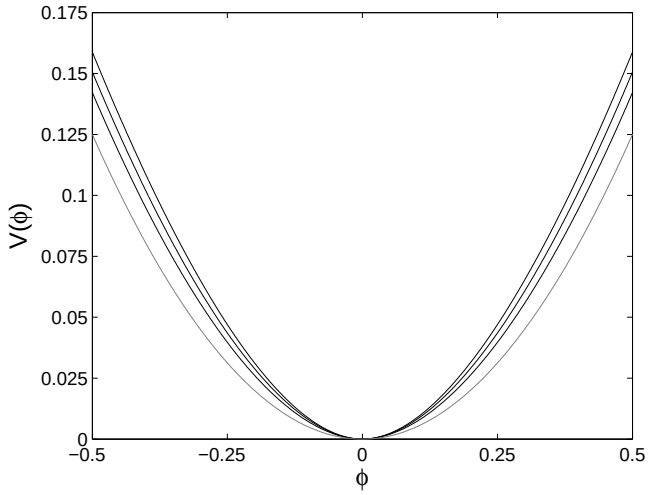

Figure 4.14. Potential V in (4.7) around the minimum for values $p = 0.4, 0.3, 0.2$ (from top to bottom). The grey line shows the quadratic potential $\phi^2/2$.

correction was reported to support long-lived lumps (called I-balls by the authors). This led us to study the effects of the form of the potential on the existence of long-lived oscillating solutions. We have chosen to study the following convex function

$$V(\phi) = \frac{\phi^2}{1+\phi^{2p}}\,, \tag{4.7}$$

which reduces to quadratic when the exponent $p = 0$. Figure 4.14 shows the potential (4.7) close to the minimum for values $p = 0.4, 0.3$ and 0.2 together with the quadratic potential $\phi^2/2$ indicated by the grey line. The potential is steeper than the quadratic one in the vicinity of the minimum where oscillations of the field take place, $|\phi| < 1$.

The potential (4.7) sets a far greater challenge for the absorbing boundary conditions than ϕ^4 theory or the sine-Gordon model. This becomes readily apparent in Figure 4.15 where the second derivative of the potential is shown for the same values of the parameter p. Already small

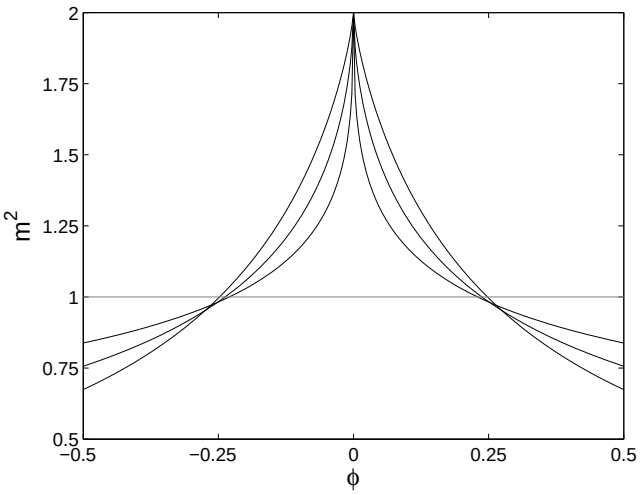

Figure 4.15. The second derivative of the potential V in (4.7) for $p = 0.4, 0.3, 0.2$ (from broader to narrower spikes around $\phi = 0$). The grey line shows the constant $m^2 = 1$ for a quadratic potential.

deviations from the vacuum $\phi = 0$ create large variations in V'', which increase when the exponent p decreases. This is a drawback from the point of view of the absorbing boundary conditions used because they are based on the assumption that the potential can be linearised in the equation of motion. Once the fluctuations create large corrections, the absorption can be expected to be only partial or, in the worst case, the update on the boundary even pumps energy into the lattice. From now on we restrict considerations to values $1/2 > p \geq 0.4$ which yield less stark variations and for which the radiation is clearly adequately removed from the lattice.

Also here the oscillon is initialised by a Gaussian deviation from the vacuum

$$\phi(r) = A \cdot \exp(-r^2/r_0^2), \tag{4.8}$$

with the same width of the distribution, $r_0 \simeq 2.9$, but due to the steepness of the potential (4.7) we set the amplitude of the displacement to be smaller, $A = 0.6$. The oscillons formed are well described by a Gaussian

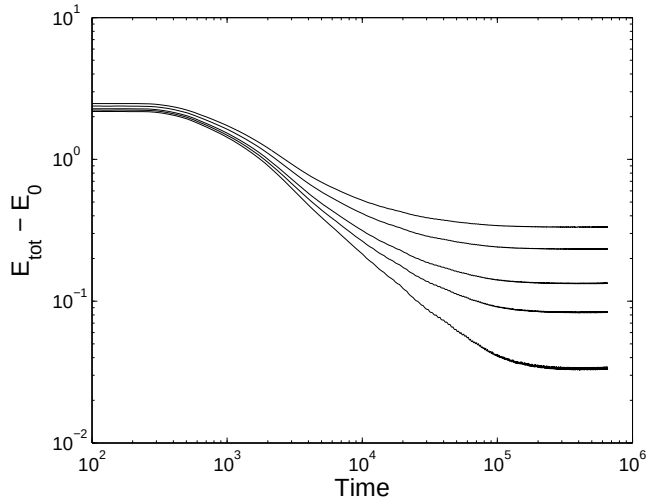

Figure 4.16. The difference of the total energy and a constant, $E_{\rm tot} - E_0$, on a logarithmic scale: $E_0 = 58.7, 58.5, 58.9, 58.95$ and 59.0 from top to bottom.

shape though with a slightly larger width. After a short initial phase of decrease in energy the oscillon settles into a state characterised by a very constant energy.

Figure 4.16 presents data from a (2+1)-dimensional simulation where the parameter p was set to $p = 0.4$. The values for total energy in the lattice are averaged over 40 measure points in a time interval of length 5000. None of the curves $E_{\rm tot} - E_0$ approaches now a straight line. This demonstrates the far greater need for fine-tuning due to the fast decay.

The enhanced accuracy in energy of the simulations assuming radial symmetry permits us to seek the constant E_0. The energy inside a shell from the (1+1)-dimensional simulation subtracted by $E_0 = 58.6621$ is shown in Figure 4.17 for the same potential $p = 0.4$. The guide to eye (grey line) shows that the decay of the radiation component is roughly inversely proportional to time. This is further demonstrated in Figure 4.18 where data is shown for $p = 0.45$. The constant $E_0 = 60.5336$ is subtracted both from the total energy in the lattice and from the energy inside a shell. These curves would overlap but the latter is displaced for clarity.

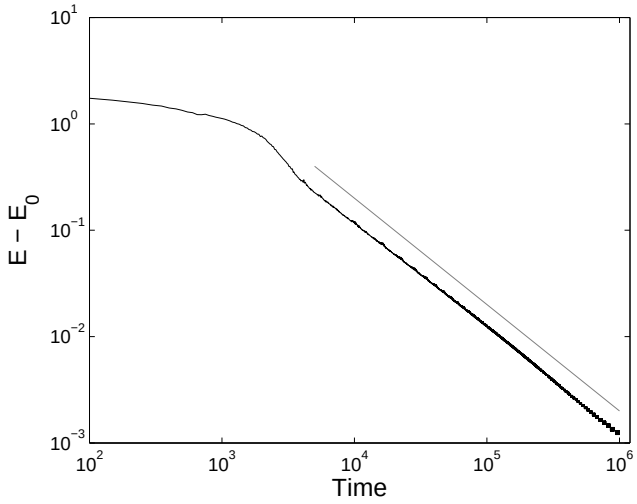

Figure 4.17. The difference of the energy inside a shell of radius $r = 5r_0$ and a constant $E_0 = 58.6621$. The fluctuations in the difference are clearly visible in the plotted curve at late times in the right. The grey straight line is a guide to eye of a power law inversely proportional to time, t^{-1}.

The constant E_0 can be principally determined more precisely than e.g. in ϕ^4 theory due to the fast suppression of the radiated power. However, this tests to a far greater extent the accuracy the energy can be measured in simulations. We naturally start to reach the accuracy of the evolution algorithm with the chosen values of the lattice spacing and time step. In both Figures 4.17 and 4.18 there appear visible fluctuations at late times when the difference $(E(t) - E_0)$ start to drop to the magnitude 10^{-3}.

We do not aim to a precise determination of the exponent in the power law, but undoubtedly the suppression of the radiative component is strong compared to ϕ^4 theory and the sine-Gordon model, where the oscillon has still approximately 10% more energy at the end of the simulations than the best fit to a power law yields for the constant E_0. For the convex potentials here the expected further energy loss is orders of magnitude less. We were able to study only very limited values of the parameter p due to numerical restrictions, but seems plausible that the potential (4.7) supports oscillons for a wider variety of the exponent governing its steepness.

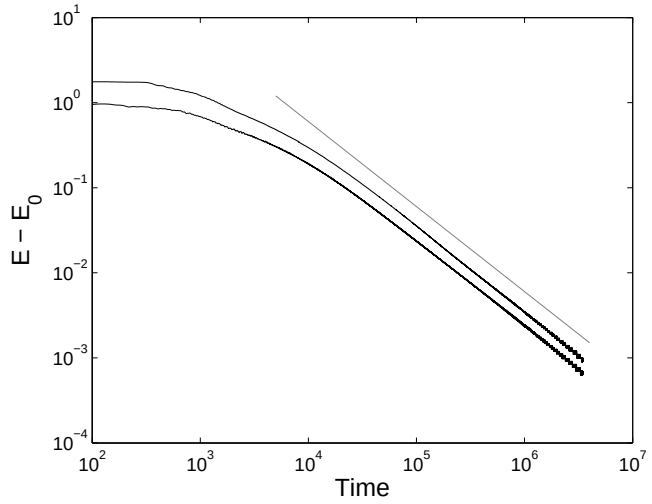

Figure 4.18. The difference of the total energy and constant $E_0 = 60.5336$ together with the difference of energy inside a shell of radius $r = 5r_0$ and the same constant E_0 but the curve displaced downwards by 30% for clarity. The grey straight line is a guide to eye of a power law inversely proportional to time, t^{-1}.

It should be noted that non-radiating oscillons have been found in one-dimensional signum-Gordon model [146]. This is governed by the potential

$$V(\phi) = g\,|\phi|. \tag{4.9}$$

The convex potential (4.7) reduces to linear for $p = 1/2$ in the limit of large field, $\phi \gg 1$. Of course, this is not the realm where oscillations of the field take place when considering oscillons. However, one cannot exclude right away any connection between oscillons we have reported here and those described in [146]. At the very least, both are examples of oscillons appearing in theories where the potential is not a smooth one.

4.6 Conclusions

We have presented absorbing boundary conditions for a massive, real scalar field in the Cartesian and polar or spherical coordinates in two and three di-

mensions. We used these in a study of oscillons in ϕ^4 theory, sine-Gordon model and in convex potentials performing both (2+1)-dimensional and (1+1)-dimensional simulations assuming radial symmetry. We presented checks to estimate the adequateness of the boundary conditions used. The good agreement of the total energy in the lattice with that only in the vicinity of an oscillon, as well as the lack of a radiation signal in frequency space, suggest that absorbing boundaries remove radiation from the simulation box. Some reflection still occurs causing anisotropy on the remnant radiation background on the lattice. It should be pointed out that the treatment of the corners of lattices is a difficult task also for massless radiation as discussed e.g. in [147]. This may provide partial explanation to the reflection we observe.

Turning to the results on oscillons, we have shown that while oscillons radiate energy during the evolution the rate of the energy loss is not constant but attenuates in the course of time. We showed that the time evolution of the energy of an oscillon is well modelled by dividing it into a constant and a decaying radiative part. Especially (1+1)-dimensional simulations permitting larger time span provide strong evidence that the decay of the radiative part is governed by a power law. We further determined the values of the constant components as well as approximate values of the exponent governing the power law decay.

What do the results tell us about the lifetime of oscillons in two dimensions? The appearance of the constant E_0 now raises the question of its physical interpretation. While it would be tempting to define it as the energy of a non-radiating oscillon, this kind of conclusion cannot be made straightforwardly. It is not obvious if there are oscillon solutions at such energy. As the energy decreases the oscillon oscillates faster and the oscillation frequency ω_0 increases as discussed in the previous chapter. Once it is close enough to the radiation frequency $\omega = m$ the oscillon decays. Both in ϕ^4 theory and in sine-Gordon model the energy E_0 is still considerably smaller than that of an oscillon we have able to study in simulations because the radiative part shows a slow decay in time. The work done for small-amplitude quasi-breathers in two-dimensional ϕ^4 theory suggests that there exist oscillon states for all frequencies $\omega < m$ [60]. If this result can be applied here, it gives some support for the possibility of an oscillon

solution with energy E_0 in the quartic potential. However, in the case of the convex potentials presented here the situation is definitely intriguing. We have shown that there the suppression of the radiation losses is quick, roughly inversely proportional to time and thus only a very small further decrease in energy is to be expected to occur. This makes it possible that these oscillons could go on indefinitely long. Another open question remaining is if it is possible to tailor potentials in which the emission of radiation from oscillon is strongly suppressed also in higher dimensions.

4.7 Appendix: Absorbing Boundaries

In this appendix the absorbing boundary conditions are presented. As the starting point consider the following linear wave equation

$$\ddot{\varphi} - \nabla^2\varphi + \varphi \cdot V''|_{\varphi=0} = 0\,, \tag{4.10}$$

where $\varphi = \varphi(t, \boldsymbol{x})$ is now a small perturbation around a chosen vacuum and V'' is evaluated at that point. For example in ϕ^4 theory $\phi \to \eta - \varphi$ and $V''(\phi)|_{\phi=\eta} = 2\lambda\eta^2 = m^2$. In two-dimensional polar coordinates the equation is already given in (3.5).

4.7.1 Cartesian Coordinates

The treatment here follows closely the one presented in [148] for a massless scalar field. Working in two spatial dimensions the solution of the wave equation (4.10)

$$\frac{\partial^2\varphi}{\partial t^2} - \frac{\partial^2\varphi}{\partial x_1^2} - \frac{\partial^2\varphi}{\partial x_2^2} + m^2\varphi \;=\; 0 \tag{4.11}$$

in the region $x_1 > 0$ is given by

$$\varphi\,(t, x_1, x_2) = \exp\Big[\, i\,(\sqrt{\omega^2 - \widetilde{\beta}^2 - m^2}\, x_1 + \omega t + \widetilde{\beta} x_2\,)\Big]\,, \tag{4.12}$$

for $\omega^2 > m^2 + \widetilde{\beta}^2$ and where ω and $\widetilde{\beta}$ are dual variables to t and x_2, respectively. This solution (4.12) is annihilated at $x_1 = 0$ by the operator

in the parenthesis

$$\left[\left(\frac{\partial}{\partial x_1} - i\sqrt{\omega^2 - \widetilde{\beta}^2 - m^2}\right)\varphi\right]\Bigg|_{x_1=0} = 0. \tag{4.13}$$

From the point of view of numerical implementation using leapfrog update we aim to reach second order equations at the boundaries. Expanding the square root to second order in (4.13) and replacing the variables ω and $\widetilde{\beta}$ by the corresponding time and spatial derivatives one obtains the boundary condition

$$\frac{\partial}{\partial t}\frac{\partial \varphi}{\partial x_1} - \frac{\partial^2 \varphi}{\partial t^2} + \frac{1}{2}\frac{\partial^2 \varphi}{\partial x_2^2} + \frac{1}{2}m^2\varphi = 0 \tag{4.14}$$

at $x_1 = 0$. The equation (4.14) permits a straightforward time evolution using leapfrog algorithm. To be more precise, the condition (4.14) yields a new evolution equation for the field momentum Π compared to that in the interior of the lattice, whereas the update of the field ϕ stays unaltered. Inward derivatives are used on the boundaries.

At the corners one demands that the wave equation (4.11) and the boundary condition (4.14) for both x_1 and x_2 are fullfilled.

By combining the equations

$$\begin{aligned}
\frac{\partial^2 \varphi}{\partial t^2} - \frac{\partial^2 \varphi}{\partial x_1^2} - \frac{\partial^2 \varphi}{\partial x_2^2} + m^2\varphi &= 0 \\
\left[2\frac{\partial}{\partial t}\frac{\partial \varphi}{\partial x_1} - 2\frac{\partial^2 \varphi}{\partial t^2} + \frac{\partial^2 \varphi}{\partial x_2^2} + m^2\varphi\right]\Bigg|_{x_1=0} &= 0 \\
\left[2\frac{\partial}{\partial t}\frac{\partial \varphi}{\partial x_2} - 2\frac{\partial^2 \varphi}{\partial t^2} + \frac{\partial^2 \varphi}{\partial x_1^2} + m^2\varphi\right]\Bigg|_{x_2=0} &= 0
\end{aligned} \tag{4.15}$$

one reaches the boundary condition at the corner $x_1 = 0 = x_2$

$$\frac{\partial}{\partial t}\frac{\partial \varphi}{\partial x_1} + \frac{\partial}{\partial t}\frac{\partial \varphi}{\partial x_2} - \frac{3}{2}\frac{\partial^2 \varphi}{\partial t^2} + \frac{3}{2}m^2\varphi = 0 \tag{4.16}$$

In the case of a massless scalar field the conditions at the corners (4.16) can be brought back to first order equations with respect to time via

integration. The mass term m^2 does not permit such a reduction here.

Though no (3+1)-dimensional simulations were carried out we give the corresponding equations. The generalisation of the boundary condition (4.13) to three dimensions is obvious, but at the corners and edges the equations are slightly different.

At the corner $x_1 = x_2 = x_3 = 0$ one combines

$$\begin{aligned}
&\frac{\partial^2\varphi}{\partial t^2} - \frac{\partial^2\varphi}{\partial x_1^2} - \frac{\partial^2\varphi}{\partial x_2^2} - \frac{\partial^2\varphi}{\partial x_3^2} + m^2\varphi = 0 \\
&\left[\frac{\partial}{\partial t}\frac{\partial\varphi}{\partial x_1} - \frac{\partial^2\varphi}{\partial t^2} + \frac{1}{2}\frac{\partial^2\varphi}{\partial x_2^2} + \frac{1}{2}\frac{\partial^2\varphi}{\partial x_3^2} + \frac{1}{2}m^2\varphi\right]\Bigg|_{x_1=0} = 0 \\
&\left[\frac{\partial}{\partial t}\frac{\partial\varphi}{\partial x_2} - \frac{\partial^2\varphi}{\partial t^2} + \frac{1}{2}\frac{\partial^2\varphi}{\partial x_1^2} + \frac{1}{2}\frac{\partial^2\varphi}{\partial x_3^2} + \frac{1}{2}m^2\varphi\right]\Bigg|_{x_2=0} = 0 \\
&\left[\frac{\partial}{\partial t}\frac{\partial\varphi}{\partial x_3} - \frac{\partial^2\varphi}{\partial t^2} + \frac{1}{2}\frac{\partial^2\varphi}{\partial x_1^2} + \frac{1}{2}\frac{\partial^2\varphi}{\partial x_2^2} + \frac{1}{2}m^2\varphi\right]\Bigg|_{x_3=0} = 0
\end{aligned} \tag{4.17}$$

to obtain

$$\frac{\partial}{\partial t}\frac{\partial\varphi}{\partial x_1} + \frac{\partial}{\partial t}\frac{\partial\varphi}{\partial x_2} + \frac{\partial}{\partial t}\frac{\partial\varphi}{\partial x_3} - 2\,\frac{\partial^2\varphi}{\partial t^2} + \frac{5}{2}m^2\varphi = 0\,. \tag{4.18}$$

Combining on the edge $x_1 = 0 = x_2$

$$\begin{aligned}
&\frac{\partial^2\varphi}{\partial t^2} - \frac{\partial^2\varphi}{\partial x_1^2} - \frac{\partial^2\varphi}{\partial x_2^2} - \frac{\partial^2\varphi}{\partial x_3^2} + m^2\varphi = 0 \\
&\left[2\frac{\partial}{\partial t}\frac{\partial\varphi}{\partial x_1} - 2\frac{\partial^2\varphi}{\partial t^2} + \frac{\partial^2\varphi}{\partial x_2^2} + \frac{\partial^2\varphi}{\partial x_3^2} + m^2\varphi\right]\Bigg|_{x_1=0} = 0 \\
&\left[2\frac{\partial}{\partial t}\frac{\partial\varphi}{\partial x_2} - 2\frac{\partial^2\varphi}{\partial t^2} + \frac{\partial^2\varphi}{\partial x_1^2} + \frac{\partial^2\varphi}{\partial x_3^2} + m^2\varphi\right]\Bigg|_{x_2=0} = 0
\end{aligned} \tag{4.19}$$

leads to

$$\frac{\partial}{\partial t}\frac{\partial\varphi}{\partial x_1} + \frac{\partial}{\partial t}\frac{\partial\varphi}{\partial x_2} - \frac{3}{2}\,\frac{\partial^2\varphi}{\partial t^2} + \frac{1}{2}\frac{\partial^2\varphi}{\partial x_3^2} + \frac{3}{2}m^2\varphi = 0. \tag{4.20}$$

The number of equations needed to cover all the boundaries of the grid in

three dimensions is already quite large.

4.7.2 Radial Wave in Two Dimensions

When one assumes radial symmetry in two dimensions the equation replacing (4.11) is

$$\frac{\partial^2\varphi}{\partial t^2} - \frac{\partial^2\varphi}{\partial r^2} - \frac{1}{r}\frac{\partial\varphi}{\partial r} + m^2\varphi = 0. \tag{4.21}$$

As mentioned the solutions of (4.21) are Bessel functions, but considering an absorbing boundary at far distance ($r \gg 1$) the approximative solution reads (we are naturally only interested in the outgoing wave, $k > 0$)

$$\varphi\,(t,r) = \frac{1}{\sqrt{r}}\exp\left[\,i\,(\sqrt{\omega^2 - m^2}\,r + \omega t\,)\right]. \tag{4.22}$$

This solution (4.22) is annihilated at the boundary $r = r_\mathrm{b}$ by the operator in the parenthesis

$$\left[\frac{\partial}{\partial r} - i\sqrt{\omega^2 - m^2} + \frac{1}{2r}\right]\varphi\Big|_{r=r_\mathrm{b}} = 0. \tag{4.23}$$

This yields an absorbing boundary condition on the edge of the one-dimensional grid

$$\frac{\partial}{\partial t}\frac{\partial\varphi}{\partial r} - \frac{\partial^2\varphi}{\partial t^2} + \frac{1}{2}m^2\varphi + \frac{1}{2r}\,\varphi = 0. \tag{4.24}$$

The last term, suppressed by the inverse of physical distance r, results from the treatment in polar coordinates. It turns out to be fairly insignificant in the numerical set-up used in this study, but in smaller grids it increases the absorption.

4.7.3 Spherical Wave in Three Dimensions

When one assumes spherical symmetry in three dimensions the solution for the wave equation

$$\frac{\partial^2\varphi}{\partial t^2} - \frac{\partial^2\varphi}{\partial r^2} - \frac{2}{r}\frac{\partial\varphi}{\partial r} + m^2\varphi = 0. \tag{4.25}$$

is given by

$$\varphi\,(t,r) = \frac{1}{r}\exp\left[\,i\,(\sqrt{\omega^2 - m^2}\,r + \omega t\,)\right]. \tag{4.26}$$

This is annihilated at the boundary $r = r_\mathrm{b}$ by

$$\left[\frac{\partial}{\partial r} - i\sqrt{\omega^2 - m^2} + \frac{1}{r}\right]\varphi\Big|_{r=r_\mathrm{b}} = 0\,, \tag{4.27}$$

which leads to following absorbing boundary condition

$$\frac{\partial}{\partial t}\frac{\partial\varphi}{\partial r} - \frac{\partial^2\varphi}{\partial t^2} + \frac{1}{2}m^2\varphi + \frac{1}{r}\,\varphi = 0 \tag{4.28}$$

appropriate when a three-dimensional system is considered in a spherically symmetric geometry.

Chapter 5

Oscillons and Domain Walls

We have already discussed how the domain walls are produced as a simple example of Kibble mechanism as well as reviewed some mechanisms that lead to formation of oscillons. While the oscillating energy concentrations have been seen to form with a tiny initial density contrast in [132], in this chapter we report oscillon formation via a much more violent process, namely, from domain collapse in ϕ^4 theory. Rather a more related study to the main topic of this chapter is [149]. There bubble collisions were investigated during a first order phase transition. The authors noticed formation of what was called long-lived quasilumps. In the context of a phase transition after inflation it was also speculated that the quasilumps could result in the formation of black holes. However, [150] came to the opposite conclusion. The size of an oscillon is well above its the Schwarzschild radius even at GUT scale models. Only at the energy scale around 10^{18} GeV these two are comparable, but at such energy the gravitational effects are inevitably important.

This chapter is organised as follows. First we examine the signal of moving oscillons in the spectral function. We apply our method to simulations with random initial conditions, and are able to detect oscillons formed from collapsing domains, and measure their velocity distribution. In an attempt to understand the resulting ensemble of oscillons and to reduce the effect of the radiation bath they move through, we also prepare an initial state of only oscillons moving into random directions and report the dynamics of this oscillon gas. Annihilation through collision seems to

play a role in reducing the density of oscillons, and so we finish our investigation by studying the off-axis collisions of oscillons and an oscillon and a stationary domain wall.

5.1 Numerical Set-up

In this chapter we concentrate exclusively on ϕ^4 theory in two spatial dimensions with the degenerate double well potential using the scaled form (3.2), but we expect that qualitatively the results would be very similar in the two-dimensional sine-Gordon model. The equation of motion (3.1) is evolved on a two-dimensional lattice using a leapfrog update. The lattice spacing is set to be $dx = 0.25$ and the time step $dt = 0.05$. Here all the simulations have been performed using periodic boundary conditions for two reasons. First, in a study of Lorentz-boosted oscillons we want to allow them to move around the lattice without hitting any boundaries. Secondly, in simulations with random initial conditions that is a standard choice that allows domains of different vacua to grow, while absorbing boundary conditions are based on an expansion in a vicinity of a single minimum of the potential that must be chosen explicitly beforehand.

5.2 Oscillon Signal in the Spectral Function

We create oscillons on the lattice by using the Gaussian ansatz (3.4) with the same width $r_0 \simeq 2.9$ and amplitude $A = 1$ as before. The signal of stationary oscillons in frequency space using the spectral function has been discussed earlier and examples are shown in Figure 4.5. Here our interest lies in moving oscillons. We perform a boost on an oscillon and allow it then to move on the lattice, whose size was set to be 400^2. During the simulation we measure the mean of the field momentum $\bar{\Pi}(t)$ in order to attain the spectral function $\Phi(t)$, given by (4.3). Figure 5.1 shows the spectral function $|\Phi(\omega)|$ at zero momentum obtained by performing a Fourier transform over the interval of length $5{\cdot}10^3$ in time units when an oscillon is stationary and when it is moving at velocity $v \simeq 0.42$. The location of the peak of the basic frequency of a moving oscillon is shifted to the left to a smaller value due to time dilation, and its multiples correspondingly. The

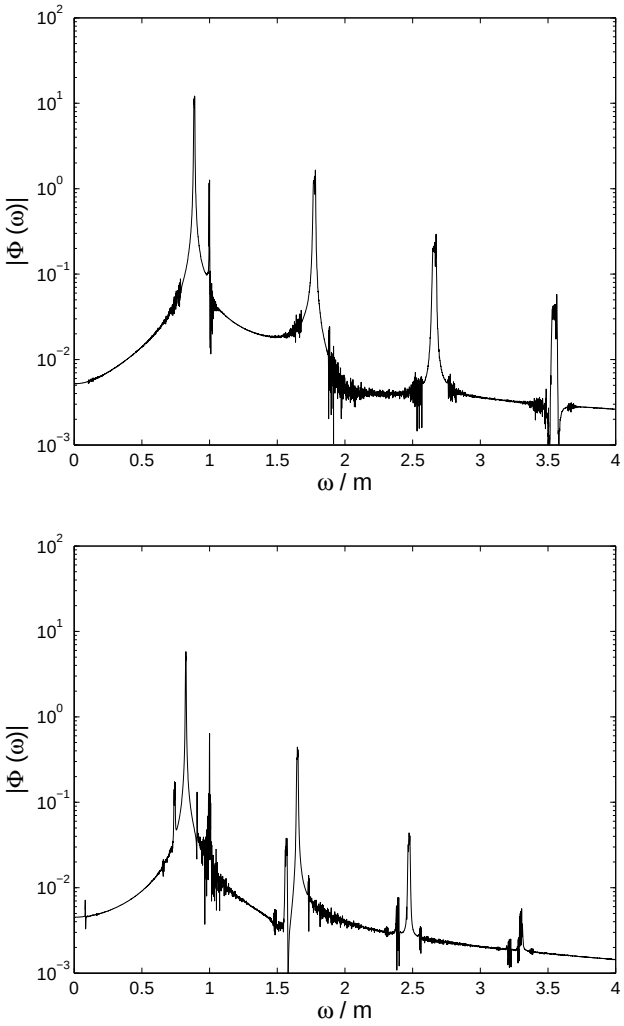

Figure 5.1. The spectral function $|\Phi(\omega)|$ at zero momentum over the time interval of length $5 \cdot 10^3$ for a stationary oscillon (above) and an oscillon with velocity $v \simeq 0.42$ (below).

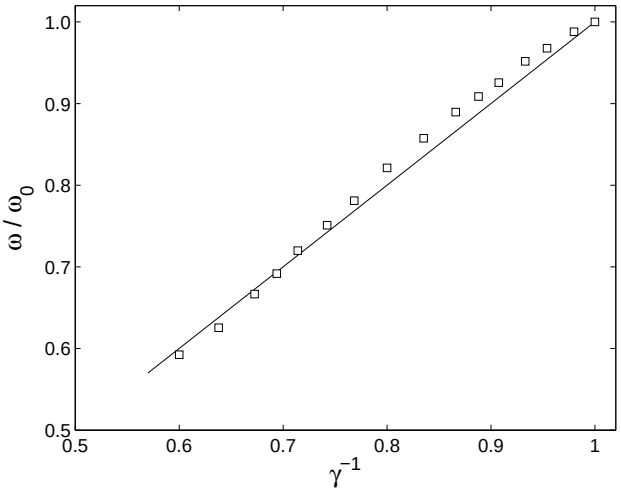

Figure 5.2. The relative frequency ω/ω_0 as a function of the inverse of the Lorentz factor γ. The solid line is $\omega = \omega_0/\gamma$, where $\omega_0 = 0.85$ is the basic frequency of a stationary oscillon.

effect is best seen by comparing the location of the fourth peaks in the pictures or the distance between the peak of the basic frequency and that of radiation. This drift is further illustrated in Figure 5.2, where the relative frequencies where the peaks appear in the spectra are shown against the inverse of the γ-factor, $\gamma = 1/\sqrt{1-v^2}$. The deviations of measured values from the straight line $\omega = \omega_0/\gamma$ illustrate the numerical limitations of determining the basic frequency in the data as well as the precision in the velocity of a moving oscillon, to be discussed later. The peaks at $\omega = m$ in Figure 5.1 indicate the presence of a dispersive radiation component in the simulation box due to emission by an oscillon. Here the radiation is left in the lattice because of the periodic boundary conditions and consequently the signal is not as clean as in Figure 4.5 where absorbing boundary conditions were used. However, periodic boundary conditions are necessary to permit a long integration time when monitoring a moving oscillon as they allow the oscillon to wrap around the lattice. Due to radiation losses and subsequent interaction with the radiation, the oscillons slows down as time

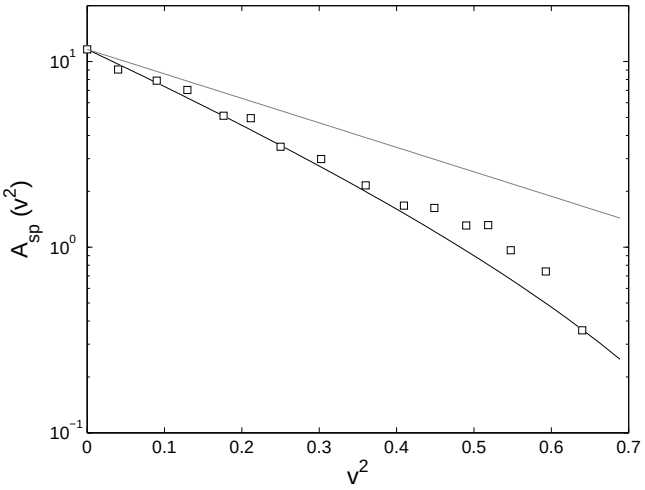

Figure 5.3. The amplitude of the basic frequency, i.e. the power in the spectral function $\Phi(\omega)$ at its peak, as a function of velocity. The black solid curve shows the amplitude of a Gaussian distribution moving with velocity v in the spectral function, given by the right-hand side of the Equation (5.6). The grey straight line demonstrates the bare exponential $\exp(-\omega_0^2 r_0^2 v^2 \,/\, 2)$ without the additional power suppression. The strong suppression with increasing velocity makes the right hand end of the graph particularly sensitive to background noise. The curves are set to coincide with the measured amplitude of a stationary oscillon: 11.63 at $v = 0$; furthermore, $\omega_0 = 0.85$ and $r_0 = 2.9$.

lapses. On the other hand, the precision with which the frequency can be determined depends linearly on the length of the time interval. These two effects work against each other and one can expect only a limited accuracy. This is manifest in the dispersion of the data points in Figure 5.2, but the general trend is clear.

In addition to the shift of the basic frequency there is a much more drastic effect in the suppression of the height of this peak as the velocity of an oscillon increases. We expect an exponential decrease (see Appendix). The value of the spectral function Φ at $\omega = \omega_0\,(\gamma)$ is shown as a function of v^2 together with the prediction in Figure 5.3. We immediately point out that the precision in measuring the amplitude is not expected to be good.

This is due to the restricted resolution in frequency (order 10^{-3} in units of ω/m) when a discrete Fourier transform in a limited interval is carried out, whereas the peak itself is generally very narrow. Furthermore, while time dilation shifts the location of the oscillation frequency further away from the radiation frequency thus easing the distinction between these two, the strength of the signal gets strongly suppressed. The background noise can therefore lift the amplitudes far more at the side of the higher velocity end of the graph. Consequently, the positions of the data points in Figure 5.3 can be considered only indicative.

5.3 Radiation of Oscillons from Collapsing Domains

The starting point of this section is an evolving domain wall network, discussed earlier together with the Kibble mechanism. Such a network can be created by using the same evolution algorithm initialised now with random conditions. Equation (3.1) is evolved numerically on a lattice of size 400^2. Keeping the lattice spacing $dx = 0.25$ throughout this study, the physical size in linear dimension L is 100. We use "false vacuum" initial conditions, the field is set to the local maximum of the potential and the field momentum is given a random value picked from a Gaussian distribution with a zero mean and width 0.1. This means that the correlation length ξ at the beginning of the simulation, if not exactly zero, is less than the lattice spacing, $\xi \lesssim 0.25$. During the early stages the evolution is damped, but at the time $t = 25$ the damping is turned off and then the field is allowed to evolve freely. Domains where ϕ is in either of the two minima of the potential (3.2) are formed and separated by domain walls. As discussed before the domains grow in size during the evolution.

Obviously, a domain wall itself is an energy concentration due to the potential and gradient energy locked up in the wall, and a moving wall has naturally also a kinetic component. When a domain collapses the energy that was trapped in the domain wall is released. Thus there is energy available for the field to execute large oscillations. The simulations carried out here demonstrate that usually the domain collapse takes place rapidly and then there tends to be large amount of energy, especially in the

kinetic form, localised around the quickly shrinking domain wall already well before the eventual disappearance. In particular, there appear some very high energy concentrations moving along the wall. A similar kind of observation of energy concentrations, often (but not necessarily) along the domain wall, was made in [122] where field dynamics of tachyonic preheating after hybrid inflation was studied. Once the domain has collapsed these energy concentrations either give rise to or turn into propagating nonlinear waves. Oscillons are born.

The process of domain collapse is illustrated with two pairs of snapshots. Figure 5.4 shows the isocontours of the field ϕ (left) and the energy density (right) before (above) and after (below) the domain collapse. Inside the contours dark grey indicates a region where the field is close to the disappearing vacuum, in the areas in lighter grey the field is around the maximum of the potential and white marks the field close to the other vacuum that becomes the dominating one. In turn, the higher the energy density the darker the corresponding area is displayed, and the pentagon-like shape of the domain is also clearly recognisable in the corresponding snapshot of the energy density where the enclosing domain wall appears black. In the second pair of snapshots the domain has collapsed - the large grey area has vanished indicating disappearance of this vacuum. Instead there are ripples where the field is far from the dominating vacuum positioned on a ringlike wave front. These small, elliptic regions show up as extremely high peaks of energy density (the view in the picture is tilted to visualise the height of peaks of energy concentration). These are oscillons which propagate along the spherical wavefront away from the location of the collapsed domain. Unlike the dispersive waves that are damped quickly, oscillons are far less dissipative and have a long range. It should be noted that the elliptic form results from Lorentz contraction and thus indicates the high velocity of emitted oscillons. Furthermore, the seeds of oscillons are not required to be spherical: asymmetric bubbles can collapse into an oscillon [142]. The production of oscillons is associated with regions of high velocity on the domain walls, rather than bubble collapse where a single oscillon is formed from a bubble: there are generally several oscillons created by one collapsing domain.

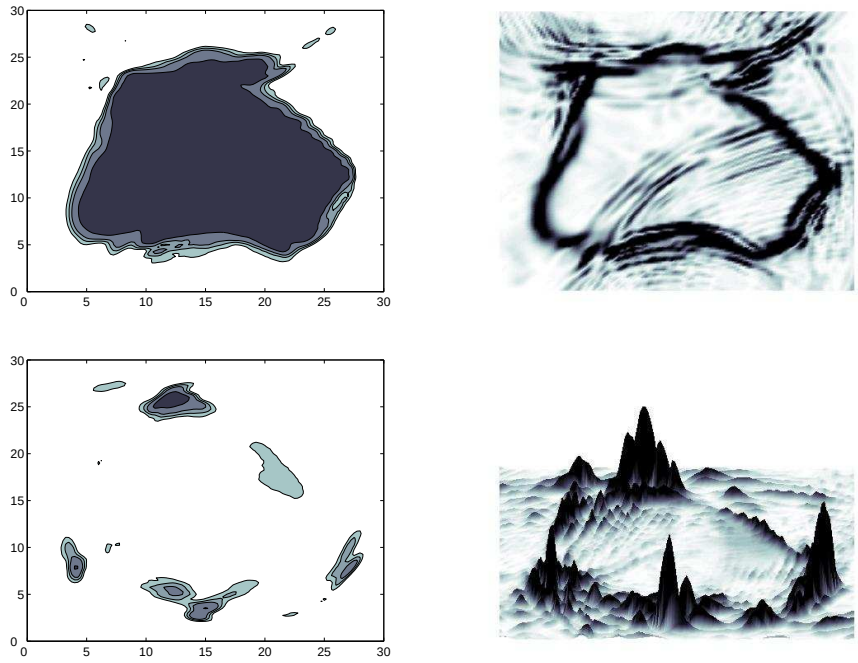

Figure 5.4. Oscillon formation in a domain collapse: the left panel shows contours of the field ϕ; the right panel presents the total energy density before the domain collapse (above) and right after (below). The snapshots are separated by 27 time units; the physical size in linear dimension of the subbox shown is 30. On the left the colours show domains of different vacua: dark grey indicates areas where the field $\phi < -0.5$ and white where the other vacuum is selected, $\phi > 0.5$. Energy density varies from zero (white) to above 0.8 (black). The view in the second snapshot of the energy density is tilted to highlight the areas of stark energy concentrations.

5.3.1 Statistical Analysis in Frequency Space

Eventually one or the other of the two vacua will completely dominate in a lattice of a finite size. This indicates the end of the scaling regime (which is not yet visible in Figure 2.4, but would be a deviation of the roughly straight line). However, if the simulation box becomes divided between two domains that span over the whole volume, typically a fairly static, intermediate state follows where there are those two domains, and domain walls, present and which last for a long time. We exploit this phenomenon in order to compare the signal of oscillons and domain walls in the spectral function.

It is relatively easy to observe if there are only one or two large domains present by monitoring the total length of domain walls in the lattice. If the total length of domain walls $L_{\rm walls}$ does not exceeds twice the linear size of the lattice L, $L_{\rm walls} > 2L$, there cannot be two domains spanning the box size. We determine the length of domain walls by counting the number of lattice sites where the field changes sign compared to its nearest neighbouring lattice points. We work under the hypothesis that oscillons are created only when larger domains collapse, thus from the last domain of the disappearing vacuum, and the ones from smaller domains created earlier disappear when colliding with the domain walls still present (though as demonstrated later on this is not inevitably the outcome).

We generated $30,000$ different initial configurations. Since our attention is in the aftermath of collapsed domains, the simulations are evolved much longer than e.g. in a study which would be only interested in the scaling of domain walls. The scaling regime typically terminates after $t = L/2$ due to boundary effects, thus here at $t \approx 100$, but we monitor the length of domain walls at two later instants: $t = 250$ and $t = 750$. Out of all the configurations, in 18,931 there is only one large domain dominating at the time of the first inspection. In 8174 cases the simulation box was divided into two large domains throughout this interval up to the final time $t = 750$. In the remaining cases the collapse of the other domain takes place during this interval and these events are discarded here.

We examine the spectral function separately for these two above mentioned cases - single domain (oscillons) or two domains (and thus long

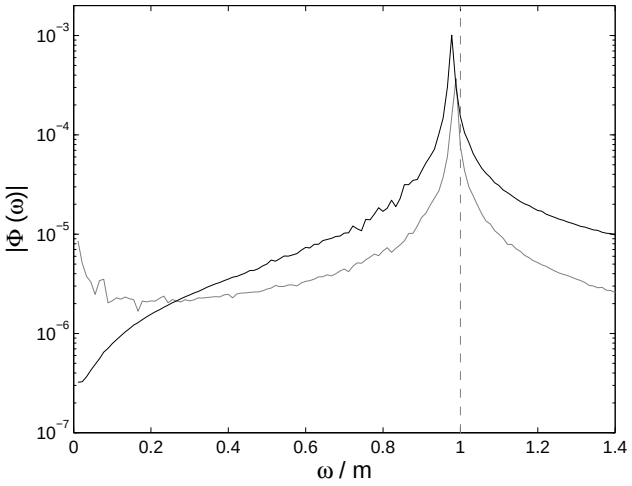

Figure 5.5. The spectral function $|\Phi(\omega)|$ at zero momentum over the time interval of length 400 for oscillons (black) and domain walls (grey). The vertical dashed line shows the radiation frequency $\omega = m$ without fluctuations.

domain walls present). Figure 5.5 shows the spectral function $|\Phi(\omega)|$ obtained an average over all the selected configurations and normalised by the number of events for one domain present (black) and for two domains (grey). The Fourier transform is made over a time interval of length 400 starting at time $t = 350$. This choice is to ensure that there are no domain walls in the observation interval. There can be shorter domain walls present at the time $t = 250$ which do not trigger the threshold $2L$ when monitoring is made, but they have time to fade during the subsequent time interval before the observation interval commences.

For a single domain with oscillons the spectral function shows a fairly broad radiation peak, and a long "shoulder" of decreasing power together with an almost complete absence of lowest frequencies. This is in stark contrast with the growing power at small frequencies in the presence of two domains. We believe this is the signal of the long domain walls that are very static objects, thus contributing to the lowest frequencies in the system. The peak at the radiation frequency is also narrower. This is easily understood by the fact that there is less kinetic energy in the system since

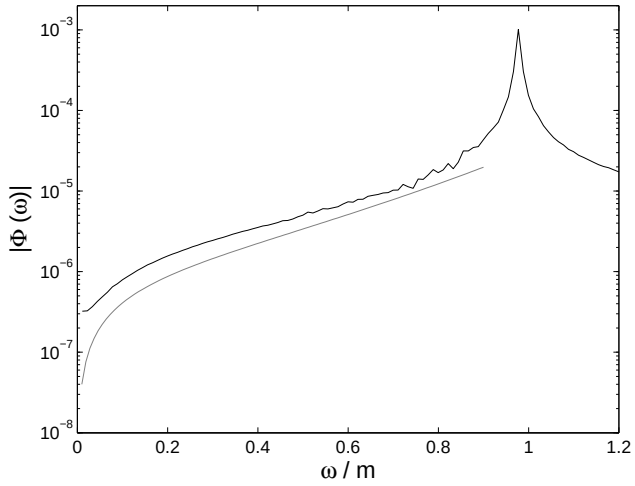

Figure 5.6. The spectral function $|\Phi(\omega)|$ for oscillons (black) as in Fig. 5.5 together with the curve $\omega \cdot \exp(b\,\omega^2)$ (grey), where $b = 2.1$. This suggests that the velocity distribution is governed by a power law when the exponential dependence of the amplitude $A_{\rm sp}$ is removed.

a large fraction of the energy remains locked up in the long domain walls. Thus these are cooler systems compared to those without domain walls. Not only the width, but also the location of the peak of radiation confirms this. In neither of the cases is the peak positioned precisely at $\omega = m$, but at a slightly lower frequency. The measurement via spectral function is sensitive to the effective mass $m_{\rm eff}$, given by (2.5). Only at zero temperature $T = 0$ the value of the effective mass $m_{\rm eff}$ coincides with the bare parameter m. Any non-zero temperature, below the critical temperature in the broken phase, reduces the value of $|m^2_{\rm eff}|$. Though we do not expose the system to a direct heat bath in the simulations, the radiation released from domains during the time evolution creates an effective thermal bath. There is some temperature associated to this heat bath and as a natural consequence $m_{\rm eff} < m$. In the case of one domain, the radiation is obviously stronger and the shift is already visible, yielding approximately a 2% displacement from $\omega = m$. Though there is undoubtedly some characteristic temperature in the system, we do not see any obvious and feasible way

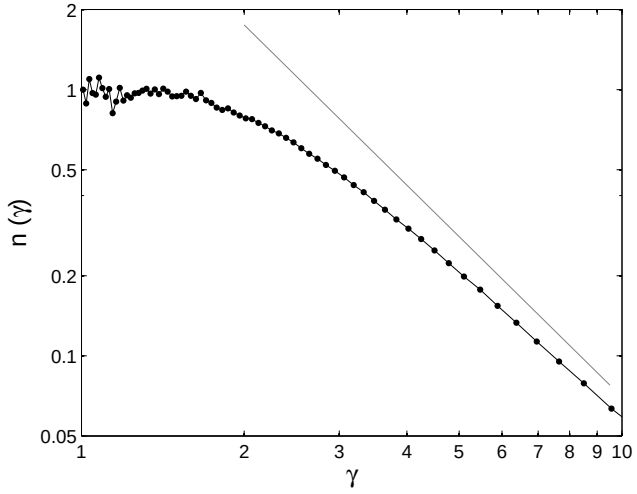

Figure 5.7. The velocity distribution $n(\gamma)$, number of oscillons in a velocity window (5.9), derived from the signal in spectral function $\Phi(\omega)$ shown in Fig. 5.6. The distribution is normalised to unity at the data point of smallest velocity $v \simeq 0.12$. The parameters ω_0 and r_0 are set to have the same values as in Fig. 5.3. The straight, grey line shows the curve γ^{-2}.

to determine it. The standard method is to derive temperature via kinetic energy, but this approach is immediately excluded here. This is due to the oscillons which carry considerable kinetic energy, but should not be considered as thermal fluctuations. As mentioned earlier other numerical studies have estimated that half or even the majority of the energy of a system could be stored in oscillons [126, 127].

The time dilation of the oscillation period relates the frequency and velocity via $\omega = \omega_0/\gamma$ and it is thus appealing to try to extract information of the velocity of oscillons from the power in the spectral function assuming that the signal in the spectral function at frequencies $\omega \lesssim 0.85$ is mainly due to the oscillons. Figure 5.6 shows that the "shoulder" can be reproduced. The signal in the spectral function $\Phi(\omega)$ can be transferred to an arbitrary velocity distribution of oscillons $n(v)$ with the use of the amplitude given by (5.6). One now needs to assume that the formed oscillons have typically size $r_0 \approx 3$ - this is supported by the simulations.

Figure 5.7 shows the velocity distribution, the number of oscillons with velocity between v and $v + dv$, as a function of γ-factor derived by (5.9) from the signal in the spectral function. The data suggest a fairly flat distribution at low velocities, whereas the region $\gamma \gtrsim 2$ is well fitted with a power law suppression γ^{-2}. It is an open question whether this velocity distribution reflects the properties of the source, or the effect of energy loss in the strongly radiative environment. Survival of oscillons in a thermal environment has been studied in [151], where it was concluded that oscillons can resist a weak thermal bath for long periods of time, but here the dispersive radiation component, and the effective heat bath, is relatively strong. Conservation of momentum indicates that the high-γ oscillons must be emitted by high-γ parts of the domain wall network. These are cusps, which are by definition regions where the walls are moving close to the speed of light.

5.4 Oscillon Gas

While simulations with random initial conditions and the subsequent formation of oscillons from collapsing domains provide a reasonably realistic model of how oscillons could be produced e.g. in conditions present in the early Universe, the drawback is the strong radiative component. Inevitably, a large fraction of the energy of the domain walls is released into dispersive modes that not only appear as the dominating signal in the spectral function, but also undoubtedly affect significantly the evolution of oscillons as discussed earlier.

In order to simulate the evolution of an ensemble of oscillons in a far less radiative environment, we follow a different approach. An *oscillon gas* is initialised by preparing an oscillon lattice where oscillons are placed initially at equal distance from each other, but boosted with a velocity v in random directions. In the subsequent evolution oscillons collide resulting in scattering, decaying and merging. The energy released from oscillons creates a radiative component, but this is starkly suppressed compared to the one present in simulations reported in the previous section.

Figure 5.8 shows three snapshots of the total energy density in a simulation where initially 36 oscillons are placed with velocity $v = 0.5$ into

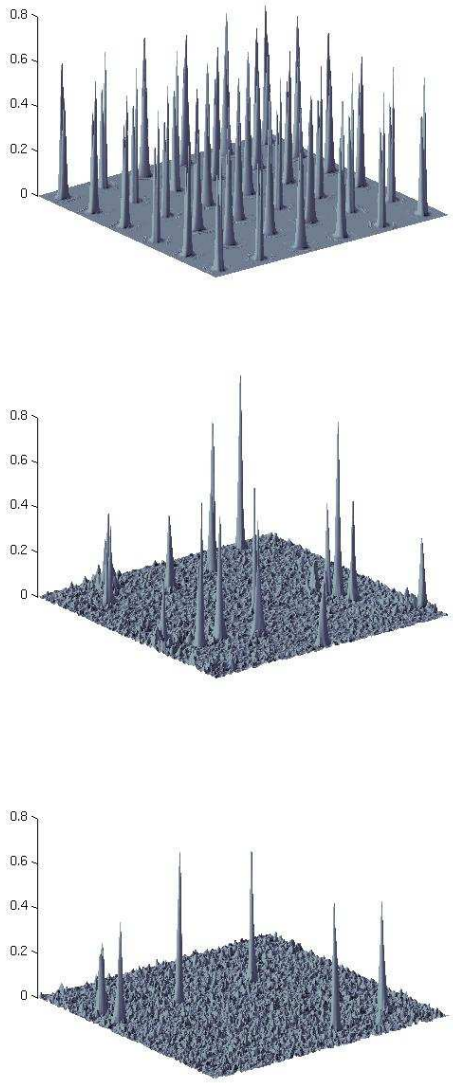

Figure 5.8. Sequence of snapshots showing the total energy density at times $t = 0$, 937.5, 10190. The high peaks are oscillons. Some of them survive, while lots of energy is released to radiation, the small amplitude fluctuations visible in the later snapshots.

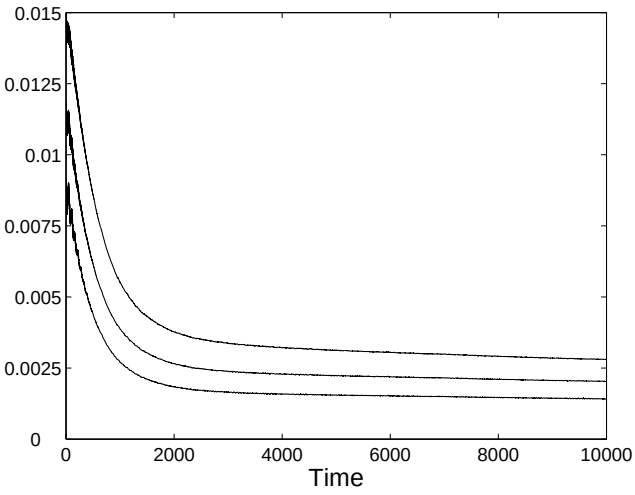

Figure 5.9. Fraction of points of the lattice where the total energy density exceeds 0.15, 0.2 or 0.25 (20, 28 and 35 times the average from top to bottom) as a function of time. The sharp decrease in the number of oscillons flattens out with time.

random directions on the lattice of size 800^2 (physical size in linear dimension is 200). There is a reduction in the number of oscillons and the energy in dispersive propagating waves is clearly visible in the two later snapshots, but this is far less strong than those originating from domain walls. Most importantly, the simulations show that a few oscillons, typically half a dozen, survive for a long period of time, far greater than e.g. the time required an oscillon at initial velocity v to travel around the lattice.

Because radiation is suppressed, higher concentrations in the energy density can be used to track oscillons. The survival of oscillons was studied more quantitatively by performing simulations of a larger ensemble. One hundred different initial states each having 121 oscillons at the beginning were evolved on a lattice of size 1500^2. Figure 5.9 shows the fraction of lattice points where the total energy exceeds 0.25, 0.2 or 0.15 as a function of time (these thresholds correspond to roughly 35, 28 and 20 times the mean value, respectively). For clarity the data is averaged over one os-

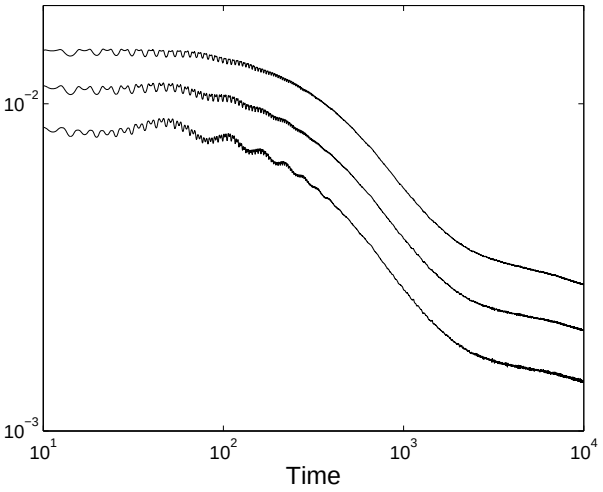

Figure 5.10. The same data as in Figure 5.9 on a logarithmic scale. The period when the curves show a roughly constant value, corresponds to an early stage when no collisions have yet taken place. The intermediate period shows a phase that can be described by a power law.

cillation period (roughly 5 in time units). This is because all the oscillons start initially at the same phase and there is considerable variation in the height and width of the energy density within the period (see Figure 3.2). Some oscillations are still visible left in Figure 5.10, where the same data is plotted on a logarithmic scale. However, the collisions cause generally a phase shift as will be discussed in the next section (see the left panel of Figure 5.11). Therefore we do not expect that the used initial state is in anyway particular, but rather that the phase distribution of oscillons soon becomes a random one. At the very least, the curves in Figure 5.10 do not show visible fluctuations after the early stage. All the curves yield also a similar time evolution: thus we conclude that there is no sensitivity to the thresholds chosen either. As the dispersive waves do not contain energy concentrations that would exceed these thresholds (as can be seen in Figure 5.8), we further argue that the signal must be due to oscillons.

The data in Figures 5.9 and 5.10 clearly show that there is a decrease

in the number of lattice sites where the energy density exceeds the thresholds corresponding to the demise of oscillons in collisions. However, the main result is that there are two phases: the steeply declining slope flattens around time $t = 10^3$ to a much less rapid decay. At the end of the simulation there is still almost 20% left of the initial number of lattice points where the thresholds are exceeded.

In the region of fast decline the slopes have values approximately -0.7. This is marginally consistent with a decay law inversely proportional to time. Such a power law is to be predicted by a simple annihilation picture: oscillons have constant velocity v and cross section σ. Then in two dimensions their number density $N = N(t)$ obeys the differential equation

$$\dot{N} = -\langle v\sigma \rangle N^2, \tag{5.1}$$

which yields an evolution inversely proportional to time, or more precisely

$$N(t) = \frac{N_0}{1 + \langle v\sigma \rangle N_0 t}\,. \tag{5.2}$$

While the steeper slopes can be understood on the basis of the differential equation (5.1), we do not have any quantitative explanation for the crossover. On the qualitative level there are at least two effects that could lengthen the life time of oscillons at a later stage of the simulations. First, collisions between oscillons, though not necessarily leading to their demise, cause considerable perturbation, and the oscillon radiates strongly before it settles back into a long-living state. If another collision occurs during this relaxation it is then presumably highly likely to destroy the already perturbed oscillon. In the simulations it is seen that the second collision is indeed often the fateful one. Lower number density and consequently a longer mean free path can yield an enhancement of the survival probability in collisions. More importantly, due to the interactions oscillons slow down drastically (a decrease in the average velocity $\langle v \rangle$ can be partially responsible of the flatter slope than the expected -1 already at the earlier stage). The reduced collision rate in turn increases the lifetime.

5.5 Oscillon Collisions - Merging and Scattering

The simulations presented in the previous section show that collisions between oscillons can, apart from scattering or demise, result in merging. Off-axis collisions of oscillons were briefly studied earlier and an attractive scattering occurs with the relatively high velocity used. A wider study at lower velocities is performed here. Reducing the velocity causes the trajectories of oscillons to bend more after the encounter. Ultimately oscillons scatter approximately at right angles after the collision. If the velocity is decreased even more, the oscillons do not scatter anymore, but merge together. Thus there is a kind of critical velocity, v_c, above which oscillons have enough translational energy to escape the attractive self interaction, but below which coalescence takes place. This is illustrated in Figures 5.11 and 5.12. Figure 5.11 shows snapshots of the value of the field in an off-axis collision of two oscillons when the displacement in the alignment between the centers of oscillons, the impact parameter, is 11.0 units. On the left panel the initial velocity is set to be $v \simeq 0.1$ whereas on the right it is approximately 10% smaller, $v \simeq 0.09$. In the first case scattering takes place, including a strong phase shift. The latter situation results in merging where a considerable amount of energy is leaked during the process as can be seen from the spiral waves in the field. However, a localised energy concentration remains as can be seen particularly clearly in Figure 5.12, which shows the energy density at same time instants as the value of the field in Figure 5.11.

The impact parameter alone, however, is not sufficient for a complete description of the scattering process of oscillons. As mentioned before, over a period of an oscillation there is a large variation in the size of the oscillon profile also in energy density ρ, see Figure 3.2. Therefore the bare impact parameter is an inadequate simplification, but also the phase at the moment of the impact affects the energy transfer and thus the final state after the collision. An exhaustive study of these effects was not carried out here. We merely finish by reporting that at low velocities even an impact parameter as large as 12 in the units used, thus greatly exceeding the approximate size of an oscillon r_0, is still sufficient to bend the trajectories to such an extent that oscillons merge together. None of the set-ups used

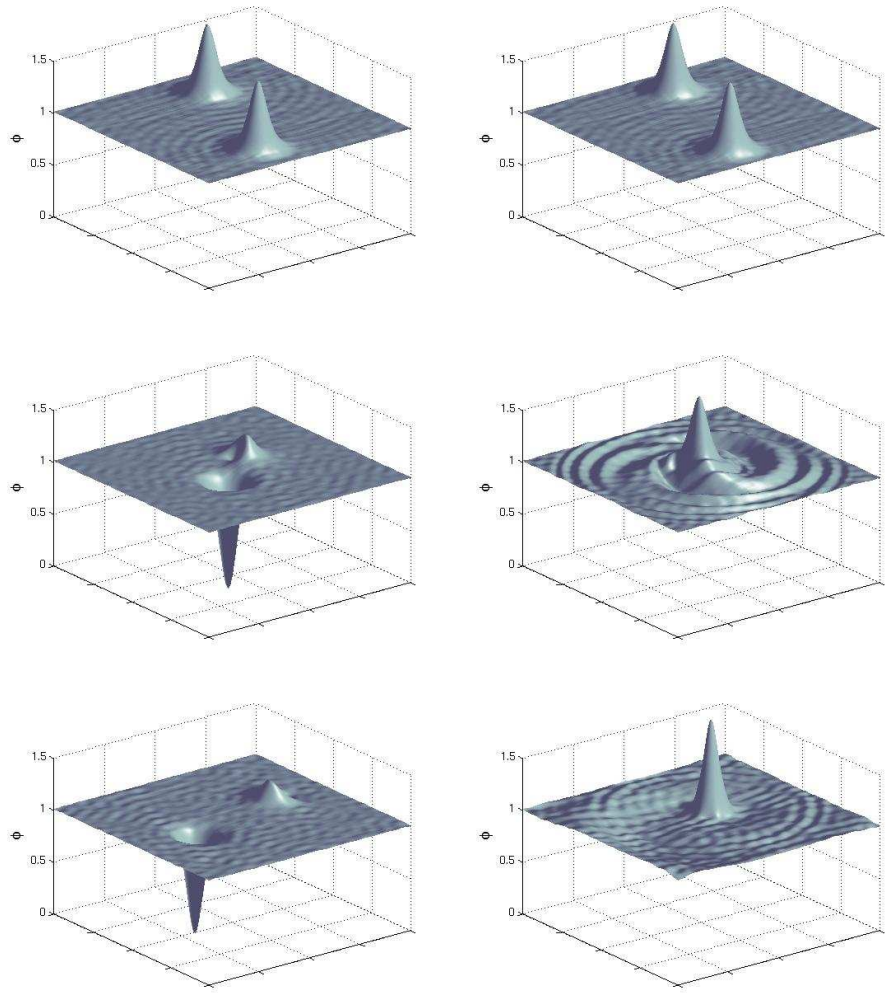

Figure 5.11. Oscillons scattering and merging: the field at three instants (chronologically from top to bottom) in an off-axis collision of oscillons at velocity $v \simeq 0.1$ (left) and $v \simeq 0.09$ (right). Alignment of the centers is displaced by 11.0 units.

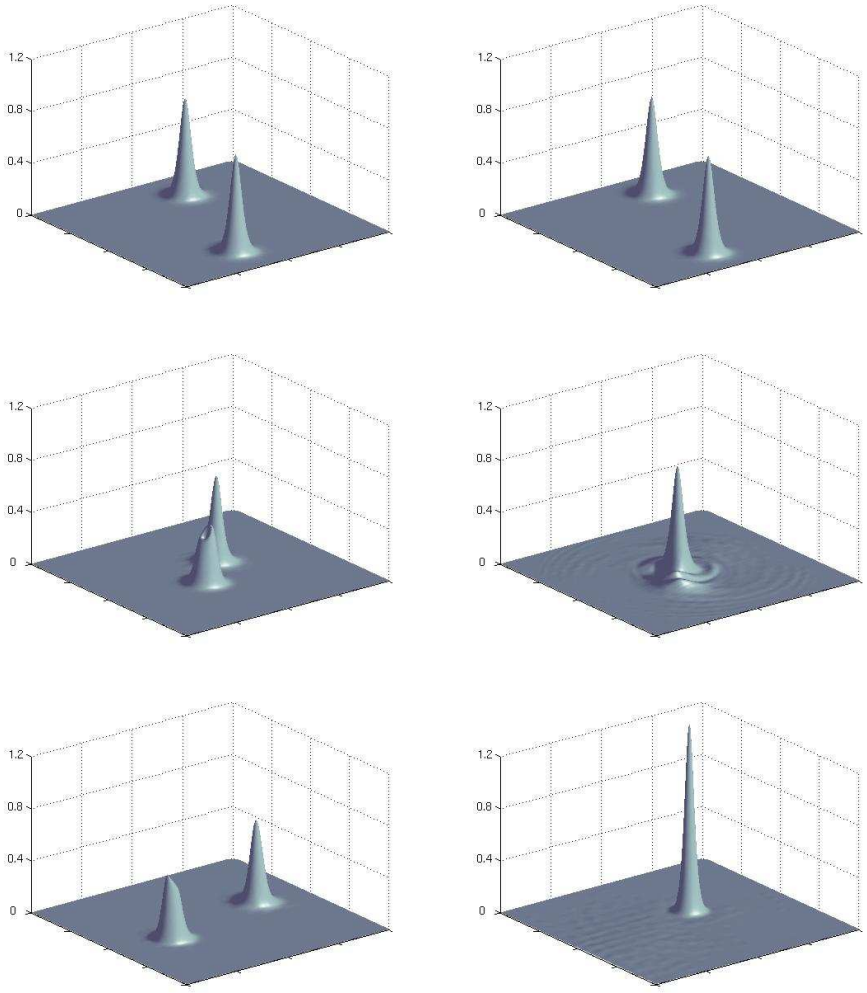

Figure 5.12. Oscillons scattering and merging: the energy density at the same time instants as in Fig. 5.11 in an off-axis collision of oscillons at velocity $v \simeq 0.1$ (left) and $v \simeq 0.09$ (right).

for collisions have led to an immediate demise of both oscillons, but the final state has always at least one localised energy concentration left.

5.6 Oscillons Crossing the Domain Walls

As oscillons are made by domain walls and survive collisions, it is natural to pose the question of what happens when an oscillon meets a domain wall. Figure 5.13 shows snapshots of an oscillon with an initial velocity $v \simeq 0.75$ crossing a domain wall. The oscillon is clearly recognisable both before the encounter and afterwards oscillating around the other vacuum. Snapshots of the total energy density show that crossing has caused a perturbation on the domain wall that propagates at the speed of light along the wall away from the interaction point. A travelling wave, a pulse moving at the speed of light along a planar domain wall, is a known solution (see e.g. [9]). Snapshots in the kinetic energy where the static domain wall is initially invisible show that while the oscillon has shed some energy to the domain wall, that is a relatively tiny fraction as the ripples along the domain wall are barely visible. Though the direct energy transfer between the oscillon and the domain wall is in this case relatively small, the oscillon is deformed, slightly elongated in the direction of the domain wall, and potentially radiates some of its energy. It should be emphasised that the presented encounter is not necessarily a typical one – at velocity $v \simeq 0.5$ a crossing and survival of large localised oscillations has not been witnessed. At $v \simeq 0.5$ the energy density of an oscillon does not greatly exceed that of a domain wall, whereas at $v \gtrsim 0.75$ it is factors larger. In addition, there are two effects that readily seem to enhance the crossing probability at higher velocities. Lorentz contraction shortens the length of the disturbance oscillons create and due to the time dilation the time-evolution of the wave is slower decreasing the energy transfer to the domain wall. Apart from the velocity, the relative phase of the oscillon seems to strongly control the amount of energy transfer in a collision. In any case, just the possibility that oscillons can cross domain walls and propagate from one vacuum to another demonstrates how surprisingly persistent objects they are.

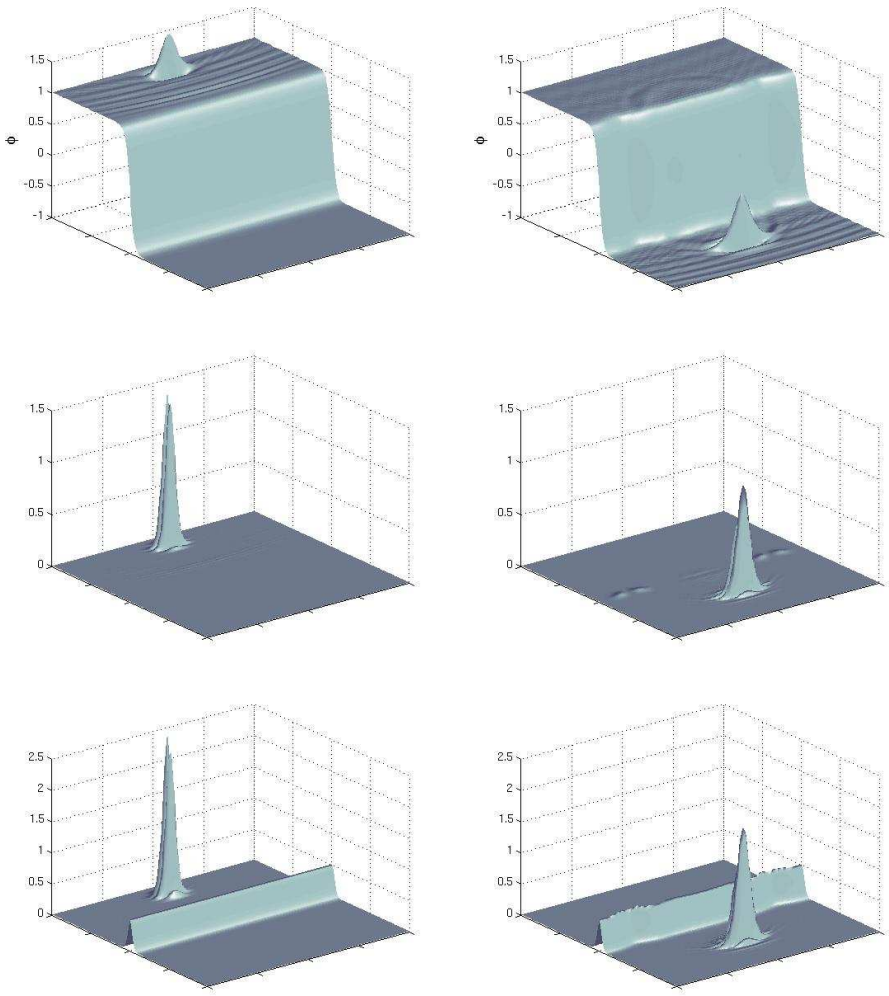

Figure 5.13. An oscillon crossing a domain wall with velocity $v \simeq 0.75$: the upper panel shows the value of field before (left) and after (right) the collision, the middle shows the kinetic energy density and total energy below.

5.7 Conclusions

We studied the field dynamics of a quartic double well potential with random initial conditions in two spatial dimensions. We have shown evidence that when the field is undamped the collapse of domains takes place so rapidly that there is enough energy to excite the field into long-lived, non-perturbative oscillating energy concentrations, oscillons. Investigating the field in the Fourier domain using a kind of classical spectral function enabled us to extract a velocity distribution for the oscillons, which extends to surprisingly high γ. This makes us believe that oscillons originate from regions from the domain wall with high velocity or cusps. We note that long domain walls also leave a very distinctive trace in the spectral function and maybe similar techniques could be used in studies of defects as well.

We further examined oscillons in a less radiative environment but still in a random system and showed that a fraction of oscillons persist for a long time. We reported on the merging of oscillons in off-axis collisions at low velocities as well as the potential of oscillons to cross a domain wall at high enough velocity. We believe these results would be qualitatively very similar in the two-dimensional sine-Gordon model that supports oscillons as well. Extrapolation to three dimensions, however, is far less straightforward as the lifetime and stability of oscillons depends strongly on the dimension of the theory. Adequate simulations would be required there.

We did not impose any damping for the system, apart from at very early times to condense it. Damping is not likely to alter the process of domain collapse considerably, unless the dissipation is really strong, while the further evolution may be different. However, it is not clear what kind of consequences dissipation would have. Damping could reduce the dispersive radiation modes and thus even enhance the oscillon lifetime. An obvious reason for friction in the system is of course the Hubble damping in the context of the early Universe. A numerical study in one dimension showed that oscillons could persist in an expanding background when the expansion rate is low enough [49]. This has been later studied analytically and the rate of energy loss was shown to be exponentially suppressed in the inverse of the Hubble parameter H [127]. Going back to moving oscillons

and their interactions, expansion can reduce velocities which may once again have twofold consequences. Oscillons may merge and decay more easily in collision, but it is also possible that expansion reduces the collision rate and then increases the lifetime of oscillons.

5.8 Appendix

We present here an analytic outline of how a moving Gaussian distribution would appear in spectral function $\Phi(\omega)$. The calculation is done in two spatial dimensions, but generalisation to any other dimension is straightforward. The starting point is the ansätze (3.4) and (1.62). Assume now further that all the modes $f_n(r)$ have the Gaussian form with the same width so that

$$\phi(r,t) = \exp(-r^2/r_0^2) \cdot \sum_{n=1}^{\infty} a_n \, \cos(n\omega_0 t)\,. \tag{5.3}$$

Consider now an arbitrary term in the sum under a boost with velocity v in x_1-direction. This yields

$$a_n \exp\Big(-\frac{\gamma^2 u^2 + x_2^2}{r_0^2}\Big) \cdot \cos\Big(n\omega_0\big(\frac{t}{\gamma} - \gamma v u\big)\Big)\,, \tag{5.4}$$

where we have defined $u = x_1 - vt$. The volume average integrating over the variables u and x_2 yields

$$\frac{a_n}{\gamma} \, \exp\Big(-\frac{n^2\omega_0^2 r_0^2}{4}\, v^2\Big) \cdot \cos\Big(\frac{n\omega_0 t}{\gamma}\Big)\,. \tag{5.5}$$

The decrease in the frequency is now explicitly readable in the time-dependent part. It is worth noticing that the higher modes $n > 1$ that appear with weaker amplitudes a_n for a stationary oscillon undergo now yet an extra suppression (this is to a certain extent visible in Figure 5.1, compared to the static situation $v = 0$). Now consider the basic frequency, $n = 1$. The spectral function in the approximation used is the product of the mean of the field and field momentum, $\bar{\phi} \cdot \bar{\Pi}$. Thus its amplitude has

a functional dependence on the kinematic variables v and γ

$$A_{\rm sp}(v) \propto \frac{1}{\gamma^3} \exp\Big(-\frac{1}{2}\,\omega_0^2\, r_0^2\, v^2 \Big)\,. \tag{5.6}$$

Consider now an arbitrary velocity distribution $n(v)$, referring the number of oscillons with velocity between v and $v + dv$. This yields a signal in the spectral function

$$\Phi(\omega) \propto \int dv\, n(v)\, A_{\rm sp}(v)\, \delta(\omega - \omega_0/\gamma(v))\,. \tag{5.7}$$

By the simple relation $\gamma = \omega_0/\omega$ this can be turned into the velocity distribution

$$n(v) = \frac{\omega_0 \sqrt{\omega_0^2 - \omega^2}}{\omega}\, \frac{\Phi(\omega)}{A_{\rm sp}(\omega)}\,. \tag{5.8}$$

It is, however, better to present the distribution $n(v)$ as a function of γ-factor

$$n(\gamma) = n(v)\, v/\gamma^3\,. \tag{5.9}$$

Bibliography

[1] S. Coleman, *Aspects of Symmetry* (Cambridge University Press, 1985).

[2] J. Scott Russell, Report of the 7th Meeting of British Association for the Advancement of Science, Liverpool, p. 417 (1838).

[3] D. J. Korteweg and G. de Vries, Philos. Mag. **39**, 422 (1895).

[4] R. F. Dashen, B. Hasslacher, and A. Neveu, Phys. Rev. **D10**, 4130 (1974).

[5] A. M. Polyakov, JETP Lett. **20**, 194 (1974).

[6] T. H. R. Skyrme, Proc. Roy. Soc. Lond. **A262**, 237 (1961).

[7] R. Rajaraman, *Solitons and Instantons* (North-Holland, 1982).

[8] N. Manton and P. Sutcliffe, *Topological Solitons* (Cambridge University Press, 2004).

[9] T. Vachaspati, *Kinks and domain walls: An introduction to classical and quantum solitons* (Cambridge University Press, 2006).

[10] R. F. Dashen, B. Hasslacher, and A. Neveu, Phys. Rev. **D11**, 3424 (1975).

[11] S. Aubry, J. Chem. Phys. **64**, 3392 (1976).

[12] M. Moshir, Nucl. Phys. **B185**, 318 (1981).

[13] D. K. Campbell, J. F. Schonfeld, and C. A. Wingate, Physica **9D**, 1 (1983).

[14] T. Sugiyama, Prog. Theor. Phys. **61**, 1550 (1979).

[15] M. Peyrard and D. K. Campbell, Physica **9D**, 33 (1983).

[16] P. Anninos, S. Oliveira, and R. A. Matzner, Phys. Rev. **D44**, 1147 (1991).

[17] H. Segur and M. D. Kruskal, Phys. Rev. Lett. **58**, 747 (1987).

[18] S. Dutta, D. A. Steer, and T. Vachaspati (2008), `arXiv:0803.0670[hep-th]`.

[19] J. Verwaest, Nucl. Phys. **B123**, 100 (1977).

[20] S. R. Coleman, Phys. Rev. **D11**, 2088 (1975).

[21] M. Salle, Phys. Rev. **D69**, 025005 (2004), `hep-ph/0307080`.

[22] Y. Bergner and L. M. A. Bettencourt, Phys. Rev. **D69**, 045002 (2004), `hep-th/0305190`.

[23] G. H. Derrick, J. Math. Phys. **5**, 1252 (1964).

[24] A. M. Polyakov and A. A. Belavin, JETP Lett. **22**, 245 (1975).

[25] W. J. Zakrzewski, *Low Dimensional Sigma Models* (Bristol, Institute of Physics Publishing, 1989).

[26] G. 't Hooft, Nucl. Phys. **B79**, 276 (1974).

[27] S. R. Coleman, Nucl. Phys. **B262**, 263 (1985).

[28] G. Rosen, J. Math. Phys. **9**, 999 (1968).

[29] T. D. Lee, Phys. Rept. **23**, 254 (1976).

[30] R. Friedberg, T. D. Lee, and A. Sirlin, Phys. Rev. **D13**, 2739 (1976).

[31] E. W. Kolb and M. S. Turner, *The Early Universe* (Addison-Wesley, 1990).

[32] S. Theodorakis, Phys. Rev. **D61**, 047701 (2000).

[33] A. Jokinen, *Affleck-Dine Mechanism and Q-balls along SUSY Flat Directions* (PhD thesis, University of Helsinki, 2002).

[34] A. Kusenko, Phys. Lett. **B404**, 285 (1997), `hep-th/9704073`.

[35] T. Multamaki and I. Vilja, Nucl. Phys. **B574**, 130 (2000), `hep-ph/9908446`.

[36] K.-M. Lee, J. A. Stein-Schabes, R. Watkins, and L. M. Widrow, Phys. Rev. **D39**, 1665 (1989).

[37] K. Enqvist and J. McDonald, Nucl. Phys. **B538**, 321 (1999), `hep-ph/9803380`.

[38] T. Multamaki and I. Vilja, Phys. Lett. **B484**, 283 (2000), `hep-ph/0005162`.

[39] T. Multamaki, *On the Properties and Cosmology of Q-balls* (PhD thesis, University of Turku, 2001).

[40] N. Graham, Phys. Lett. **B513**, 112 (2001), `hep-th/0105009`.

[41] R. Battye and P. Sutcliffe, Nucl. Phys. **B590**, 329 (2000), `hep-th/0003252`.

[42] T. Multamaki and I. Vilja, Phys. Lett. **B482**, 161 (2000), `hep-ph/0003270`.

[43] S. Kasuya and M. Kawasaki, Phys. Rev. **D62**, 023512 (2000), `hep-ph/0002285`.

[44] T. Multamaki, Phys. Lett. **B511**, 92 (2001), `hep-ph/0102339`.

[45] K. Enqvist and J. McDonald, Nucl. Phys. **B570**, 407 (2000), `hep-ph/9908316`.

[46] E. W. Kolb and I. I. Tkachev, Phys. Rev. **D49**, 5040 (1994), `astro-ph/9311037`.

[47] L. Stenflo and M. Y. Yu, Phys. Fluids **B1**, 1543 (1989).

[48] J. Garcia-Bellido (Personal Communications, 2006).

[49] N. Graham and N. Stamatopoulos, Phys. Lett. **B639**, 541 (2006), hep-th/0604134.

[50] I. L. Bogolyubsky and V. G. Makhankov, JETP Lett. **24**, 12 (1976).

[51] I. L. Bogolyubsky and V. G. Makhankov, Pisma Zh. Eksp. Teor. Fiz. **25**, 120 (1977).

[52] M. Gleiser, Phys. Rev. **D49**, 2978 (1994), hep-ph/9308279.

[53] E. J. Copeland, M. Gleiser, and H. R. Muller, Phys. Rev. **D52**, 1920 (1995), hep-ph/9503217.

[54] E. P. Honda and M. W. Choptuik, Phys. Rev. **D65**, 084037 (2002), hep-ph/0110065.

[55] G. Fodor, P. Forgacs, P. Grandclement, and I. Racz, Phys. Rev. **D74**, 124003 (2006), hep-th/0609023.

[56] M. Gleiser and D. Sicilia, Phys. Rev. Lett. **101**, 011602 (2008), arXiv:0804.0791[hep-th].

[57] M. Gleiser, Phys. Lett. **B600**, 126 (2004), hep-th/0408221.

[58] R. Watkins, DART-HEP-96/03, unpublished (1996).

[59] P. M. Saffin and A. Tranberg, JHEP **01**, 030 (2007), hep-th/0610191.

[60] G. Fodor, P. Forgacs, Z. Horvath, and A. Lukacs, Phys. Rev. **D78**, 025003 (2008), arXiv:0802.3525[hep-th].

[61] J. Geicke, Phys. Rev. **E49**, 3539 (1993).

[62] E. Farhi, N. Graham, V. Khemani, R. Markov, and R. Rosales, Phys. Rev. **D72**, 101701 (2005), hep-th/0505273.

[63] N. Graham, Phys. Rev. Lett. **98**, 101801 (2007), hep-th/0610267.

[64] N. Graham, Phys. Rev. **D76**, 085017 (2007), arXiv:0706.4125[hep-th].

[65] E. Witten, Phys. Rev. Lett. **38**, 121 (1977).

[66] P. Forgacs and N. S. Manton, Commun. Math. Phys. **72**, 15 (1980).

[67] E. Farhi, K. Rajagopal, and R. L. Singleton, Phys. Rev. **D52**, 2394 (1995), hep-ph/9503268.

[68] M. Gleiser and J. Thorarinson, Phys. Rev. **D76**, 041701 (2007), hep-th/0701294.

[69] P. W. Higgs, Phys. Lett. **12**, 132 (1964).

[70] P. W. Higgs, Phys. Rev. Lett. **13**, 508 (1964).

[71] H. B. Nielsen and P. Olesen, Nucl. Phys. **B61**, 45 (1973).

[72] P. Arnold and L. D. McLerran, Phys. Rev. **D37**, 1020 (1988).

[73] C. Rebbi and J. Singleton, Robert L., Phys. Rev. **D54**, 1020 (1996), hep-ph/9601260.

[74] N. J. Zabusky and M. D. Kruskal, Phys. Rev. Lett. **15**, 240 (1965).

[75] C. S. Gardner and G. K. Morikawa, Courant Inst. Math. Sci. Res. Rep. NYO-9082 (1960).

[76] E. Fermi, J. Pasta, and S. Ulam, Fermi Collected Papers **II**, 978 (1955).

[77] C. S. Gardner, J. M. Greene, M. D. Kruskal, and R. M. Miura, Phys. Rev. Lett. **19**, 1095 (1967).

[78] M. Onorato, A. R. Osborne, M. Serio, and S. Bertone, Phys. Rev. Lett. **86**, 5831 (2001), cond-mat/0104055.

[79] P. B. Umbanhowar, F. Melo, and H. L. Swinney, Nature **382**, 793 (1996).

[80] P. B. Umbanhowar, F. Melo, and H. L. Swinney, Physica **249A**, 1 (1998).

[81] D. Blair, I. S. Aranson, G. W. Crabtree, V. Vinokur, L. S. Tsimring, and C. Josserand, Phys. Rev. **E61**, 5600 (1994), `cond-mat/9910099`.

[82] L. S. Tsimring and I. S. Aranson, Phys. Rev. Lett. **79**, 213 (1997).

[83] O. M. Umurhan, L. Tao, and E. A. Spiegel, Ann. N. Y. Acad. Sci. **867**, 298 (1998), `astro-ph/9806209`.

[84] J. Dunkley et al. (WMAP) (2008), `arXiv:0803.0586[astro-ph]`.

[85] E. Komatsu et al. (WMAP) (2008), `arXiv:0803.0547[astro-ph]`.

[86] A. D. Sakharov, Pisma Zh. Eksp. Teor. Fiz. **5**, 32 (1967).

[87] M. Dine and A. Kusenko, Rev. Mod. Phys. **76**, 1 (2004), `hep-ph/0303065`.

[88] I. Affleck and M. Dine, Nucl. Phys. **B249**, 361 (1985).

[89] A. Vilenkin and E. P. S. Shellard, *Cosmic Strings and other Topological Defects* (Cambridge University Press, 1994).

[90] K. Kajantie, M. Laine, K. Rummukainen, and M. E. Shaposhnikov, Phys. Rev. Lett. **77**, 2887 (1996), `hep-ph/9605288`.

[91] A. Tranberg, *Cold Electroweak Baryogenesis* (PhD thesis, University of Amsterdam, 2004).

[92] T. W. B. Kibble, J. Phys. **A9**, 1387 (1976).

[93] W. H. Zurek, Nature **317**, 505 (1985).

[94] W. H. Press, B. S. Ryden, and D. N. Spergel, Astrophys. J. **347**, 590 (1989).

[95] B. S. Ryden, W. H. Press, and D. N. Spergel, Astrophys. J. **357**, 293 (1990).

[96] T. Garagounis and M. Hindmarsh, Phys. Rev. **D68**, 103506 (2003), hep-ph/0212359.

[97] P. P. Avelino, C. J. A. P. Martins, J. Menezes, R. Menezes, and J. C. R. E. Oliveira, Phys. Lett. **B647**, 63 (2007), astro-ph/0612444.

[98] S. Borsanyi and M. Hindmarsh, Phys. Rev. **D77**, 045022 (2008), arXiv:0712.0300[hep-ph].

[99] M. Hindmarsh and A. Rajantie, Phys. Rev. Lett. **85**, 4660 (2000), cond-mat/0007361.

[100] J. Preskill, Phys. Rev. Lett. **43**, 1365 (1979).

[101] A. H. Guth, Phys. Rev. **D23**, 347 (1981).

[102] R. Jeannerot, Phys. Rev. Lett. **77**, 3292 (1996), hep-ph/9609442.

[103] Y. B. Zeldovich, I. Y. Kobzarev, and L. B. Okun, Zh. Eksp. Teor. Fiz. **67**, 3 (1974).

[104] J. A. Frieman, G. B. Gelmini, M. Gleiser, and E. W. Kolb, Phys. Rev. Lett. **60**, 2101 (1988).

[105] K. Griest and E. W. Kolb, Phys. Rev. **D40**, 3231 (1989).

[106] J. A. Frieman, A. V. Olinto, M. Gleiser, and C. Alcock, Phys. Rev. **D40**, 3241 (1989).

[107] D. Metaxas, Phys. Rev. **D63**, 083507 (2001), hep-ph/0009225.

[108] A. Kusenko and M. E. Shaposhnikov, Phys. Lett. **B418**, 46 (1998), hep-ph/9709492.

[109] M. Dine, L. Randall, and S. D. Thomas, Nucl. Phys. **B458**, 291 (1996), hep-ph/9507453.

[110] A. Kusenko, Phys. Lett. **B405**, 108 (1997), hep-ph/9704273.

[111] S. Kasuya and M. Kawasaki, Phys. Rev. **D61**, 041301 (2000), hep-ph/9909509.

[112] K. Enqvist, A. Jokinen, T. Multamaki, and I. Vilja, Phys. Rev. **D63**, 083501 (2001), hep-ph/0011134.

[113] K. Enqvist and A. Mazumdar, Phys. Rept. **380**, 99 (2003), hep-ph/0209244.

[114] A. G. Cohen, S. R. Coleman, H. Georgi, and A. Manohar, Nucl. Phys. **B272**, 301 (1986).

[115] G. R. Dvali, A. Kusenko, and M. E. Shaposhnikov, Phys. Lett. **B417**, 99 (1998), hep-ph/9707423.

[116] H. P. Nilles, Phys. Rept. **110**, 1 (1984).

[117] M. Laine and M. E. Shaposhnikov, Nucl. Phys. **B532**, 376 (1998), hep-ph/9804237.

[118] E. Palti, P. M. Saffin, and E. J. Copeland, Phys. Rev. **D70**, 083520 (2004), hep-th/0405081.

[119] A. Kusenko, Phys. Lett. **B406**, 26 (1997), hep-ph/9705361.

[120] E. W. Kolb and I. I. Tkachev, Phys. Rev. Lett. **71**, 3051 (1993), hep-ph/9303313.

[121] M. van der Meulen, *Cold Electroweak Baryogenesis and Quantum Cosmological Corrections* (PhD thesis, University of Amsterdam, 2008).

[122] E. J. Copeland, S. Pascoli, and A. Rajantie, Phys. Rev. **D65**, 103517 (2002), hep-ph/0202031.

[123] G. N. Felder and L. Kofman, Phys. Rev. **D75**, 043518 (2007), hep-ph/0606256.

[124] G. N. Felder and O. Navros, JCAP **0702**, 014 (2007), hep-ph/0701128.

[125] M. van der Meulen, D. Sexty, J. Smit, and A. Tranberg, JHEP **02**, 029 (2006), hep-ph/0511080.

[126] M. Broadhead and J. McDonald, Phys. Rev. **D72**, 043519 (2005), hep-ph/0503081.

[127] E. Farhi et al., Phys. Rev. **D77**, 085019 (2008), arXiv:0712.3034[hep-th].

[128] M. Broadhead and J. McDonald, Phys. Rev. **D68**, 083502 (2003), hep-ph/0305298.

[129] M. Beltran, J. Garcia-Bellido, and J. Lesgourgues, Phys. Rev. **D75**, 103507 (2007), hep-ph/0606107.

[130] J. N. Hormuzdiar and S. D. H. Hsu, Phys. Rev. **C59**, 889 (1999), hep-ph/9805382.

[131] V. A. Gani, A. E. Kudryavtsev, T. I. Belova, and B. L. Druzhinin, Phys. Atom. Nucl. **62**, 895 (1999), hep-ph/9712526.

[132] S. Kasuya, M. Kawasaki, and F. Takahashi, Phys. Lett. **B559**, 99 (2003), hep-ph/0209358.

[133] M. Gleiser and R. C. Howell, Phys. Rev. **E68**, 065203 (2003), cond-mat/0310157.

[134] M. Gleiser and R. C. Howell, Phys. Rev. Lett. **94**, 151601 (2005), hep-ph/0409179.

[135] M. Gleiser, B. Rogers, and J. Thorarinson, Phys. Rev. **D77**, 023513 (2008), arXiv:0708.3844[hep-th].

[136] A. Riotto, Phys. Lett. **B365**, 64 (1996), hep-ph/9507201.

[137] M. Gleiser, Int. J. Mod. Phys. **D16**, 219 (2007), hep-th/0602187.

[138] S. H. Henry Tye (2006), hep-th/0611148.

[139] E. J. Copeland, A. Padilla, and P. M. Saffin, JHEP **01**, 066 (2008), arXiv:0709.0261[hep-th].

[140] P. M. Saffin, A. Padilla, and E. J. Copeland (2008), arXiv:0804.3801[hep-th].

[141] M. Gleiser and A. Sornborger, Phys. Rev. **E62**, 1368 (2000), patt-sol/9909002.

[142] A. B. Adib, M. Gleiser, and C. A. S. Almeida, Phys. Rev. **D66**, 085011 (2002), hep-th/0203072.

[143] B. Piette and W. J. Zakrzewski, Nonlinearity **11**, 1103 (1998).

[144] G. Aarts and J. Smit, Nucl. Phys. **B511**, 451 (1998), hep-ph/9707342.

[145] G. Aarts, Phys. Lett. **B518**, 315 (2001), hep-ph/0108125.

[146] H. Arodz, P. Klimas, and T. Tyranowski, Phys. Rev. **D77**, 047701 (2008), arXiv:0710.2244[hep-th].

[147] A. Bamberger, P. Joly, and J. E. Roberts, SIAM Journal on Numerical Analysis **27**, 323 (1990).

[148] R. A. Battye, *String Radiation, Interactions and Cosmological Constraints* (PhD thesis, University of Cambridge, 1995).

[149] I. Dymnikova, L. Koziel, M. Khlopov, and S. Rubin, Grav. Cosmol. **6**, 311 (2000), hep-th/0010120.

[150] E. P. Honda, *Resonant dynamics within the nonlinear Klein-Gordon equation: Much ado about oscillons* (PhD thesis, Texas U., 2000), hep-ph/0009104.

[151] M. Gleiser and R. M. Haas, Phys. Rev. **D54**, 1626 (1996), hep-ph/9602282.

Samenvatting

Als je een steen in het water gooit, zie je ringvormige golven die zich verwijderen van het punt waar de steen het wateroppervlak raakt. De energie die door de steen is vrijgemaakt, wordt door de golven getransporteerd en raakt zo verspreid over een steeds groter oppervlak. Anders gezegd: de energie wordt gedissipeerd. In water ziet men echter ook een soort gedrag dat in alles het tegenovergestelde van dissipatie is. Een bekend voorbeeld van het inperken van het aantal richtingen waarin een golf zich kan voortbewegen is een kanaal. Als je een grote boot volgt in een kanaal (een veel voorkomend schouwspel als je de trein van Amsterdam naar Utrecht neemt) kun je zien dat de golven achter de boot zich over lange afstanden ongestoord voortbewegen. Dit is precies de observatie die leidde tot de ontdekking van *solitonen*: gelokaliseerde niet-dissipatieve pakketjes energie.

Het geval van golven in ondiep water is aan het eind van de 19^{e} eeuw verklaard door Diederik Korteweg en Gustav de Vries; zij leidden een niet-lineaire vergelijking af die nu hun naam draagt en een soliton-oplossing heeft. Later werd ontdekt dat solitonen en vrij lopende golven in een aantal relativistische veldentheorieën voorkomen en deze oplossingen zijn veel bestudeerd. Ze worden geclassificeerd in twee categorieën: topologische en niet-topologische solitonen. De topologische soliton oplossing heeft andere randvoorwaarden in het oneindige dan het fysische vacuüm van de theorie en het soliton kan niet op een continue manier worden vervormd tot de vacuüm toestand. Het simpelste voorbeeld is de kink-oplossing in één dimensie, die interpoleert tussen twee verschillende vacua. Het bestaan van niet-topologische solitonen is gerelateerd aan een extra behoudswet en er is geen ontaard vacuüm nodig in de theorie. De stabiliteit van niet-

topologische solitonen vergt dat ze energetisch voordelig zijn.

Er is een belangrijk theorema van Derrick dat stelt dat er geen statische oplossingen zijn met eindige energie in scalaire theorieën met meer dan één ruimtelijke dimensie. Er zijn twee manieren om onder dit theorema uit te komen: ten eerste door ijkvelden in de theorie te stoppen en ten tweede door niet naar stationaire oplossingen van de scalaire theorie te zoeken, maar naar tijdsafhankelijke. Magnetische monopolen zijn een voorbeeld van topologische solitonen en semi-lokale snaren zijn een voorbeeld van niet-topologische solitonen in theorieën met ijkvelden. Een voorbeeld van tijdsafhankelijke, niet-topologische solitonen zijn Q-ballen. Deze bestaan in een complex scalair veld en dragen een behouden, globale lading die verhindert dat ze vervallen.

Als men minder velden in de theorie stopt en een enkel reëel scalair veld beschouwt, dan is er geen behouden lading die de stabiliteit kan verklaren. Er is dan dus niets dat het energiepakketje principieel verhindert om te vervallen. Echter, voor een aantal potentialen heeft zo'n theorie nog steeds een veldconfiguratie die gelokaliseerd blijft en bijna periodiek in de tijd is, dat wil zeggen zonder dissipatie. Deze objecten worden vaak *oscillonen* genoemd en zijn het onderwerp van deze dissertatie. Oscillonen zijn niet-topologisch en stralen zeer langzaam een beetje energie uit.

In dit proefschrift worden oscillonen beschouwd in twee ruimtelijke dimensies, waarbij we ons voornamelijk concentreren op twee relativistische veldentheorieën, namelijk de ϕ^4-theorie en het *sine-Gordon* model. Uit numerieke resultaten blijkt dat oscillonen in deze theorieën in veel opzichten lijken op meer conventionele solitonen of vrij lopende golven, waarvan de eigenschappen beter zijn begrepen. De studie van verstrooiing van oscillonen onderling in hoofdstuk drie demonstreert dat ze weer tevoorschijn kunnen komen na een botsing, wat een onderscheidende eigenschap is voor solitonen. Er treden echter energieverliezen op bij deze interacties. Dit lijkt veel op wat er gebeurt bij de botsing tussen een kink en antikink in een ϕ^4 theorie, waarbij de kinks kunnen annihileren, en zelfs als ze terugkaatsen gaat een deel van hun oorspronkelijke energie verloren in de vorm van straling.

De stabiliteit van oscillonen wordt bestudeerd in hoofdstuk drie en vier. Ze leven extreem lang en in simulaties kan men ze niet zien verdwij-

nen. We stellen vast dat het stralingsdeel van de oscillonenergie afvalt als een machtswet. Verder beschouwen we een model waarin de hoeveelheid straling per tijdseenheid sterk onderdrukt wordt over de tijd, wat suggereert dat zo'n oscillon een voorbeeld zou kunnen zijn van een gelokaliseerde, eindige oplossing in een tweedimensionale, reële, scalaire theorie die oneindig lang leeft.

Niet-dissipatieve oplossingen zijn op zichzelf al interessant om te bestuderen, maar het wordt nog interessanter als ze via een of ander proces in de natuur gevormd kunnen worden en kunnen voortbestaan in een realistische omgeving. In het geval van relativistische veldentheorieën is het vroege universum een geschikte omgeving om te bestuderen omdat daar verschillende soorten defecten gevormd zouden kunnen worden, zoals kort beschreven in hoofdstuk twee. Op hun beurt kunnen defecten, zoals domeingrenzen, een sterke invloed uitoefenen, welke, in het geval van het vroege universum vaak aan waarnemingen kunnen worden getoetst. Als oscillonen tevoorschijn komen in een systeem, vertragen ze het proces van equipartitie, zoals de solitonen van de Korteweg-De Vriesvergelijking in het Fermi-Pasta-Ulammodel. Een productiemechanisme voor oscillonen wordt gepresenteerd in hoofdstuk vijf, waar domeingrensnetwerken worden bestudeerd. Simulaties wijzen uit dat het heftige proces van het ineenstorten van domeinen over het algemeen oscillonen produceert en dat hun snelheidsdistributie zich tot hoog-relativistische snelheden uitstrekt. Een studie van een diffuus gas van oscillonen laat zien dat een bepaalde fractie van de oscillonen voor langere tijd blijft bestaan. Men moet in het achterhoofd houden dat het dynamisch bereik van veldentheoriesimulaties een kleine fractie is van kosmologische tijdsschalen, maar net zoals andere structuren kunnen oscillonen belangrijke consequenties hebben.

Publications

- M. Hindmarsh and P. Salmi,
  Oscillons and Domain Walls
  Phys. Rev. D **77** (2008) 105025 [arXiv:0712.0614 [hep-th]].

- P. Salmi, A. Achúcarro, E. J. Copeland, T. W. B. Kibble, R. de Putter, and D. A. Steer,
  Kinematic Constraints on Formation of Bound States of Cosmic Strings – Field Theoretical Approach
  Phys. Rev. D **77** (2008) 041701 R [arXiv:0712.1204 [hep-th]].

- A. Achúcarro, P. Salmi and J. Urrestilla,
  Semilocal string networks
  Phys. Rev. D **75** (2007) 121703 R [arXiv:astro-ph/0512487].

- M. Hindmarsh and P. Salmi,
  Numerical investigations of oscillons in 2 dimensions
  Phys. Rev. D **74** (2006) 105005 [arXiv:hep-th/0606016].

- F. Freire, N. D. Antunes, P. Salmi and A. Achúcarro,
  The role of dissipation in biasing the vacuum selection in quantum field theory at finite temperature
  Phys. Rev. D **72** (2005) 045017 [arXiv:hep-ph/0502220].

- R. Kinnunen, S. Lehti, A. Nikitenko and P. Salmi,
  On the discovery potential of the lightest MSSM Higgs boson at the LHC
  J. Phys. G **31** (2005) 71 [arXiv:hep-ph/0503067].

- S. Abdullin *et al.*,
  Summary of the CMS potential for the Higgs boson discovery
  Eur. Phys. J. C **39S2** (2005) 41.

- P. Salmi, R. Kinnunen, and N. Stepanov,
  Prospects of detecting massive charged Higgs from hadronic decay $H^{\pm} \rightarrow tb$ in CMS
  CMS Note 2002/024 [arXiv:hep-ph/0301166].

- E. K. O. Hellén, P. E. Salmi, and M. J. Alava,
  Cluster Persistence in One-Dimensional Diffusion-Limited Cluster–Cluster Aggregation
  Phys. Rev. E **66**, (2002) 051108 [arXiv:cond-mat/0206139].

- E. K. O. Hellén, P. E. Salmi, and M. J. Alava,
  Cluster Survival and Polydispersity in Aggregation
  Europhys. Lett. **59**, (2002) 186 [arXiv:cond-mat/0111522].

Curriculum Vitæ

I was born on 6th October 1975 in Kuorevesi, which is today part of Jämsä. I attended the secondary school in the nearby Mänttä graduating from Mäntän lukio in 1994.

I enrolled at the University of Helsinki in 1995. Part of my MSc degree studies were done at the Ruprecht-Karls-Universität Heidelberg where I spent one semester in the ERASMUS exchange program in 1999. In the summer of 2001 I worked at the European Centre for Particle Physics CERN within the program of the Helsinki Institute of Physics which participates the Compact Muon Solenoid (CMS) Experiment at the LHC. My master thesis dealt with time-dependent random walks the reasearch being carried out at the Laboratory of Physics of the Helsinki University of Technology. I graduated in physics in 2002.

I worked in the fall of 2002 as an acting assistant at the Department of Physics at the University of Helsinki. Early 2003 I worked at the Helsinki Institute of Physics in the CMS project. I came to Instituut-Lorentz in 2003 with the help of a grant from Magnus Ehrnrooth Foundation. I spent nine months at the Department of Physics & Astronomy at the University of Sussex in 2004-2005 within the European Community's Marie Curie Program.

Acknowledgements

The research work presented in this thesis has been done at Instituut-Lorentz at the University of Leiden and at the University of Sussex, both during a nine-month stay through the Marie Curie fellowship (in 2004-2005) and numerous visits afterwards.

I am greatly indebted to Mark Hindmarsh, without whom this thesis would not exist. First of all, I must thank him for spotting oscillons in the simulations - I considered them a mere nuisance. Furthermore, I am grateful to him for discussions, sharing of ideas and encouragement in what followed. I also want to thank the University of Sussex for hospitality over the past three and a half years. Also thanks to Ana Achúcarro for painstakingly reading the manuscript.

On the side of external funding two sources played a very important role. The already mentioned Marie Curie Fellowship of the European Community Program is gratefully acknowledged. Secondly, I want to thank Magnus Ehrnrooth Foundation for the grant that enabled me to start my PhD research in the first place.